Remote sensing of solar-induced chlorophyll fluorescence (SIF) in vegetation: 50 years of progress

Gina H. Mohammed[a,*], **Roberto Colombo**[b], **Elizabeth M. Middleton**[c], **Uwe Rascher**[d], **Christiaan van der Tol**[e], **Ladislav Nedbal**[d], **Yves Goulas**[f], **Oscar Pérez-Priego**[g], **Alexander Damm**[h,i], **Michele Meroni**[j], **Joanna Joiner**[c], **Sergio Cogliati**[b], **Wouter Verhoef**[e], **Zbyněk Malenovský**[k], **Jean-Philippe Gastellu-Etchegorry**[l], **John R. Miller**[m], **Luis Guanter**[n], **Jose Moreno**[o], **Ismael Moya**[f], **Joseph A. Berry**[p], **Christian Frankenberg**[q], **Pablo J. Zarco-Tejada**[j,r,s,t]

[a]P&M Technologies, Sault Ste. Marie, Ontario, Canada [b]Remote Sensing of Environmental Dynamics Lab., University of Milano - Bicocca, Milan, Italy [c]NASA/Goddard Space Flight Center, Greenbelt, Maryland, United States [d]Forschungszentrum Jülich, Institute of Bio- and Geosciences, IBG-2: Plant Sciences, Jülich, Germany [e]University of Twente, Faculty of Geo-Information Science and Earth Observation, Enschede, The Netherlands [f]CNRS, Laboratoire de Météorologie Dynamique (LMD), Ecole Polytechnique, Palaiseau, France [g]Department of Biogeochemical Integration, Max Planck Institute for Biogeochemistry, Jena, Germany [h]Department of Geography, University of Zurich, Zurich, Switzerland [i]Eawag, Swiss Federal Institute of Aquatic Science and Technology, Duebendorf, Switzerland [j]European Commission, Joint Research Centre (JRC), Ispra (VA), Italy [k]Department of Geography and Spatial Sciences, School of Technology, Environments and Design, College of Sciences and Engineering, University of Tasmania, Hobart, Australia [l]Centre d'Etudes Spatiales de la BIOsphère – UPS, CNES, CNRS, IRD, Université de Toulouse, Toulouse, France [m]Department of Earth and Space Science and Engineering, York University, Toronto, Canada [n]German Research Center for Geosciences (GFZ), Remote Sensing Section, Potsdam, Germany [o]Department of Earth Physics and Thermodynamics, University of Valencia, Valencia, Spain [p]Department of Global Ecology, Carnegie Institution of Washington, Stanford, California, United States [q]Jet Propulsion Laboratory, California Institute of Technology, Pasadena, California, United States [r]Instituto de Agriculture Sostenible (IAS), Consejo Superior de Investigaciones Científicas (CSIC), Córdoba, Spain [s]Department of Infrastructure Engineering, Melbourne School of Engineering, University of Melbourne, Melbourne, Victoria, Australia [t]School of Agriculture and Food, Faculty of Veterinary and Agricultural Sciences, University of Melbourne, Melbourne, Victoria, Australia

Abstract

Remote sensing of solar-induced chlorophyll fluorescence (SIF) is a rapidly advancing front in terrestrial vegetation science, with emerging capability in space-based methodologies and diverse application prospects. Although remote sensing of SIF – especially from space – is seen as a contemporary new specialty for terrestrial plants, it is founded upon a multi-decadal history of

---

[*]Correspondence: gina.mohammed@pmtech.Ca.

research, applications, and sensor developments in active and passive sensing of chlorophyll fluorescence. Current technical capabilities allow SIF to be measured across a range of biological, spatial, and temporal scales. As an optical signal, SIF may be assessed remotely using highly-resolved spectral sensors and state-of-the-art algorithms to distinguish the emission from reflected and/or scattered ambient light. Because the red to far-red SIF emission is detectable non-invasively, it may be sampled repeatedly to acquire spatio-temporally explicit information about photosynthetic light responses and steady-state behaviour in vegetation. Progress in this field is accelerating with innovative sensor developments, retrieval methods, and modelling advances. This review distills the historical and current developments spanning the last several decades. It highlights SIF heritage and complementarity within the broader field of fluorescence science, the maturation of physiological and radiative transfer modelling, SIF signal retrieval strategies, techniques for field and airborne sensing, advances in satellite-based systems, and applications of these capabilities in evaluation of photosynthesis and stress effects. Progress, challenges, and future directions are considered for this unique avenue of remote sensing.

Keywords

(1) Sun-induced fluorescence; (2) Steady-state photosynthesis; (3) Stress detection; (4) Radiative transfer modelling; (5) SIF retrieval methods; (6) Satellite sensors; (7) Airborne instruments; (8) Applications; (9) Terrestrial vegetation; (10) Passive techniques; (11) Review

1. Introduction

The first recorded observation of solar-induced fluorescence (SIF) was made almost two centuries ago when Sir David Brewster, a Scottish preacher, discovered that a beam of sunlight striking a green alcoholic extract of laurel leaves elicited a brilliant red light (Brewster, 1834). He also noted that, as the light passed through successive 'thicknesses' of the extract, the emission changed colour from red to orange to yellow – this transition possibly being the first evidence of re-absorption by chlorophyll (Govindjee, 1995). Professor G.G. Stokes (1852) later coined the term 'fluorescence' to describe the emission. The likelihood of a link between the emission and photosynthetic assimilation was suggested by Müller (1874), and this idea was confirmed in the seminal work of Kautsky and Hirsch (1931), who revealed the kinetics of chlorophyll-a fluorescence (CF) emission in dark-adapted, suddenly illuminated leaves. Using only their eyes to track the initial fluorescence peak and its prompt decay to a lower steady-state level, they correlated this signature with the time course of CO_2 assimilation.

The theme of covariation between CF and photosynthesis was studied by McAlister and Myers (1940), who described two processes, one involving an inverse relation between rate of CO_2 uptake and intensity of fluorescence, the other a direct relationship. The key to this dual response was offered by Duysens and Sweers (1963), who pioneered the use of modulated excitation light – as is used in modern-day pulse-amplitude modulation (PAM) fluorimetry – and were the first to describe the active regulation of fluorescence yield by the process we now call "non-photochemical quenching" (Krause and Weis, 1991; Weis and Berry, 1987). The Duysens and Sweers (1963) approach was used to establish a quantitative

relationship between fluorescence yield and the rate of electron transport (Genty et al., 1989; Weis and Berry, 1987).

These pioneers prepared the stage for analysis of CF to become an established protocol in photosynthesis research and applications in forestry, crop science, horticulture, and ecophysiology (reviews by Baker and Rosenqvist, 2004; DeEll and Toivonen, 2003; Govindjee, 2004; Krause and Weis, 1991, 1984; Lichtenthaler, 1989; Lichthentaler and Rinderle, 1988; Mohammed et al., 1995; Papageorgiou and Govindjee, 2004). PAM fluorimetry is now used routinely to monitor photosynthetic responses. CF is informative about the light reactions of Photosystem II (PSII) especially, and is non-invasive, rapidly performed, and field-portable (Duysens, 1963; Franck and Herzfeld, 1941; Franck et al., 1941; Papageorgiou and Govindjee, 2004; Porcar-Castell et al., 2014; Schreiber, 2004; Schreiber et al., 1986). The catch is that PAM requires active manipulation of the light environment, limiting the approach to small scale (e.g., single leaf) applications.

As an optical signal, CF can be remotely sensed. This generally relies on passive measurement of SIF instead of active techniques using artificial excitation light. Remote sensing of fluorescence, already well-established in aquatic science since the early 1960s (reviews by Blondeau-Patissier et al., 2014; Gower, 2016), is a more recent endeavour in terrestrial science (reviews by Frankenberg and Berry, 2018; Malenovský et al., 2009; Meroni et al., 2009; Middleton et al., 2018; Moya and Cerovic, 2004; Moya et al., 1992; Zhang et al., 2009). Passive airborne sensors for fluorescence assessment include hyperspectral imaging systems able to retrieve discrete emission bands and potentially the full SIF emission spectrum, with high spatial granularity for field applications (e.g., Damm et al., 2011; Frankenberg et al., 2018; Meroni et al., 2009; Rascher et al., 2015; Zarco-Tejada et al., 2018, 2013b).

Atmospheric satellite sensors from several missions have been used to measure far-red SIF in terrestrial vegetation. They include: the Greenhouse gases Observing SATellite (GOSAT) – Thermal And Near-infrared Sensor for carbon Observation Fourier Transform Spectrometer (TANSO-FTS); the Meteorological Operational satellite (MetOp) – Global Ozone Monitoring Experiment-2 (GOME-2) sensor; the Environmental Satellite (EnviSat) – SCanning Imaging Absorption spectroMeter for Atmospheric CHartographY (SCIAMACHY), and MEdium Resolution Imaging Spectrometer (MERIS); the Orbiting Carbon Observatory (OCO-2); the Sentinel-5 Precursor (S-5P) – TROPOspheric Monitoring Instrument (TROPOMI); and the Carbon Dioxide Observation Satellite (TanSat) – Atmospheric Carbon dioxide Grating Spectrometer (ACGS) (Du et al., 2018; Frankenberg et al., 2011b; Guanter et al., 2007; Joiner et al., 2012, 2011; Köhler et al., 2018a; Sun et al., 2018). Applications of this satellite data are being studied for estimation of photosynthesis and stress effects (e.g., He et al., 2017; Köhler et al., 2018b; Li et al., 2018b; MacBean et al., 2018; Middleton et al., 2018; Qiu et al., 2018; Smith et al., 2018; Verma et al., 2017). None of those satellite systems were intended originally for measuring SIF, and only recently was the first global mission approved that is designed specifically for SIF measurement in terrestrial vegetation – the FLuorescence EXplorer (FLEX) (Drusch et al., 2017).

The vision to utilize remotely-detected fluorescence for ecological purposes is not entirely new. Almost 30 years ago, Krause and Weis (1991) presciently speculated that "…extension of fluorescence measurements to large-scale spectroscopy may be useful in basic and applied environmental research, such as mapping of the photosynthetic activity of terrestrial and marine vegetation." Progress in that direction was realized when chlorophyll fluorescence was shown experimentally and analytically to be a signal superimposed upon apparent reflectance spectra in leaves and canopies (Zarco-Tejada et al., 2000a, 2000b). Later, Moya and Cerovic (2004) commented that "…it is surprising that, even after a quarter of a century of research on satellite detection of chlorophyll fluorescence, no operational system has yet even been developed" (a situation they considered true to some extent for airborne systems as well). Today, there are exceptional breakthroughs on these fronts – in SIF sensor technologies, retrieval algorithms, and the modelling of leaf and canopy fluorescence and photosynthesis (Cogliati et al., 2015b; Damm et al., 2014; Frankenberg et al., 2012; Gastellu-Etchegorry et al., 2017; Hernández-Clemente et al., 2017; Joiner et al., 2016; Pedrós et al., 2010; Van der Tol et al., 2014, 2009a, 2009b; Verhoef et al., 2018; Vilfan et al., 2016; Zarco-Tejada et al., 2013b, 2006; Zhao et al., 2016). Much has occurred in fluorescence science since Brewster recorded that first observation! Now, fluorescence may be 'viewed' at multiple and complementary scales, even from space.

This review synthesizes developments in terrestrial SIF remote sensing over the last 50 years. It covers essential fluorescence basics, historical progress delineating fluorescence effects upon leaf and canopy reflectance spectra, advances in modelling, SIF retrieval methods, remote sensing technologies, and applications. As a synoptic overview, it complements recent reviews focused more specifically on fluorescence-photosynthesis linkages, SIF retrieval methods, applications, and/or instrumentation (A   et al., 2015; Frankenberg and Berry, 2018; Garbulsky et al., 2014a, 2014b; Malenovský et al., 2009; Meroni et al., 2009; Middleton et al., 2018; Porcar-Castell et al., 2014; Zhang et al., 2009).

This paper is dedicated to Dr. Marvin Bauer, who was pivotal for the communication of scientific advances on remote sensing of chlorophyll fluorescence during his tenure as Senior Editor of *Remote Sensing of Environment*. Dr. Bauer engaged this emerging specialty with curiosity and caution, weighing its application and relevance to the field of remote sensing. Subsequent reporting of fluorescence science in this journal (and others) over the decades attests to his willingness to debut many advances in this field.

2. Steady-state chlorophyll fluorescence and vegetation physiology

2.1. Fluorescence basics

The CF spectral emission spans approximately 650-800 nm in intact leaves, with two maxima – one in the red spectral region around 685-690 nm (F_{685}) and the other a shoulder in the far-red (near-infrared) around 730-740 nm (F_{740}). Two photosystems are involved: PSII, which emits in both the red and far-red regions of the spectrum, and PSI, which emits mainly in the far-red (Boardman et al., 1966; Govindjee, 1995; Pfündel, 1998) (Figure 1). Emission of CF is one of the pathways by which plants dissipate excitation energy absorbed from Photosynthetically Active Radiation (PAR), the others being photochemical electron transport, and two types of thermal energy dissipation – constitutive (i.e., internal

conversions at the level of the chlorophyll molecule that operate over the longer term or seasonally), and regulated (i.e., photosystem and molecular processes that respond rapidly to short-term changes in light intensity) (Hendrickson et al., 2004; Krause and Weis, 1991; Lichtenthaler and Rinderle, 1988; Papageorgiou and Govindjee, 2004; Porcar-Castell et al., 2014).

The dynamic nature of fluorescence emission from plants – evident in response to varying light intensity or, in the extreme, to sudden dark-light transition – is due to changing photochemical and non-photochemical quenching in the photosystem. The term quenching may be used to represent all processes that reduce fluorescence emission (Krause and Weis, 1991). Photochemical quenching (PQ) indicates the availability of open PSII reaction centers for photochemistry. In dark-adapted foliage that is suddenly exposed to strong light, PQ is quickly saturated, causing fluorescence to rise to a maximum (F_{max}); concomitantly, non-photochemical processes are triggered to harmlessly dissipate absorbed excessive light energy until PQ is re-established and allowing fluorescence to decline to a 'steady-state' level after a few minutes of illumination (Demmig-Adams et al., 2012). Outdoors, steady-state fluorescence is dynamically tuned by the balance of photochemical and non-photochemical processes responding to light intensities and other environmental conditions. CF quantum yield *in vivo* usually is less than 10%, with typical values of 0.5-3% under steady-state illumination (Porcar-Castell et al., 2014, and references therein).

Steady-state fluorescence is sometimes called terminal or stationary fluorescence (in Kautsky induction kinetics) and denoted as F_T, Ft, or F_S (Maxwell and Johnson, 2000; Van Kooten and Snel, 1990). Specific metrics quantify F_T, Ft, or F_S (Toivonen and Vidaver, 1984; Schreiber et al., 1986); PSII maximal or effective quantum yield (Genty et al., 1989); amplitude of the individual emission peaks, or their ratio (Agati et al., 1995; Campbell et al., 2007; Kuckenberg et al., 2009; Lichtenthaler and Rinderle, 1988); fluorescence lifetime (Cerovic et al., 1996); spectral wavelength position of the peaks (Kancheva et al., 2007); fluorescence band width (Subhash and Mohanan, 1997); area under the spectral emission curve (Srivastava and Pandey, 2012; Subhash, 1995); and fluorescence spatial patterns (Lichtenthaler and Rinderle, 1988).

Sensitivity of PSII reactions to abiotic and biotic stresses results in impairments of photochemical electron transport capacity, often readily echoed in changes to the fluorescence emission (A   et al., 2015). Strategies for photoprotection are thus needed and involve multiple mechanisms in addition to thermal dissipation. These include scavenging of reactive oxygen species, regulation of light absorption via leaf or chloroplast movements, redistribution of light energy between PSII and PSI via state transitions (migration of light harvesting complexes), and adjustments in photosystem stoichiometry (relative amounts of PSII and PSI) (Dall'Osto et al., 2014; Demmig-Adams et al., 2012; Krause and Weis, 1991). Although these are 'non-photochemical' in a generic sense, the more specific, regulated thermal dissipation is usually intended by the term 'non-photochemical quenching' (NPQ), which is assessed by active fluorescence sensors (albeit imperfectly as they cannot exclude all the other forms of photoprotection during measurement). Two NPQ mechanisms are the xanthophyll cycle involving interconversion of violaxanthin, antheraxanthin, and zeaxanthin

pigments (Demmig-Adams et al., 2012; Goss and Lepetit, 2015), and the xanthophyll lutein-epoxide cycle (Matsubara et al., 2007).

By the time fluorescence emission reaches a remote sensor, it has been subjected to the influences of diverse drivers in the vegetation, environment, and atmosphere, which can affect quenching, light absorption, re-absorption and scattering of fluorescence signals [see also Sections 4 and 8]. Disentangling the effects and importance of the various factors in a given situation is a focus of mechanistic interpretation of fluorescence data [Section 4] and is relevant to the effective usage of fluorescence as an optical proxy for photosynthesis and associated stress effects (Ac et al., 2015; Paul-Limoges et al., 2018; Verrelst et al., 2016, 2015b).

2.2.   Methodological advances in measuring steady-state fluorescence under controlled conditions

Fluorescence assessment in the laboratory, growth chamber, or greenhouse has utilized a suite of measurement devices, including fluorescence microscopes, spectroscopic or spectrofluorimetric devices, portable fluorometers, and imaging tools (Kalaji et al., 2012; Mohammed et al., 1995). These have allowed study of fluorescence induction kinetics and steady-state behaviour scales ranging from isolated photosystems to small vegetation canopies (Table 1) (reviews by Bolhàr-Nordenkampf et al., 1989; Fernandez-Jaramillo et al., 2012; Kalaji et al., 2012; Mohammed et al., 1995), and visualization of leaf fluorescence to better understand ultrastructural influences on light absorption, scattering, transmission, and fluorescence re-absorption (Kalaji et al., 2012). They have been helpful for examining spatial distribution of fluorescence in the leaf, and non-chlorophyll fluorophores and absorbers in leaf tissues (Bornman et al., 1991; Buschmann et al., 2000; Chappelle and Williams, 1987; Kalaji et al., 2012; Vogelmann and Evans, 2002).

Imaging reveals spatial and temporal heterogeneities in CF on leaf or plant surfaces due to biotic and abiotic stress factors (Barón et al., 2016; Buschmann et al., 2009; Donaldson and Williams, 2018; Gorbe and Calatayud, 2012; Nedbal and Whitmarsh, 2004; Nedbal et al., 2000; Oxborough, 2004; Rascher and Lüttge, 2002; Rascher et al., 2001). Imaging techniques have also been combined with other methods like gas exchange or infrared thermography for comprehensive details on spatial distribution of photosynthetic variables, stomatal function, and water use efficiency (Chaerle et al., 2007; Lawson, 2009; Murchie and Lawson, 2013).

Laboratory spectroscopic methods have allowed examination of fluorescence induction and decay kinetics, derivation of excitation-emission matrices (Louis et al., 2006), and discrimination of PSII and PSI fluorescence bands (Franck et al., 2002; Palombi et al., 2011; Papageorgiou, 1975; Vácha et al., 2007). They have also supported the development of leaf and canopy fluorescence models (Pedrós et al., 2010, 2008; Van der Tol et al., 2009a, 2009b). Combinations and special configurations of various devices have also been used – such as a PAM fluorometer with a spectroradiometer to probe changes in the green spectral region related to NPQ (Gamon et al. 1997, 1992, 1990; Wong and Gamon, 2015); a fluorescence spectrometer and an integrating sphere to quantify fluorescence re-absorption by chlorophyll (Gitelson et al., 1998); an integrating sphere with spectral detectors to study

CF in whole plants or branches (Toivonen and Vidaver, 1984) or fluorescence effects on apparent reflectance (Zarco-Tejada et al., 2003, 2000a, 2000b); and passive with active sensors to follow induction kinetics (Moya et al., 2004), spectrally-resolved fluorescence emission signatures, quenching parameters, and other photosynthetic variables (Magney et al., 2017; Wyber et al., 2017).

2.3. Transitioning from lab to field

Since the late 1980s, portable devices increasingly dominated laboratory and field-based CF science. The PAM systems have been used extensively for leaf-level work (Schreiber, 2004; Schreiber et al., 1986) (e.g., from Heinz Walz GmbH, Germany; Hansatech Instruments Ltd., UK; Photon Systems Instruments, Czech Republic; Opti-Sciences, USA). Some systems also measure gas exchange, chlorophyll content, and other spectral characteristics (e.g., from PP Systems, USA; LI-COR, USA; PhotosynQ, USA). Fluorescence lifetime has also been analyzed, as it is correlated with CF yield and feasible for short-distance assessments (e.g., a few meters) (Cerovic et al., 1996; Moya and Cerovic, 2004; Moya et al., 1995; Terjung, 1998). Micro-lidars have been used in short-range work (1-10 meters) (Flexas et al., 2000; Ounis et al., 2001), but delivering high intensity light pulses from great distances in order to saturate photosynthesis has been technically challenging. LIFT methods (Kolber et al., 2005) use fast repetition of high-power laser diode pulses to partially reduce the plastoquinone pool and can allow distances up to 50 m. A recent refinement is smaller and still allows a full suite of active fluorescence parameters and canopy reflectance in a fast scanning mode (Keller et al. in press).

Airborne lasers for excitation of fluorescence generally require high-peak-power sources (Chekalyuk et al., 2000; Hoge and Swift, 1981; Kim, 1973) that can pose risks to eye safety. However, Ounis et al. (2016) found that eye safety is achievable with appropriate operational conditions using an airborne platform for laser-induced fluorescence (LIF), SIF, reflectance, and waveform analysis of the backscattered laser signal – thereby deriving a multiple set of vegetation variables to help disentangle the various SIF drivers.

2.4. Lessons from the laboratory for remote sensing of SIF

Research into fluorescence-photosynthesis relationships, stress effects, and confounding factors has been greatly facilitated by the variety of measurement tools and the use of controlled studies. Such studies have been helpful for development and refinement of models representing fluorescence-photosynthesis linkages in different vegetation types, radiative transfer of fluorescence in leaves and small canopies, and fluorescence superimpositional effects upon reflectance [Sections 3 & 4]. Key messages have emerged from such research. First, steady-state fluorescence is influenced not only by PQ and NPQ, but also light absorption by chlorophyll, environmental conditions, structural traits, and stress factors (Buschmann, 2007; Cecchi et al., 1994; Chappelle and Williams, 1987; Stober et al., 1994; Valentini et al., 1994). Therefore – ancillary information is needed to reduce sources of error in interpretation of fluorescence changes and for parameterization of models (Mohammed et al., 2016, 2003, 1995). Second, since re-absorption reduces the visible fluorescence below that initially produced by the photosystems (e.g., Gitelson et al., 1998; Lichtenthaler and Rinderle, 1988), quantification of the re-absorption effect requires

radiative transfer theory [Section 4] and understanding of leaf anatomical effects on light penetration, scattering, transmission, and re-absorption. Third, it can be advantageous to measure more than one fluorescence variable. Having both red and far-red fluorescence has been shown empirically to be advantageous for studying fluorescence-photosynthesis associations, stress effects, and influences due to vegetation type (Chappelle and Williams, 1987; Valentini et al., 1994). Several steady-state fluorescence indicators have been identified from fundamental studies and are relevant for the design of future remote sensors and associated ground-based activities (Drusch et al., 2017; Fernandez-Jaramillo et al., 2012; Maxwell and Johnson, 2000; Mohammed et al., 2003, 1995; Rohá ek et al., 2008).

Transferability of lab-based fluorescence results to field situations, and of active to passive methods, is subject to caveats. Laboratory results might not mirror in-situ behaviour due to differences in growing environment, sampling protocols, and sensor operating conditions (Maxwell and Johnson, 2000; Stober et al., 1994). Data from active and passive techniques might not be consistently comparable (Goulas et al., 2017; Porcar-Castell et al., 2014; Rascher et al., 2009), and this continues to be investigated (A et al., 2015; Cecchi et al., 1994; Magney et al., 2017; Wyber et al., 2017). Artificial excitation light sources differ from sunlight in spectral composition, intensity and directionality (affecting light penetration, emission wavelength, and re-absorption) (Cerovic et al., 1999). Portable fluorometers using red excitation light can be biased toward the far-red region of the emission (to avoid overlap between excitation and emitted light) (Kalaji et al., 2014; Porcar-Castell et al., 2014), whereas blue light stimulates the full CF emission but mainly from superficial leaf layers. A helpful approach is to analyze excitation-emission matrices to reveal illumination effects (Corp et al., 2003; Louis et al., 2006; Middleton et al., 2008). Further comparative work is warranted, and assumptions must be well understood (Porcar-Castell et al., 2014).

Recognizing those caveats, future lab-scale or controlled-environment trials can support SIF remote sensing activities in several ways: (i) creation of spectral-fluorescence-physiology databases and libraries to support calibration, modelling and interpretation of remotely sensed SIF; (ii) elucidation of confounding factors for interpretation of SIF changes; (iii) identification of ancillary data types needed for airborne or space-based missions; (iv) prototyping and refinement of remote sensor specifications and spatio-temporal sampling protocols; (v) testing of field sensors to be used in ground-truthing and validation; and (vi) determination of confidence margins and constraints for applications, based on vegetational and environmental variables.

3.   Early evidence of steady-state chlorophyll fluorescence effects on leaf and canopy spectra

Before the year 2000, measurement technology was limited in its capacity to provide convincing evidence that for vegetation in natural light the very small upwelling fluorescence signal could be reliably distinguished in the presence of the dominant reflected radiance signal.

Consequently, first references on the topic were qualitative or tentative. Buschmann and Lichtenthaler (1988) inspected reflectance and fluorescence signatures using the Visible

Infrared Reflectance Absorbance Fluorescence (VIRAF) spectrometer and concluded that the fluorescence emission could probably influence the red edge spectral region – in particular around 750 nm. McFarlane et al. (1980) and Carter et al. (1996, 1990) used a Fraunhofer Line Radiometer and the Fraunhofer Line Depth (FLD) measurement principle to study fluorescence in the Hα line (656 nm) and the O_2-B absorption band (687 nm), revealing changes in SIF from leaves or canopies with treatments of herbicide, water stress, or light regime. Later, other studies evaluated relationships between reflectance indices and fluorescence, especially the trends obtained between the PRI vs. fluorescence-based indicators of PSII photochemical efficiency in the context of radiation-use-efficiency estimations (Gamon et al., 1997; Peñuelas et al., 1998, 1997). Using calculations of reflectance-difference spectra between dark-adapted and light-adapted leaves, Gamon and Surfus (1999) showed that xanthophyll pigment de-epoxidation and CF emission affected the reflectance signatures of vegetation after exposure to white light (Figure 2). Nevertheless, the main focus of this work was on the PRI, and particularly its relative increment (PRI) as a direct indicator of xanthophyll cycle pigment activity. As yet, no quantitative assessments were carried out to demonstrate the reliability of the fluorescence emission extracted from the leaf spectral radiance or apparent spectral reflectance.

After these first qualitative demonstrations of the potential effects of chlorophyll fluorescence superimposed on the apparent reflectance, a series of laboratory-based experiments were undertaken aimed at its quantitative assessment both at the leaf level (Zarco-Tejada et al., 2000a, 1999a) and at the canopy level using the Compact Airborne Spectrographic Imager (CASI) (Zarco-Tejada et al., 2000b, 1999b). Experiments were conducted with an integrating sphere to examine the leaf optical properties with and without a cut-off bandpass filter (<695 nm), allowing leaves to be illuminated thereby without and with fluorescence-exciting radiation (Figure 3, left). These experiments were also carried out with the CASI to acquire imagery over plant seedlings (Figure 3, centre), which enabled the quantitative demonstration at the image level (i.e., canopy level) of a fluorescence signal superimposed upon the apparent reflectance. These results were further validated via the development of a leaf radiative transfer model (RTM), named the Fluorescence–Reflectance–Transmittance (FRT) model, based on the doubling method that accounted for the within-leaf fluorescence signal (Zarco-Tejada et al., 2000a) (Figure 3, right). These leaf- and canopy-level experiments, along with the physical modelling approach, served as a quantitative demonstration that the fluorescence emission could be extracted and, more importantly, that the observed fluorescence signal effects on the apparent reflectance agreed with independently acquired fluorescence data using the PAM-2000 instrument. It was further demonstrated that the experimental protocols used to extract the fluorescence signal from the leaf reflectance spectra were consistent with basic radiative transfer theory.

Those experiments and the modelling work proved that the SIF emission was superimposed upon the apparent reflectance acquired by the *"narrow-band"* imaging spectrometers of that time (i.e., imagers with spectral resolution, SR, in the range of 2.5 to 10 nm full-width-at-half-maximum, FWHM). Further efforts attempted to quantify the fluorescence signal under natural illumination (Zarco-Tejada et al., 2002, 2001) using CASI imagery acquired over *Acer saccharum* M. (sugar maple) sites in Canada. Flights conducted over the course of diurnal experiments under natural light conditions and over forest sites with different levels

of stress demonstrated that the SIF signal could be extracted by reflectance subtraction methods. Reflectance differences calculated between early and midday imagery acquired by CASI showed spectral differences that at the time were associated with the diminution of the fluorescence emission as a function of stress over the course of the diurnal cycle. Moreover, the derivative reflectance calculated from canopy-level CASI airborne imagery showed a peak at the 700-730 nm region which was experimentally shown to relate to stress conditions and potentially to be caused by fluorescence emission and chlorophyll content changes in vegetation under stress.

The derivative-based peak feature discussed in Zarco-Tejada et al. (2002), which responded as a function of forest health condition, was further investigated in a series of laboratory experiments (Dobrowski et al., 2005; Zarco-Tejada et al., 2003). The studies of this feature, observed on the derivative reflectance with heat- and light-induced stress in growth chambers, demonstrated that the diurnal dynamics of the chlorophyll fluorescence emission could be tracked at the canopy level, mimicking the dynamics of the steady-state fluorescence measured concurrently and corresponding with induced stress levels. Dobrowski et al. (2005) successfully extracted the fluorescence signal in diurnal experiments designed to induce stress, analyzing the dynamics of the recovery from stress in the reflectance spectra. They proved the link between the fluorescence variables extracted from canopy reflectance and plant photosynthesis measured at the same time. Later, Campbell et al. (2008) showed the contribution of CF to the apparent reflectance of corn leaves in time-resolved laboratory measurements using a solar simulator and blocking filters (which blocked incoming light in the PAR region to prevent fluorescence excitation, similarly to what was done by Zarco-Tejada et al., 2000a).

New experiments to extract chlorophyll fluorescence signals using the FLD principle with the oxygen absorption feature became possible with spectrometers able to provide sub-nanometer resolutions [Section 5] (Meroni and Colombo, 2006; Pérez-Priego et al., 2005). In water stress experiments conducted under natural light and field conditions, Pérez-Priego et al. (2005) demonstrated that the radiance in-filling within the O_2-A feature was related to steady-state fluorescence, an indicator of the water stress dynamics over the course of diurnal experiments. More importantly, they proved experimentally that sub-nanometer spectrometers could be used to understand the radiance variations embedded in the O_2-B and O_2-A absorption bands (Figure 4). This approach would be used several years later, along with narrow-band spectrometers, as standard protocols for validation of fluorescence results. The FLD principle has been successfully applied to leaf radiance spectra track changes in the photosynthetic apparatus of herbicide-treated vegetation (Meroni and Colombo, 2006), demonstrating the feasibility of the oxygen features for fluorescence quantification using high-resolution spectrometers [Section 5].

The experiments described here were critical for the understanding of the fluorescence emission effects on apparent reflectance and for convincing the scientific community of the feasibility of measuring fluorescence from passive reflectance spectra. (Although now widely accepted, doubts still existed until the late 1990s.) The initial qualitative descriptions by Buschmann and Lichtenthaler (1988) followed by Gamon and Surfus (1999) served to encourage further progress on the quantitative assessments as part of detailed experiments

carried out in the laboratory and under natural light conditions, both at the leaf and at the canopy levels (Zarco-Tejada et al., 2000a, 2000b). The conclusions of these studies seeded the development of the first robust RTMs to account for the fluorescence emission at both the leaf and canopy levels, and stimulated an in-depth analysis of more advanced methodologies for the retrieval of chlorophyll fluorescence using the FLD principle – widely used currently, but poorly understood at the beginning of the millennium.

4. Modelling the effects of chlorophyll fluorescence through the canopy

4.1. Fundamentals of chlorophyll fluorescence modelling

The development of technologies and retrieval algorithms to evaluate fluorescence has progressed hand in hand with model developments. Measurement of active chlorophyll fluorescence in plant leaves, often combined with analysis of gas exchange [Section 2], has played a crucial role in fundamental research on plant photosynthesis and has supported the development of mathematical models for leaf photosynthesis (Farquhar et al., 1980). . These models have been implemented in global land surface models for climate research (for a review, see Pitman, 2003), which has entailed upscaling of modelled photosynthetic processes from the leaf to the stand level (or 'vegetation canopy') and differentiation between sunlit and shaded leaves (De Pury and Farquhar, 1997). In general, two-stream (simulating direct and diffuse fluxes) RTMs have been implemented in dynamic vegetation models such as the Boreal Ecosystems Productivity Simulator (BEPS) (Liu et al., 1997), Biome-BGC (Chen et al., 1999), and land surface models such as CLM2 (Dai et al., 2004), CLM4 (Bonan et al., 2011), and the Breathing Earth System Simulator (BESS) (Ryu et al., 2011). Contemporary analyses of airborne and satellite fluorescence have further stimulated the development of models as scaling tools.

In contrast to measurements of conducted on individual leaves, SIF retrieved from Top-of-Canopy (TOC) data is subject to complexities of canopy structure and coverage, solar illumination angle, soil brightness, stem and branch effects, leaf pigments, and other drivers [Sections 2, 8] (Fournier et al., 2012; Middleton et al., 2018; Porcar-Castell et al., 2014; Rosema et al., 1991). Quantitative modelling of such effects allows a way to integrate them and to use SIF in parameterizing terrestrial vegetation traits in land surface models (Lee et al., 2015; Norton et al., 2018).

In essence, models for canopy photosynthesis describe light absorption and utilization, whereas a canopy-level model for fluorescence describes three key processes: (i) the absorption of incident radiation; (ii) the subsequent emission as fluorescence; and (iii) the scattering and re-absorption of fluorescence through the canopy after emission.

Knowledge about the relationships between fluorescence, electron transport and photochemistry in leaves (e.g., Schreiber et al., 1995) did not include the variability caused by the canopy structure on absorption and scattering. These aspects have been addressed in a different disciplinary field, using radiative transfer theory (Jacquemoud et al., 2009). During the last two decades, that work has resulted in models that quantify the key processes and their interdependencies (Figure 5).

4.2. Leaf physiological models of steady-state fluorescence

Leaf physiological models have aimed to quantify the partitioning of absorbed radiation to the pathways of photochemical and non-photochemical quenching [Section 2]. To overcome the lack of modulated light and saturating flashes (available with active methods), predictive models for the relationship between PQ and NPQ were needed. To that end, Andries Rosema and co-workers developed the Laser Environmental Active Fluorosensor (LEAF-NL), which they used to acquire active and passive fluorescence and to develop a quantitative model for steady-state fluorescence that describes NPQ as a function of irradiance with two empirical parameters (Rosema et al., 1998). Their measurements on poplar seedlings and their modelling results showed that NPQ causes a positive relationship between fluorescence emission and photochemistry efficiency at high light intensities, which challenged a common perception that a fluorescence increase generally implies a reduction in photochemistry (McFarlane et al., 1980) – although Rosema's findings were consistent with the comments of McAlister and Myers (1940) regarding the existence of both an inverse and a direct relationship [Section 1].

The values of the fitting parameters in Rosema's model appeared to depend not only on irradiance but also on the temperature and water stress status of the plants, which was consistent with studies on PAM fluorescence showing positive correlation of steady-state fluorescence with actual photosynthesis rate as assessed via gas exchange. Flexas et al. (2002), for instance, observed drought effects on NPQ and gas exchange, confirming feedback mechanisms between actual photosynthesis and NPQ (Bilger and Bjorkman, 1990). Van der Tol et al. (2009a) modelled this feedback by introducing the fluorescence emission, the pH-gradient across the thylakoid membrane, and NPQ, into the photosynthesis model of Farquhar et al. (1980). Later Lee et al. (2013) and Van der Tol et al. (2014), on the initiative of Joe Berry, parameterized and calibrated a simpler model for this feedback, using a calibrated non-linear relationship between NPQ and the relative light saturation of photosynthesis. This relative light saturation is the ratio of the actual over the theoretical maximum electron transport.

These models are fairly simple and can easily be implemented in canopy-level or global-scale models, but they still rely on empirical coefficients and lack a mechanistic process description of the feedback mechanism. Zaks et al. (2012), Bennett et al. (2018), and Morris and Fleming (2018) developed a dynamic (time-resolved) model that simulates the pools of excited chlorophyll and the concentrations of the quenchers zeaxanthin and antheraxanthin using the rate coefficients of the involved processes in a more mechanistic way. Such mechanistic representations could be used in remote sensing models for satellite fluorescence as well.

All of the models for fluorescence, photochemistry and NPQ quantify the initial emission of fluorescence after incident photons have been captured by photosystems. They do not answer the questions of 'how much light is absorbed by the photosystems in the first place?', nor 'what happens to the fluorescence after emission by the photosystems?'. These questions have been addressed with RTMs, for both individual leaves and vegetation canopies.

4.3. Leaf radiative transfer models for fluorescence

The absorption of incident light and the (re-)absorption of emitted fluorescence inside leaves has been described in detail by Gitelson et al. (1999, 1998) and Buschmann (2007). A part of the incident light is reflected by the leaf surface before entering the leaf. The remaining light penetrates into the leaf – where it may be absorbed by different pigments, including chlorophyll – or scattered. When fluorescence is produced, a certain part is (re-)absorbed by pigments on its way out of the leaf. The absorption of the incident light and thus the emission of fluorescence increases asymptotically with chlorophyll content of the leaf. But as the fluorescence emission spectrum (~650-800 nm) overlaps with the chlorophyll absorption spectrum (~400-720 nm), some of the emitted fluorescence is re-absorbed by chlorophyll again. This absorption by chlorophyll is strong in the red region, thus red fluorescence quickly saturates and then decreases with increase in leaf chlorophyll content. As the leaf is far less absorbent in the far-red region, the saturation of fluorescence is much lower there. Gitelson et al. (1999) showed that for this reason, the fluorescence peak ratio, i.e., the ratio of far-red to red fluorescence is correlated with chlorophyll content. Due to the re-absorption, only a little red fluorescence (~ 690 nm) escapes from the shaded (usually abaxial) side of the leaf compared to the illuminated (usually adaxial) leaf side, resulting in different spectral shapes (Louis et al., 2006; Van Wittenberghe et al., 2013).

For modelling of fluorescence it was necessary to describe these processes mathematically. Several leaf RTMs (without fluorescence) had emerged already in the 1960s. Most prominent was one by Allen et al. (1970, 1969), using the analogy of a pile of glass plates. An improved successor is the widely used PROSPECT (from the French PROpriétés SPECTrales) model, created by Jacquemoud and Baret (1990), which relaxed the number of plates to be a non-integer to gain more control over the variability of mesophyll scattering properties of the modelled leaves. Calibration of the specific absorption coefficients of chlorophyll, water and dry matter was accomplished by numerical optimization techniques. This provided a good correspondence with spectra of leaf reflectance and transmittance, which were determined for leaves of known (laboratory-assayed) concentrations of leaf constituents.

To support the interpretation of fluorescence data from the laser-induced fluorescence instrument of Rosema in the early 1990s, an early attempt was made to incorporate fluorescence in RTMs for single leaves as well as vegetation canopies. Thus, the FLSAIL model was developed by Rosema et al. (1991). Also called KMF ('Kubelka-Munk Fluorescence'), since it included fluorescence by using the two-stream approach of Kubelka and Munk (1931), the model solved the radiative transfer equations numerically using an efficient layer doubling algorithm, a variant of the adding algorithm of Van de Hulst (1957; cited in Van de Hulst, 1981). The doubling algorithm scales from an extremely thin layer to an optically thick layer by repeated stacking of identical layers. The doubling method was used also in the FRT leaf RTM, and was developed to provide theoretical support for fluorescence contribution to apparent reflectance (Zarco-Tejada et al., 2000a, 2000b; see also Section 3). A later-published model for leaf fluorescence, FluorMODleaf (Pedrós et al., 2010), was based on the PROSPECT concept of parallel plates but used a different way to simulate the leaf fluorescence, calculating first the emission and subsequent re-absorption of

fluorescence in a plate, then the stacking of an integer number of plates, and finally interpolating to a real number of plates. The more recent Fluspect model (Vilfan et al., 2016) uses the doubling algorithm for fluorescence calculation, but the rest of its algorithm is based entirely on PROSPECT.

4.4. Canopy radiative transfer models for fluorescence

To study vegetation canopy fluorescence in relation with in-situ (i.e., Bottom Of Atmosphere, BOA), airborne, and satellite (i.e., Top Of Atmosphere, TOA) observations, a canopy fluorescence model should simulate two types of products: (i) Canopy spectral radiative budget, including fluorescence emission; and (ii) Fluorescence signal measured at any altitude. In the case of canopy spectral radiative budget, depending on the spatial extent of the area and the selected spatial resolution, the calculation of the three-dimensional (3D) radiative budget can be very demanding in terms of computer time and memory. It must track radiation along any direction, which explains the inefficiency of reverse ray tracing Monte Carlo models (Disney et al., 2000) that trace sample photon paths from the sensor to the illumination sources. For remotely sensed fluorescence signals at any altitude, this involves simulating radiative transfer in the atmosphere in addition to the vegetation canopy. A common modelling solution is to couple a canopy model and an atmospheric RTM (e.g., the MODerate resolution atmospheric TRANsmission, MODTRAN) (Berk et al., 2014), or 6-S (Kotchenova et al., 2008)). But this solution cannot accurately simulate the complex neighboring effects (i.e., local surface irradiance depends on surrounding surfaces and topography) due to the 3D Earth-Atmosphere radiative coupling.

Canopy fluorescence models rely on embedding a leaf fluorescence model into a canopy reflectance model (Disney, 2016). One-dimensional (1D) models with the vegetation canopy being simulated as homogeneous layers – such as the canopy FLSAIL model (Rosema et al., 1991) – appeared first. Using the doubling approach, this model solves the four-stream differential equations of radiative transfer, including bi-directional scattering terms. FLSAIL and also its successors FluorSAIL (Miller et al., 2005) and the Soil-Canopy-Observation of Photosynthesis and Energy fluxes (SCOPE) (Van der Tol et al., 2009b) models are all based on the 'Scattering of Arbitrarily Inclined Leaves' (SAIL) model, in which the vegetation is represented by identical leaves with stochastically described orientation that scatter the four streams of incident solar light, the diffuse upward and downward fluxes and the radiance in the observation direction (Verhoef, 1985, 1984). SAIL, in turn, is based on the predecessor models of Allen et al. (1970) and Suits (1972). These 1D models do not simulate the effects of spatial and structural heterogeneity of vegetation in the horizontal plane, such as crown shadows or row culture effects, nor do they simulate effects of vertical variability of leaf types, leaf orientation angles or leaf pigment concentrations, as might be present in, say, a real forest stand with an understory and overstory. Although approaches exist to handle clumping in RTMs (Ni-Meister, Yang and Kiang, 2010), the effect of clumping on SIF has received little attention. Modifications to the four-stream radiative transfer concept have been made to overcome these limitations. For example, the FluorFLIM model (Zarco-Tejada et al., 2013a), based on FluorSAIL and FLIM (Rosema et al., 1992), simulates vegetation clumping (crowns), while mSCOPE (Yang et al., 2017) simulates fluorescence emanating from vertically heterogeneous canopies. He et al. (2017) derived a relatively simple

correction for the solar-viewing geometry, in which the observed signal of SIF is decomposed into contributions from sunlit and shaded fractions of the canopy. Their model is based on a RTM for discrete objects with internal structures ('4-scale'), such as forest stands (Chen and Leblanc, 1997). The model of He et al. (2017) should also work for clumped vegetation and recent models that derive the scattering of SIF directly from reflectance take effects of clumping on SIF implicitly into account via the reflectance (Köhler et al., 2018b; Yang and Van der Tol, 2018).

3D photon and flux tracing RTMs can work with realistic descriptions of actual vegetation canopies, either by representing all plant parts as facets (i.e., triangles) or by discretizing canopies into so-called voxels, small spatially distinct volumes filled with a turbid medium of leaves, possibly with different optical properties. Several 3D models have been extended to include simulation of passive fluorescence, notably FluorFLIGHT for forest canopies (Hernández-Clemente et al., 2017), the Fluorescence model with Weight Photon Spread (FluorWPS) for row crops (Zhao et al., 2016), and the Discrete Anisotropic Radiative Transfer (DART) model for any 3D explicit vegetation architecture (Gastellu-Etchegorry et al., 2017). All three models simulate leaf-emitted fluorescence with Fluspect, after which within-canopy radiation propagation is tracked with ray or flux tracing algorithms. Their spatially detailed simulations potentially can provide deep insight into interactions of fluorescence fluxes in structurally complex canopies.

The DART model (Gastellu-Etchegorry et al., 2017, 2015, 1996) was designed to simulate both the 3D radiative budget and remote sensing observations (i.e., in-situ/airborne/satellite LiDAR and imaging spectrometers from visible to thermal infrared) of any urban and natural landscape with any topography. The Earth-Atmosphere radiative coupling is simulated for any user-defined atmosphere. Vegetation can be simulated with facets or turbid voxels. The 3D SIF emission is simulated using Fluspect, based on the fluorescence quantum yield efficiencies that can be specified per leaf facet or per type of leaf in relation to the leaf biochemistry and optical properties. The foliage can be divided into sunlit and shaded by simulating instantaneous leaf irradiance, and also into sun- and shade-adapted classes by simulating time series of scene diurnal radiative budgets (e.g., simulations of multiple days with a time-step of one hour). Subsequent computation of diurnal leaf irradiance integrals combined with user-specified leaf irradiance thresholds determines respective duration of sun and shade exposure.

3D models like DART do not include an energy balance and do not work with the environmental parameters (e.g., air temperature) driving apparent leaf fluorescence. Hence, for computation of the emission by photosystems and the quenching mechanisms, DART imports values precomputed in SCOPE. DART chlorophyll fluorescence products, namely canopy BOA and TOA SIF radiance and reflectance images and the 3D leaf radiative budget (i.e., PSI and PSII fluorescence exitance and sun-scattered exitance per triangular facet), allow computation of advanced outputs, such as the canopy fluorescence escape factor (Guanter et al., 2014). At this time, SCOPE is the only canopy model that includes the energy balance at the leaf level and thus the consistent estimation of photosynthesis and fluorescence.

Figure 6 shows an example of DART-simulated BOA chlorophyll fluorescence for a maize field at an early growth stage. Simulation of diurnal radiative budgets of solar irradiation (Figure 6a) allowed for classification of the maize stand into sun and shade-adapted parts (Figure 6b), further used for simulation of canopy reflectance (Figure 6c) and fluorescence (Figures 6d & 6e) images. Advantages of the ray or flux tracing models are that they allow not only quantification of processes leading to modelled canopy fluorescence but also their visualization. Although producing more accurate results, the use of triangular facets is computationally more demanding than the use of turbid voxels that represent a large set of foliar elements. (DART is currently being adapted in order to simulate the fluorescence of canopies that are modelled with turbid voxels.)

4.5. Integrated canopy fluorescence and photosynthesis models

Interpreting fluorescence results of a canopy in terms of photosynthesis and stress requires modelling of not only the radiative fluxes but also the non-radiative energy fluxes. Non-radiative fluxes are not commonly taken into account in remote sensing observation models, but they are an important component of land surface models (Anderson, 1963; Kalma et al., 2008). Non-radiative fluxes include the energy involved in metabolism (photosynthesis and respiration), the turbulent exchange of latent and sensible heat flux, and the conduction of heat into biomass and soil. These fluxes eventually determine the temperature of the leaves and the humidity in vegetation canopies, both of which are crucial variables for stomatal aperture (Ball et al., 1987; Leuning, 1995), photosynthesis (Collatz et al., 1991) and fluorescence quenching (Bilger and Bjorkman, 1990). For a complete modelling of fluorescence, it was therefore considered necessary to include these processes in canopy fluorescence models.

Integration of radiative with non-radiative energy fluxes and photosynthesis has been a subject of inquiry since the 1960s. De Wit (1965) and Goudriaan (1977) were among the first to develop computer simulation models combining radiative transfer with micro-meteorology for vegetation, maintaining energy and water budgets. Norman (1979) presented Cupid, a comprehensive model for the soil-plant-atmosphere continuum that also simulates visible, near infrared and thermal radiation. The more recent SCOPE model (Van der Tol et al., 2009b)additionally simulates the fluorescence radiance spectrum for a given viewing and illumination geometry (Figure 7). SCOPE is an extension of the FluorMOD model (Miller et al., 2005), which already included a fluorescence quenching model (Rosema et al., 1998) and a canopy RTM, but without considering thermal radiative transfer and non-radiative energy fluxes. SCOPE has been used in a number of trials to interpret SIF in vegetation measured using field devices (Migliavacca et al., 2017b; Rossini et al., 2016; Van der Tol et al., 2016) and airborne sensors (Damm et al., 2015b). It has been used also for retrieval of vegetation parameters using satellite sensors (Lee et al., 2013; Zhang et al., 2018a, 2014). A limitation of SCOPE is that it is not valid for clumped or sparse or vegetation as it uses the original SAIL model representation for radiative transfer (Verhoef, 1984).

4.6.   Lessons learned using these models

As Porcar-Castell et al. (2014) pointed out, leaf-to-canopy scaling associated with the change from active methods of fluorescence measurement to remote sensing of SIF is not just a matter of application of existing models to a larger area. Rather, it has been necessary to describe all SIF-relevant processes: absorption, emission, scattering, and re-absorption. The challenges in scaling from leaf to canopy also present opportunities to improve understanding of photosynthesis at the canopy scale.

Various papers have reported a close correlation between far-red SIF and GPP (Cui et al., 2017a; Frankenberg et al., 2011b; Goulas et al., 2017; Guanter et al., 2012; Joiner et al., 2011; Rossini et al., 2010; Verma et al., 2017; Wagle et al., 2016; Yang et al., 2015). The question of which processes are responsible for the close correlation has been discussed in most of these studies. It is now clear that SIF and GPP rely on the incident radiation and the absorption of light by chlorophyll in the whole canopy leaf area, which are both responsible for their strong correlation at diurnal and seasonal time scales (Goulas et al., 2017; Joiner et al., 2014; Yang et al., 2018b, 2015) . The dominance of total chlorophyll absorption is confirmed by sensitivity analyses of the SCOPE model (Koffi et al., 2015; Verrelst et al., 2015b).

Furthermore, Migliavacca et al. (2017b) evaluated changes in fluorescence of grassland vegetation after fertilization, differentiating effects of canopy structure on scattering from photosynthetic effects on fluorescence emission. They showed that the relative abundance of species affects canopy structure and the scattering of fluorescence, and that these changes in canopy structure dominate the variations in observed SIF between vegetation communities observed at the same time. This confirms model sensitivity analyses demonstrating that leaf area index and leaf inclination have a significant effect on SIF (Verrelst et al., 2015b), and demonstrates that scattering and re-absorption can cause substantial differences in SIF among various vegetation communities. A significant step in quantifying the scattering and reabsorption of fluorescence in the canopy was made by Romero et al. (2018). who developed a quantitative model for re-absorption in the canopy, and also performed active fluorescence measurements at the canopy level, using a lamp producing blue light to obtain fluorescence spectra above the tree crowns for validation. Their model confirmed the change in spectral shape (the relative reduction of red fluorescence), when moving from the leaf to the canopy scale, as found earlier with SCOPE.

Because scattering depends on the geometry of illumination and observation directions, quantification of fluorescence scattering in the canopy is crucial for meaningful comparisons between fluorescence observations taken under different solar and observation angles. Köhler et al. (2018b) analyzed the directional scattering of fluorescence in the canopy. They showed that the seasonality in SIF observed by GOME-2 is affected by the angular anisotropy of the canopy fluorescence and that correction for this effect is needed. Subsequently, Liu et al. (in press) used SCOPE and DART SIF simulations of vegetation canopies combined with the spectral invariant theory, in the random forest machine-learning algorithm to devise a new means for scaling a canopy SIF signal down to the level of single photosystems. Downscaling of SIF by correcting for scattering and re-absorption appeared to be an efficient way to obtain a solar-view geometry-independent measure, and a measure

for the fluorescence emission at leaf level before re-absorption. Yang and Van der Tol (2018) analytically compared the radiative transfer of incident radiation to the radiative transfer of scattered fluorescence radiation and showed that far-red fluorescence scattering in a 1D canopy is proportional to far-red reflectance normalized by the leaf albedo and canopy interceptance. With this simple equation, far-red SIF can be corrected for illumination and observation geometry and for re-absorption within the canopy at the same time, using reflectance along with SIF.

Due to the similarities between reflectance and fluorescence, it makes sense to combine the two together. One way of doing this is to invert quantitative RTMs and retrieve from reflectance the parameters necessary to quantify the light absorption by chlorophyll and the scattering and reabsorption of fluorescence. It then may be possible to estimate the efficiency of fluorescence emission and the fluorescence quenching mechanisms (Van der Tol et al., 2016).

4.7. Challenges and future directions in modelling

Challenges and opportunities still lie ahead for modellers in the fields of remote sensing of fluorescence and plant physiology.

One issue with current models for passive fluorescence is the empirical parameterization of NPQ and the lack of quantitative mechanistic parameterizations for NPQ as a function of measurable quantities. A possible strategy is to use reflectance in the region of 500-600 nm, as leaf optical properties in this spectral region are affected by a number of pigments, including those involved in photoprotection and non-photochemical heat dissipation (e.g., zeaxanthin). Spectral changes in this region are the basis of the PRI (Gamon et al., 1997). The leaf RTM Fluspect was extended recently with a more precise simulation of the reflectance and transmittance between 500 and 600 nm, by including spectral changes associated with NPQ (Vilfan et al., 2018). Including these effects in Fluspect and SCOPE or other RTMs could help to retrieve a measure of NPQ and constrain the modelled fluorescence–photosynthesis relationship. Spectrally contiguous reflectance of the far-red (red edge) shoulder (700-800 nm) is also being investigated for spectral absorbance features related to the pigment-pigment excitation interactions and xanthophyll conversion, as possible evidence of NPQ manifestation (S. van Wittenberghe, personal communication).

Laboratory and field experiments continue to provide new insights (Section 2.4), based on joint acquisition of active and passive SIF and gas exchange information to examine fluorescence-photosynthesis linkages, drought and ozone stress effects, and diurnal and seasonal relationships between SIF and other photosynthetic parameters (Magney et al., 2017; Rosema et al., 1998; Wyber et al., 2017). These data, which may be combined with the fluorescence lifetime (Sylak-Glassman et al., 2016), can be helpful for better understanding of the dynamics of fluorescence originating from PSI and PSII and their interdependence. This could lead to methods for differentiating fluorescence from the two photosystems from retrieved SIF spectra corrected for re-absorption. High spatial resolution imaging fluorescence is another promising tool, as shown by Pinto et al. (2016) who set a hyperspectral camera above a vegetation canopy to retrieve fluorescence images and

differentiate contributions from individual leaves with different insolation and orientation; this is an excellent data source for model validation.

Advances in computational power facilitate utilization of 3D ray and flux tracing models to explore canopy structural effects (e.g., for row crops or savannah type vegetation) on fluorescence, with realistic vegetation parameterizations obtained from LiDAR or orthophoto data (Fawcett et al., 2018). Also the influence of landscape spatial heterogeneity – originating from topographical gradients and landcover variability – on large-scale space-based SIF observations is anticipated in upcoming versions of 3D RTMs. Significant progress in the use of machine learning, neural networks and emulation of models (Rivera et al., 2015; Verrelst and Rivera, 2017), and the development of End-to-End simulators for satellite missions (Vicent et al., 2016) , will bring the operational use of more complex RTMs at large spatial scales within reach. This would expedite assimilation of fluorescence data into global land surface models, as has been initiated by Lee et al. (2015) for the Community Land Model, Norton et al. (2018) for BETHY, and MacBean et al. (2018) for the Organising Carbon and Hydrology In Dynamic Ecosystems (ORCHIDEE) model.

5. SIF estimation methods

5.1. General strategies

Approaches used to quantify SIF emission from vegetation TOC radiance are anchored by a simple equation describing the additive contributions of solar-reflected (*r*) and SIF radiance to the total TOC radiance $L(\lambda)$ (assuming isotropic surface reflectance and neglecting canopy-sensor atmospheric effects and adjacency):

$$L(\lambda) = r(\lambda)E(\lambda)/\pi + SIF(\lambda) \tag{1}$$

where λ is wavelength and $E(\lambda)$ the known (measured or modelled) incident irradiance at the surface (direct and diffuse). All the terms of Equation 1 are spectrally variable, making retrieval of the two unknowns challenging. Fluorescence retrieval algorithms are built mostly on the key assumption that prior knowledge of the spectral shape of all terms of the equation can be leveraged to estimate the unknown terms. Specifically, unlike *L* and *E, r* and SIF are smooth functions of wavelength and this knowledge is exploited to retrieve SIF at specific spectral absorption bands by assuming that these two variables are either constant or vary linearly over a narrow wavelength range (a few nm), or vary in a more complex way over larger spectral ranges (e.g., the full SIF emission spectrum).

Retrieval methods further exploit the larger relative contribution of SIF to the total TOC radiance at selected absorption bands as compared to over the whole spectrum (Figure 8). The proportional contribution of SIF to total TOC radiance is larger for red wavelengths because, despite the red fluorescence being strongly re-absorbed by chlorophyll, the canopy reflected radiance is very low for the same reason. Conversely, the SIF contribution is proportionally lower in the far-red where the reflected radiance is dominated mainly by canopy scattering. Besides the overall effect of fluorescence in these spectral regions, it is the specific in-filling effect within absorption bands that is key for retrieving SIF in most approaches. When observed at high SR, the fluorescence in-filling effect within the

terrestrial oxygen absorption bands (i.e., O_2-A and O_2-B at 760 nm and 687 nm, respectively) can exceed 10% (Figure 8). A similar effect occurs in the Fraunhofer Lines (FLs), but here the fluorescence proportional contribution is generally smaller as these absorption bands are less dark than oxygen bands for a given SR. In contrast to the O_2 bands, absorption in the FLs does not occur in the terrestrial atmosphere, an advantage in that modelling of atmospheric influence is much easier (as detailed in this section).

The depth of the absorption bands varies greatly over very narrow spectral ranges, hence, sensor capability to accurately detect such radiance variations through fine SR and high signal-to-noise ratio (SNR) is essential for SIF retrieval. Recent technological developments have produced a number of high-performance spectrometers (ground, airborne, and satellite) providing sufficiently high SRs and SNR for SIF retrieval [Sections 6 and 7].For satellite instruments, these features also must be balanced with spatial resolution and, in some cases, a coarse resolution of several (or more) kilometers is necessary to achieve the required SNR.

Most retrieval algorithms can quantify fluorescence at selected absorption bands, but a novel group of approaches allows derivation of the full fluorescence emission spectrum (Zhao et al., 2018). This capability affords new opportunities for better understanding SIF with respect to leaf composition, canopy structure and plant functional status (Verrelst et al., 2016, 2015b). Herein, the methods are grouped into two main classes based on whether they allow retrieval within restricted absorption bands or over the full SIF emission region (Table 2). Within the first class, we can distinguish methods based on O_2 bands and those for FLs, and in the second class methods based on parametric functions to describe *r(λ)* and *SIF(λ)* (i.e., spectrum fitting) are distinguished from those using a full radiative transfer approach (i.e., model inversion). Most retrieve SIF at different scales, from ground to satellite, using different acquisition techniques.

For airborne and satellite observations, different physically-based or empirical approaches have been explored to account for atmospheric effects. Table 2 also summarizes characteristics of the methods such as: capability of retrieving red, far-red, or full fluorescence; number of spectral bands employed (e.g., multispectral, hyperspectral); spectral range used in the retrieval; main assumptions; use of parametric expressions vs. model-based functions; and treatment of the atmospheric effect. We focus mainly on developments subsequent to the review of Meroni et al. (2009), with a few earlier ones included for historical context and completeness.

5.2. Retrieval of SIF at selected absorption bands

The first class of retrieval methods targets restricted spectral regions associated with strong absorption from gases in the terrestrial or solar atmosphere (i.e., O_2 bands or FLs, respectively). Retrieval at selected wavelengths exploits the contrast between (i) spectral wavelengths where the radiance signal is mostly dominated by the reflected solar flux, and (ii) narrow spectral regions where the solar incident flux is largely attenuated.

5.2.1.   Oxygen absorption bands—A classical strategy to disentangle reflected radiance and SIF contributions is to compare the radiance outside and inside the O_2 absorption bands. The approach is an extension of a technique originally developed for FLs,

the FLD principle (Plascyk, 1975; Plascyk and Gabriel, 1975), which relies on two radiance measurements – one inside and one outside the absorption feature – to solve Equation 1. A refinement particularly relevant for red fluorescence uses more spectral bands to introduce a spectral dependency of reflectance and fluorescence, as exemplified by the 3FLD (Maier, 2002), cFLD (Gómez-Chova et al., 2006), and iFLD (Alonso et al., 2008), reviewed by Meroni et al. (2009).

Spectral Fitting Methods (SFMs) are a more sophisticated approach that uses all available (hyper)spectral bands to quantify the spectrally variable fluorescence and reflectance contribution over a restricted spectral range. The upwelling radiance spectrum is modelled over a broader spectral window (i.e., ~ tens of nm) including multiple absorption lines (i.e., O_2 bands and FLs), with fluorescence and reflectance as continuous parametric functions. The resulting mathematical system (one equation per spectral wavelength considered) is solved to retrieve the underlying unknown function parameters. Several types of functions have been proposed to approximate the reflectance and fluorescence spectral behaviour within spectral windows around the main oxygen absorption bands (Table 2). Because SFMs use all of the high-resolution spectral information along the absorption region – theoretically hundreds of bands – the impact of instrument noise is reduced.

5.2.2.   Fraunhofer lines—In contrast to methods using oxygen absorption bands, those using solar absorption features do not require complex atmospheric modelling, hence, they have been extensively applied to current space-based SIF retrievals. This family of algorithms may be categorized into two main groups: (i) simplified physically-based schemes applied to specific FLs, and (ii) data-driven statistical approaches involving Principal Component Analysis (PCA) or Singular Value Decomposition (SVD) analysis. When the retrieval is fitting only FLs (e.g., spectral windows 745-758 nm, as in GOSAT, OCO-2 or S-5P), both simple physically-based (e.g., Frankenberg et al., 2011a) and data-driven (e.g., Guanter et al., 2012) methods can be used. When the fitting window is wider and includes atmospheric bands, as in SIF retrievals from GOME-2 data, spanning either water vapor around 740 nm or O_2 in 760 nm, then data-driven approaches are the only way to avoid the complex explicit modelling of atmospheric radiative transfer (e.g., Joiner et al., 2013; Köhler et al., 2015). Several methods have been proposed and all these strategies have allowed determination of the far-red fluorescence (Table 2).

Terrestrial SIF in the red spectral region is more difficult to detect from space using FLs as the lines in the red region are not as wide, nor as deep, as those in the far-red. Also, red SIF signal levels are typically lower overall than those in the far-red for healthy vegetation, because of reabsorption by chlorophyll and also because the emitted red fluorescence by leaves within a canopy conceivably can add to the directly emitted far-red fluorescence (i.e., the re-emission phenomenon). The sharp upturn of the red edge also complicates retrievals and may necessitate smaller fitting windows. Quantification of the red SIF emission was reported by Wolanin et al. (2015) using SCIAMACHY and GOME-2 data and by Joiner et al. (2016).

Recently, FL-based methods developed for satellite sensors also are being used for ground-based and airborne spectrometers operating at high SR (Grossmann et al., 2018; Frankenberg et al., 2018).

5.3. Retrieval of the full SIF spectrum

Two main different approaches have been developed to retrieve the continuous SIF emission spectrum (Table 2).

5.3.1. Spectrum fitting—Spectral fitting techniques are an evolution of SFMs to encompass the broader spectral region where fluorescence emission occurs. Methods such as the Fluorescence Spectrum Reconstruction (FSR) (Zhao et al., 2014), the Full-spectrum Spectral Fitting (F-SFM) (Liu et al., 2015), and the advanced FSR (aFSR) (Zhao et al., 2018) are examples that use linear combinations of basis spectra to model the SIF spectrum at TOC. The basis spectra are derived from PCA (Liu et al., 2015) or SVD (Zhao et al., 2014) on a large dataset of SIF spectra simulated by the canopy RT model SCOPE. In general, these methods are structured as follows: first, SIF is retrieved at selected absorption bands (i.e., O_2 bands, Hα FL, etc.) by means of a modified version of SFM; then, the SIF spectrum is reconstructed as a linear combination of the basis spectra matching the SIF SFM retrievals. Alternatively, the full SIF spectrum is estimated by considering simultaneously all the wavelengths in the spectral window where fluorescence occurs, as in the SpecFit model and using piecewise cubic spline to fit the reflectance (Cogliati et al., 2015b).

5.3.2. Model-inversion methods—An emerging approach for quantifying SIF is based on numerical inversion of canopy RTMs. This route permits retrieval also of relevant biophysical parameters (e.g., chlorophyll content, leaf area index, etc.), and related variables (e.g., fraction of photosynthetically active radiation, fAPAR), as side-products of the fluorescence retrieval. This additional information is crucial for interpretation of SIF with respect to plant photosynthetic activity.

An inversion approach was first developed by Verhoef et al. (2018) and is suited to the spectral and directional outputs of the tandem mission of FLEX and Sentinel-3 (S-3). The method is based on model inversion of simulated TOA radiance where the SIF and canopy parameters are retrieved simultaneously and in a consistent manner. It employs a 'light' version of SCOPE to generate the canopy reflectance signature; then SIF is modelled as an additional source of radiance using a linear combination of principal components (PCs). Actually, this approach represents a hybrid solution between model inversion (reflectance modelling) and the spectrum fitting methods (fluorescence modelling).

A more complete canopy model-inversion procedure was recently proposed by Celesti et al. (2018) based on simulations and experimental TOC observations collected during controlled stress induction experiments. It employs both the fluorescence and reflectance SCOPE subroutines. These routines are used to forward model the TOC apparent reflectance to be matched with spectral observations. The use of the fluorescence routine allows quantification of the fluorescence quantum yield, one of the key variables for understanding fluorescence and its link to photosynthesis. Because the work of Celesti et al. (2018) involved extreme contrasts in vegetation properties induced by a chemical treatment, the

operational applicability of their approach to natural vegetation canopies or TOA satellite data remains to be studied.

In the model inversion approach, Visible and Near-Infrared (VNIR) information are needed for adjusting the canopy reflectance model parameters. Unfortunately, due to current techological constraints, wide-spectral-range high-resolution spectra cannot be collected by the same spectrometer, potentially giving rise to some inconsistencies between spectral datasets with respect to spatial co-registration, radiometric intercalibration, etc. For this reason, accurate co-registration and intercalibration methods must be applied prior to fluorescence determination whenever more than one sensor is used.

5.4. Atmospheric correction, illumination, and surface anisotropy

Some of the retrieval methods require atmospheric correction before SIF retrieval (two-steps), whereas others explicitly include atmospheric correction in the design of the algorithm in a complete TOA scheme (one-step). Atmospheric effects depend on the type of absorption feature used (terrestrial vs. solar). Satellite-based FL methods explicitly include the atmospheric effect directly in a single-step algorithm design facilitated by the relatively simple behaviour of the atmosphere at these wavelengths. The assumption is that the atmospheric interference is caused mainly by scattering that, within the narrow FLs, can be considered spectrally invariant or varying as linear or polynomial functions. Thus, the simplified physically-based methods and the data-driven approaches working with FLs correct for this scattering but do not require characterization of the atmospheric status (such as aerosol optical depth or height distribution) which can strongly impact the O_2-A feature (Frankenberg et al., 2011a). By contrast, retrieval at the O_2 bands requires very accurate atmospheric modelling. High-resolution atmospheric RT codes are used to compute the spectrally-resolved atmospheric RT functions (i.e., two-way direct and diffuse transmittance, bidirectional reflectance and spherical albedo) to represent accurately the TOA reflected radiance in addition to SIF. Verhoef et al. (2018, 2014) proposed a means to couple atmospheric and surface RT at high SR based on the so-called T-18 system of atmospheric transfer functions – a method specifically designed to accommodate the finite spectral band effect. This effect concerns the fact that the atmospheric transmittance of absorption lines does not follow Beer's Law when there are large variations of the spectral absorption within the interval (spectral band), therefore the product of two atmospheric functions (e.g., downward and upward transmittance) is not equivalent to the product of these functions convolved. This strategy has been employed in several schemes based on FLD, spectral fitting, and model inversion (Cogliati et al., 2015b; Damm et al., 2014; Mazzoni et al., 2010; Wieneke et al., 2016).

The atmospheric correction at the O_2 bands may be performed either as a two-step or one-step procedure. Cogliati et al. (2015a) used a two-step approach where the TOA spectrum is converted to TOC followed by decoupling of the SIF and reflectance, based on SFM and SpecFit. A two-step approach including a more realistic atmospheric correction was presented in Sabater et al. (2017, 2015) and implemented within the FLEX End-to-End simulator (Vicent et al., 2016). A direct TOA radiance optimization approach has instead been introduced by Verhoef et al. (2018), in which at-sensor spectra are calculated by

coupling a canopy model with an atmospheric RT model. The procedures described here for satellite instruments also have been adapted for airborne imaging spectrometers. For example, FL approaches have been used with the *HyPlant* airborne sensor (Colombo et al., 2018; Rossini et al., 2015) and with the novel Chlorophyll Fluorescence Imaging Spectrometer (CFIS) (Frankenberg et al., 2018) [Section 6]. The physical methods at the O_2 bands were adapted for *HyPlant* by Cogliati et al. (2018) and a semi-empirical technique making use of fluorescence-free reference pixels (i.e., bare soils) was shown to improve characterization of the atmospheric transfer functions (Damm et al., 2014; Wieneke et al., 2016).

Retrievals that rely on O_2 absorption bands are sensitive to the direct-to-diffuse ratio of the incident light and its coupled effect with canopy anisotropy. To reach the sensor, diffuse light traverses a longer pathway compared to direct light, making the depth of the absorption sensitive to the fraction of diffuse light. This effect might be confused with in-filling by fluorescence, leading to over/under-estimation of fluorescence. Evidence of such effects based on RT simulations has been reported in Fournier et al. (2014), Cogliati et al. (2015b), and Verhoef et al. (2018). Liu and Liu (2018) considered in more detail the impact of direct/ diffuse radiation on the in-filling effect and SIF retrieval using simulated data. They found that this effect can have a marked impact on estimated SIF (up to 20% at the O_2-A band). These studies have been developed mainly with turbid-medium canopy RTMs, but the fluorescence angular distribution is also affected significantly by the structural arrangement of the canopy – with respect to sun and sensor viewing angles – which determines the actual fraction of illuminated and shaded leaves observed by the instrument. This is commonly observed from diurnal continuous measurements of fluorescence using ground-based and tower-mounted instruments viewing a fixed spot of the canopy. Understanding whether changes in fluorescence are related to canopy self-shadowing or to more relevant physiological processes is not trivial and still a challenge. Detailed consideration of anisotropic effects and the impact on retrieval accuracy of fluorescence was provided in Damm et al. (2015b) and Yang et al. (in press). Sensor technical characteristics (e.g., spatial resolution, spectral range and resolution, and SNR) are relevant to such aspects and play an important role in determining the accuracy of SIF retrieval.

5.5. Assessment of SIF retrieval accuracy

Validation of SIF retrieval methods, especially for satellite-based acquisitions, is still a challenge due to issues such as large footprint sizes and instrument errors [Section 7]. Also, until recently there has been a lack of direct ways to observe SIF independently; however, this situation is changing with the advent of new portable sensors for leaf/canopy-scale work, platform-mounted devices, drones, and other airborne sensors for SIF detection [Section 6].

So far, retrieval accuracy has been evaluated mainly through numerical experiments in which RT simulations – ones that consider comprehensive variability of reflectance, fluorescence and atmospheric conditions – are performed according to specific instrument characteristics (sampling interval, FWHM, SNR, etc.). But the reliability of accuracy statistics obtained in this way depends on the overall assumptions included in the canopy and atmospheric RT

models and how accurately the models are coupled. Most numerical simulations are based on homogenous 1D surfaces and Lambertian assumption (e.g., Damm et al., 2011; Liu et al., 2015; Meroni et al., 2010; Zhao et al., 2014), and in only a few cases has a full bidirectional reflectance distribution function (BRDF) scenario been included in the forward model (Cogliati et al., 2015b; Liu and Liu, 2018; Mazzoni et al., 2010; Verhoef et al., 2018). More recently, full 3D RT models incorporating fluorescence (e.g., FluorWPS, FluorFLIGHT, and DART) [Section 4] were developed, offering more complex strategies to calculate retrieval accuracy in heterogenous canopies and landscapes.

A more direct evaluation of SIF retrieval accuracies from airborne and satellite sensors is possible using direct comparisons with ground-based data. These data can provide more reliable estimations of fluorescence because surface irradiance is measured, and atmospheric effects may be neglected. This has been used successfully for airborne observations from the *HyPlant* sensor, operating at spatial resolution of one meter (Rascher et al., 2015; Rossini et al., 2015). However, since ground-based methods (e.g., from towers) sample a footprint of only a few square meters, it presents difficulties for validation of medium and coarse-spatial-resolution data. Validation of SIF retrievals from medium-resolution satellite missions such as FLEX (300 x 300 m^2) could be feasible by combining data from field spectroscopy instruments – to get continuous temporal data – with less frequent acquisitions over larger spatial areas using robotic systems, UAVs, or other airborne sensors in selected sites.

5.6. Challenges and future directions in SIF retrieval

Main novelties in retrieval strategies include protocols for satellites using FLs and derivation of the full SIF spectrum. A recent shift from the use of terrestrial oxygen absorption bands – nearly all papers reviewed by Meroni et al. (2009) – to FLs alone, or in parallel with O$_2$ bands, is seen also in applications using atmospheric satellite sensors. Development of FL procedures was prompted by the convenient availability of atmospheric chemistry satellites, which allowed researchers to capitalize on the simplified modelling of atmospheric effects in the solar absorption bands to quantify SIF at coarse spatial resolution [Section 7]. However, such results have suffered from the fact that the sensors employed were not specifically designed for SIF. Therefore, the instantaneous retrievals are aggregated to improve their quality at the cost of spatio-temporal resolution. However, improved observational capabilities and better SNR are offered by new atmospheric sensors (e.g., TROPOMI aboard the S-5P satellite) (Guanter et al., 2015).

Retrieval methods that use O$_2$ absorption features have their pros and cons. On the one hand, they have access to features where the fluorescence contribution is more prominent, but on the other hand they require much more complex modelling to correct for atmospheric absorption and scattering inside the O$_2$ bands. The particular design of the tandem FLEX/S-3 mission concept, aimed at SIF retrieval using the O$_2$ bands, was developed specifically to address requirements for an accurate atmospheric correction and SIF detection. The broad spectral coverage (from blue bands to IR wavelengths), the high-spectral resolution in the red and far-red region, and the dualview (nadir and oblique) offered by the tandem mission provide the spectral and directional information for an accurate atmospheric characterization (Drusch et al., 2017; ESA, 2015; Sabater et al., 2017).

Most methods emphasize selected absorption bands at both O_2 and FLs to provide independent fluorescence values, neglecting the possible functional relationship between red and far-red fluorescence emission peaks. Only the new generation of methods – full SIF spectrum and model-based inversion – offers a broader spectral characterization of SIF, and makes consistent use of the spectral detail available from the two fluorescence emission regions. The perspective of exploiting the full SIF spectrum is relevant for future work on fluorescence in relation to different canopy species, chemical/physical variables, and physiology. Knowledge of the entire fluorescence spectrum may be helpful to better quantify canopy re-absorption, as well as for deriving the respective PSI/PSII contributions and the fluorescence quantum efficiency. However, the full SIF spectrum is influenced at leaf and canopy levels by diverse factors which are not necessarily related directly to the photosynthetic activity of the plants [Section 2]. To further help understanding of all these combined effects, model inversion methods have the additional advantage of offering physiologically consistent estimates of canopy parameters that are essential to better interpretation of fluorescence. Nonetheless, in the model inversion approach VNIR information is needed for adjusting the canopy reflectance model parameters. Given that two spectrometers will likely be needed to acquire such data, accurate co-registration and intercalibration methods will be critical.

6. SIF measurement technologies – Field and airborne systems

6.1. Technological overview

A range of field sensors have been developed over the years, from hand-held and clip-on devices to TOC sensors deployable from stationary or mobile ground-based platforms, unmanned aerial vehicles (UAVs), and traditional aircraft. These technologies provide complementary capacity for measuring and interpreting fluorescence in the context of physiological processes. Airborne imaging allows mapping of fluorescence over plant canopies and derivation of indicators of photosynthetic functionality and pre-visual stress at ecological and management-relevant scales. Field and airborne systems also support satellite-based measurements through validation, interpretation, and provision of data inputs to models. The types of field systems are compared in Figure 9, indicating relative merits with respect to operational and biological considerations.

6.2. Hand-held leaf instrumentation

Portability is a priority for passive SIF field devices. But unlike the availability of active fluorometers that detect steady-state fluorescence in leaves – for which there are multiple commercial devices – instruments designed specifically for SIF are still rare. One such device is FluoWat, a hand-held leaf clip designed for use in natural sunlight. When coupled to a field-portable spectrometer, the device allows quantification of the full SIF emission and also reflectance and transmittance. FluoWat uses a short-pass filter (<650 nm) to control incoming light, so only the fluorescence emission is measured when the filter is in place. Its fiber-optic probe may be positioned to measure upward- or downward-directed fluorescence (typically from adaxial or abaxial leaf surfaces, respectively), thereby allowing study of the interplay among vertical pigment gradients, re-absorption, scattering properties, and leaf fluorescence emission. The instrument has been used to facilitate linking canopy and leaf-

level SIF data, and for stress detection (Cendrero-Mateo et al., 2016; Van Wittenberghe et al., 2015, 2014, 2013).

6.3. Top-of-canopy spectrometers

Early work in passive detection of TOC fluorescence was inspired by the development of the MKII Fraunhofer line discriminator, an airborne instrument for remote sensing of solar-induced 'luminescence' (Hemphill et al., 1977; Plascyk, 1975). Used with leaves and canopies to reveal subtle changes at the Ha FL (656.3 nm), was applied successfully by McFarlane et al. (1980) to identify water stress in citrus crops, and by Carter et al. (1990) to relate SIF to carbon assimilation in field vegetation. But limitations to using the Ha band were its distance from the fluorescence peaks and its narrow width (~0.1 nm FWHM) which necessitated very high SNR.

Detection of SIF in the O_2 bands has been researched intensively in the last twenty years [Section 5], and assorted instruments have emerged (Meroni et al., 2009). Kebabian et al. (1999) introduced a plant fluorescence sensor to detect photons re-emitted after absorption of fluorescence by oxgen contained in a low-pressure cell. Carter et al. (1996) used a Fraunhofer Line Radiometer measuring in the O_2-B band to study herbicide effects on leaf fluorescence. Moya et al. (2004) invented an instrument using narrow-band interference filters to derive fluorescence in the O_2-A band. And Evain et al. (2001) introduced a Passive Multi-wavelength Fluorescence Detector (PMFD) to measure fluorescence and reflectance at 760 nm and at 687 nm. Quantification of SIF in the O_2-B and O_2-A bands also was done by Fournier et al. (2012) using their SpectroFLEX canopy instrument, able to perform continuous and automatic measurements over several weeks. Finally, Pérez-Priego et al. (2005) illustrated the sensitivity of fluorescence (in-filling) at the O_2-A band to water stress by using a high-resolution spectrometer housed in a temperature-controlled box and connected to a 15-m-long fiber-optic cable for acquisition of reflectance from single tree crowns.

Developments in sensor technologies have sought to harness the combined information of reflectance and fluorescence (Burkart et al., 2015; Cheng et al., 2013; Migliavacca et al., 2017a; Panigada et al., 2014; Pérez-Priego et al., 2015, 2005; Yang et al., 2015). Well-calibrated ASD FieldSpec devices, for example, which have high SNR (even though the O2 absorption bands are not well resolved), have been used to capture diurnal courses of canopy SIF and reflectance (Damm et al., 2014, 2010; Liu et al., 2005), an approach also tested with some success from low-flying research aircraft (Damm et al., 2014; Schickling et al., 2016).

Sophisticated apparatus have emerged to better resolve absorption features and leverage the availability of low-cost miniaturized spectrometers. A fully automatic system, consisting of three miniature high-resolution HR2000+ spectrometers (Ocean Optics, Florida, USA) enclosed in a temperature-stabilized box and connected to collimated optic fibers, was installed atop a crane to continuously monitor SIF and reflectance spectra at a high repetition rate (1 Hz) (Daumard et al., 2012, 2010; Goulas et al., 2017). Two inter-calibrated spectrometers allowed almost simultaneous determinations of incoming and reflected radiation, with an automated routine continuously adjusting integration time to the intensity of incoming radiation in order to optimize SNR.

New instrument architectures introduced by researchers at the University of Milano and their colleagues combined high-resolution spectrometers in a temperature-stabilized box, with optical multiplexers and a dedicated intercalibration routine, creating a stable TOC measurement system (Cogliati et al., 2015a). In ecosystem studies, this apparatus provided the first concise comparison of fluorescence emissions across different plant functional types (Rossini et al., 2016) . The Milano system, known commercially under the name 'FloX' (Julitta et al., 2017), houses two spectrometers (one broadband, one high-resolution) with bifurcated fibers to allow almost simultaneous measurements of incoming and reflected irradiance. Precise calibration of the integrated system and automated data retrieval algorithms permit estimation of red and far-red fluorescence. The systems have been installed on about a dozen observation towers internationally to date.

An automated, tower-based canopy system called FUSION, developed by NASA-GSFC, integrates multi-directional spectral, thermal, and SIF observations (Middleton et al., 2018). Its two dual-channel systems (upward- and downward-looking spectrometers) simultaneously collect high-spectral-resolution data of reflected light and fluorescence and can operate continuously during daylight hours to capture diurnal and seasonal dynamics. Data products include VNIR surface reflectance spectra from ~350-1100 nm, red and far-red SIF, and surface temperature.

Other tower-based examples include FluoSpec, PhotoSpec, and AutoSIF. FluoSpec (Yang et al., 2018c, 2015) is an automated system that provides high SR (~0.13 nm FWHM) between 680 and 775 nm for red and far-red SIF; it has been used since 2012 in a site network called FluoNet. PhotoSpec assesses the red (670-732 nm) and far-red (729-784 nm) wavelength ranges and also canopy reflectance (400-900 nm); it has a high SNR and SR to allow FL retrievals and has been used successfully for continuous daytime monitoring of SIF (Grossmann et al., 2018). AutoSIF (Zhou et al., 2016; Xu et al., 2018) uses a single spectrometer to capture a spectral range of ~480-850 nm, with a spectral resolution of 0.9 nm, SNR of 1000:1, and spectral sampling interval of 0.4 nm; it has been used to quantify red and far-red SIF (Xu et al., 2018).

6.4. Airborne systems

6.4.1. Low-altitude systems – Unmanned aerial vehicles—Unmanned aerial vehicles (UAVs) (also called unmanned aircraft systems, UAS) provide observations of vegetation optical properties at the intermediate scales between ground-based and higher-altitude airborne systems. The appeal of this approach is the flexibility to provide on-demand hyperspectral imagery at high spatial and temporal resolutions (Berni et al., 2009; Garzonio et al., 2017; Lucieer et al., 2014; Malenovský et al., 2017; Zarco-Tejada et al., 2012, 2009). UAV deployments over vegetation is a fairly recent undertaking, with first prototypes developed in the early 2000s used in agricultural applications (e.g., Herwitz et al., 2004; Johnson et al., 2003). Subsequent trials were restricted primarily to multispectral and broad-band thermal imagery acquisition (e.g., Turner et al., 2014) – but in the last decade UAV systems suitable for SIF retrieval have emerged.

UAV capability to retrieve SIF has been demonstrated in several investigations. Some early experiments used a fixed-wing type of unmanned aircraft equipped with a micro-

hyperspectral imager and thermal camera (Figure 10) (Zarco-Tejada et al., 2013b, 2012). SIF emission (O_2-A) derived from the extracted spectral radiance of pure-crown 30-cm or 40-cm pixels showed, along with independent ground observations and models, that SIF signals from individual trees with different water stress status could be discriminated (using the 3FLD method with a 6-nm FWHM and 1.85 nm sampling spectra). Other systems followed, such as the HyUAS (Garzonio et al., 2017) , a non-imaging multi-rotor-platform apparatus designed to optimize optical and data acquisition, e.g., under changing meteorological conditions (Cogliati et al., 2015a) and for provision of a more homogenous footprint at a given flight height. Another development, the Piccolo doppio (Mac Arthur et al., 2014), incorporates two fiber-optic-based spectrometers and allows near-simultaneous measurements of reflectance and fluorescence in the oxygen bands. Finally, there is AirSIF, which uses a QE PRO spectrometer (Ocean Optics) with bifurcated two-channel optical fibers, and was designed to achieve accurate ground localization and shape reconstruction of the SIF and reflectance footprints – by considering exact UAV posture, geographic position, and detailed digital surface modelling of the vegetation canopy (Bendig et al., 2018).

Technical advantages of UAVs include the capability for highly customized deployments (e.g., low and slow flights allowing for high spatial resolutions and long integration times) and quick response and turn-around for planning and investigation. Although miniaturized and lightweight, UAV systems need to have a stable high spectral performance, with sufficient SNR and precision to provide accurate SIF retrievals. On the other hand, for some applications, the primary value might be a high spatial resolution with a more accurate geolocation rather than precise SIF estimates (Gautam et al., 2018), to allow e.g., mapping of SIF spatial variability in in stressed vegetation. In controlled studies, high spatial resolution can also help to discriminate the many confounding influences on SIF magnitude (e.g., shadows, vegetated background with different structure, pigment contents, etc.), thereby complementing coarser-resolution airborne and satellite systems.

6.4.2. Medium- or high-altitude systems

Line scanners: Over 30 years ago, it was shown that, despite the low emission of SIF in natural environments, it was detectable using airborne sensors in marine systems. Using the fluorescence line height feature, the fluorescence peak at 685 nm emitted by phytoplankton was clearly discriminated from background radiance of the sea surface (Gower and Borstad, 1990; Neville and Gower, 1977). But this differential technique was not applicable to terrestrial vegetation owing to its very different spectral properties such as higher reflectance – the shape of which is controlled mainly by photosynthetic pigment content and strong re-absorption of the red fluorescence (Zarco-Tejada et al., 2000b). Instead, passive detection of vegetation SIF using airborne systems came to rely on narrow absorption features of the incident radiation. To the best of our knowledge, the first reported airborne test over vegetation was performed with the MKII Fraunhofer Line Discriminator deployed onboard a helicopter (Watson and Hemphill, 1976). Later, using the enhanced sensitivity provided by the oxygen bands, the AIRFLEX line scanner became the first dedicated airborne instrument for measuring SIF in terrestrial vegetation (Moya et al., 2006). AIRFLEX is a multichannel radiometer that uses narrowband interference filters (FWHM between 0.5 and 1 nm, depending on the channel) to sample the in-band and out-of-band radiances at 687 nm and

760 nm. Interference filters allow for the detection of a high flux, enhancing SNR (albeit at the expense of spectral resolution). AIRFLEX was first tested in campaigns of the SENtinel-2 and FLuorescence EXperiment (SEN2FLEX) program, and it demonstrated clearly the feasibility of analysis in the O_2 bands (Moya et al., 2006). These early experiments were crucial in proving the distinctive nature of the fluorescence signal compared to conventional reflectance (Rascher et al., 2009).

Airborne imaging spectrometers: Until airborne imaging sensors specialized for measuring SIF became available, spectrometers with lower SR were used. They included, for example, the Reflective Optics System Imaging Spectrometer (ROSIS) (Maier et al., 2003), the CASI (Zarco-Tejada et al., 2002, 2001), and the Airborne Prism Experiment (APEX) (Damm et al., 2015a) – to retrieve SIF in the wider O_2-A band. From today's perspective, such instruments are considered sub-optimal due to their low SR (e.g., 2.2 nm for CASI-1500, 5.7 nm for APEX, and 7 nm for ROSIS), which allows fluorescence maps only in relative units, but some of these imagers (e.g., APEX) benefited from a high SNR, partly compensating for the lower SR (Damm et al., 2011). These case studies propelled the entire field by providing relevant and interesting insight into the spatial and temporal variability of SIF. They demonstrated the value of the 3FLD technique (Maier et al., 2003), the feasibility of using airborne data to validate maps of SIF retrieved from satellite sensors (Guanter et al., 2007), and the possibility to derive multi-year data to study relationships between SIF and ecosystem GPP (Damm et al., 2015a).

After some attempts to use existing imaging spectrometers in a reprogrammed mode (Rascher et al., 2009), the *HyPlant* airborne imaging spectrometer was developed as a cooperative endeavour between Germany's Forschungszentrum Julich and the Finnish company SPECIM. As the core reference instrument and demonstrator for the FLEX satellite mission, *HyPlant* was the first airborne sensor optimized optically for full-spectrum SIF retrieval, taking advantage of the oxygen absorption and FLs near 685 and 760 nm. *HyPlant*'s core module operates with high SR (0.25 nm) and a spectral sampling interval of 0.11 nm to resolve the spectral window between 670 and 780 nm (Rascher et al., 2015). Initial testing staring in 2012 confirmed that SIF could be retrieved successfully in the O_2-A band from such an airborne platform to provide information not discernible from reflectance (Figure 11) (Rascher et al., 2015; Rossini et al., 2015; Simmer et al., 2015). While the first version of the instrument had an imperfect point-spread function and limited SNR, subsequent improvements have increased SNR and pointing accuracy. The optical path of the fluorescence module has been redesigned and upgraded to achieve a stable optical performance of the detector, also helping retrieval of both fluorescence peaks using the O_2-A and Gerhards et al. 2018, Liu et al. 2018, von Hebel et al. 2018, Yang et al. in press).

Two airborne imaging spectrometers were developed recently in the US. One is the NASA/JPL CFIS, an imaging system developed for validation of OCO-2 SIF retrievals. CFIS has a high SR (<0.1 nm) and spectral coverage between 737-772 nm for estimation of far-red SIF (Frankenberg et al., 2018; Sun et al., 2017). It has been used in airborne campaigns to under-fly orbital tracks of the OCO-2 satellite, revealing strong agreement between SIF retrieved from OCO-2 and CFIS along latitudinal gradients (Sun et al., 2017). A second imager, the Hyperspec High Resolution Chlorophyll Fluorescence Sensor, is a

lightweight sensor developed by Headwall Photonics, Inc. (Bolton, Massachusetts) in partnership with NASA/Goddard to capture the spectral range of 670-780 nm (~0.2 nm SR), allowing retrieval of both red and far-red SIF. This sensor has been integrated into NASA/ Goddard's G-LiHT airborne package which also collects lidar, thermal, and hyperspectral visible-NIR optical data (Middleton et al., 2017).

6.5. Adapting theory to the 'real world'

The study of fluorescence in natural field conditions and at different biological and spatial scales requires consideration of multiple factors to acquire coherent measurements, to avoid retrieval artefacts, and to correctly interpret results. Sensor technologies, retrieval strategies, and the specific influential factors in a given situation can all affect robustness and reliability of fluorescence results. Aspects that change between proximal and remote sensing with implications for fluorescence retrievals include (i) non-uniformities and instabilities of the detectors, (ii) spatial footprint of the instrumentation, and (iii) impact of atmospheric effects. Also important is the appropriate use and the relative height placement of canopy versus reference sensors for accurate SIF measurements (Sabater et al., 2018).

With field spectrometers positioned within a short distance of the surface target, information on atmospheric functions (including atmospheric transmittances, path scattered radiance, and spherical albedo) can be provided by measuring reference panels. But with increasing distances (i.e., using tower, airborne or satellite sensors), a combination of measured and modelled atmospheric functions is required, necessitating accurate dynamic calibration status of the sensors during operation (i.e., SR, center wavelength position, stray light, etc.). It is common for spectrometers to change their spectral and radiometric performance due to pressure or temperature variations during operations. As a result, spectral non-uniformities associated with changing center wavelength position or SR during operations eventually impact the point spread function of the spectral detector element. Radiometric non-uniformities are associated with, for instance, temperature-dependent changes in dark noise (D'Odorico et al., 2010; Schlapfer et al., 2007). In situations where sensors deviate during operations from their nominal lab performance, or where they were imperfectly calibrated, the combination of modelled atmospheric functions with measured radiances is prone to error and even substantial uncertainties in retrieved fluorescence (Damm et al., 2011; Moreno et al., 2014).

The spatial footprint measured by instrumentation can have implications for the validity of assumptions used in atmospheric correction [Section 5]. For example, SIF retrievals using tower-based or airborne instrumentation with very small pixels (e.g., < 2 m) may be subject to artefacts due to greater dominance of geometric optical scattering by canopy components and higher likelihood of measuring (partly) shaded surfaces (i.e., a reduced fraction of direct irradiance) (Damm et al., 2015b). This could violate atmospheric correction tools that assume fully illuminated, homogeneous, and Lambertian reflecting surfaces, with isotropic and volumetric scattering being the dominant scattering processes.

While the emphasis here is on passive sensing of SIF, the broader context of fluorescence evaluation includes active sensors and other spectral technologies helpful for studying fluorescence characteristics and the influence of multiple factors [Section 2]. Active

technologies tend to allow better control of excitation conditions and are well suited to measurement of parameters such as fluorescence yield (the metric often associated to plant physiology). They can be an important complement to passive devices for proximal field work.

6.6. Challenges and future directions in field and airborne sensing of SIF

Substantial progress has been achieved in measuring SIF in field settings using ground-based and airborne systems, with noteworthy prospects for applications [Section 8]. Airborne SIF sensors, for example, have been used to reveal pre-visual stress effects from a bacterial pathogen (*Xylella fastidiosa*) currently infecting economically vital crops worldwide (Zarco-Tejada et al., 2018) or were applied to early signs of photosynthetic down regulation during drought stress in various crop species (Yang et al., in press). Such applications will be supported by an expanding choice of available instruments which allows analysis of SIF across spatial scales. We expect that UAV-based sensors will become more available in the near future and that a next generation of *HyPlant-like* instruments will be developed. In light of the recommendations from Section 5 – for improved spatio-temporal capacity; flexibility to measure both red and far-red fluorescence (including the full emission spectrum of SIF); sufficiently high SR and SNR to allow accurate SIF retrieval; and the provision of surface reflectance VNIR spectra to support model inversion – it is evident that modern options are well the way to realizing those objectives.

Some of the required techniques and corrections are well established for high-performance airborne systems, and they are being refined for miniaturized or lightweight sensors so as to avoid instrument and retrieval artefacts. Priorities for improvements include the correction of sensor stray light, non-linearity, and point-spread-function artefacts. [Straylight aspects have been covered by Coppo et al. (2017) in their discussion of the FLEX sensors, and it is instructive for sensors in general.] Overcoming the problem of illumination artefacts originating from geometric optical scattering in high-spatial-resolution data (i.e., individual scattering elements dominate the sensor's field-of-view; Kückenbrink et al., in press) is still an open issue. With controlled field observations, it appears to be of smaller impact, but when airborne spectrometers with high spatial resolution are used, retrieval artefacts are possible and new retrieval concepts accounting for varying fractions of direct and diffuse irradiance components must be developed (Damm et al., 2015b). We expect that technical advances in ground-, tractor-, UAV-, and aircraft-based instruments will facilitate realization of the full potential of SIF techniques for applications in vegetation and crop management, and in validation and interpretation of SIF retrievals from satellite spectrometers. In this context, these sensors will complement satellite based measurements and will provide SIF data at higher spatial and temporal scales, necessary for local mapping of natural ecosystems and in agriculture. .

7. SIF measurement technologies – Satellite systems

7.1. Technological overview

Breakthroughs in understanding the effects of fluorescence on apparent reflectance, coupled with advances in modelling, SIF retrieval approaches, and sensor capabilities, have

contributed to the realization of satellite-based SIF detection. In 1999, Marc-Philippe Stoll and colleagues proposed to the European Space Agency that a satellite mission, FLEX, be developed to measure SIF from terrestrial vegetation to support science and applications in agriculture, forestry and global change issues (Stoll et al., 1999). This concept was developed, evaluated, and refined over the ensuing years (ESA, 2015; Moreno et al., 2006; Rascher et al., 2008), and in 2015 FLEX was approved to be ESA's 8th Earth Explorer, with a projected launch date of 2022 (Drusch et al., 2017) . During the preparatory activities, ESA commissioned scientific studies, field and airborne campaigns with prototype sensors, and modelling developments foundational to satellite-based SIF science (e.g., A et al., 2015; Magnani et al., 2009; Miller et al., 2005; Mohammed et al., 2016, 2014; Moreno et al., 2014; Pedrós et al., 2010; Rascher et al., 2015, 2009; Van der Tol et al., 2014, 2009b; Verhoef et al., 2018; Verrelst et al., 2016, 2015a; Zarco-Tejada et al., 2006).

Meanwhile, researchers independently working with the atmospheric chemistry satellite GOSAT reported that chlorophyll fluorescence could indeed be retrieved in the very narrow far-red wavelengths adjacent to the O_2-A band, albeit at very coarse spatial resolution (0.5°), from which global maps could be produced (Frankenberg et al., 2011a, 2011b; Joiner et al., 2011). This exciting finding affirmed the earlier work of Guanter et al. (2007) who had shown that far-red SIF could be discriminated in terrestrial vegetation using the MERIS satellite sensor onboard EnviSat. Several satellite sensors designed primarily for measurement of atmospheric trace gases (e.g., CO_2, methane, and cloud parameters) have since been used to quantify SIF regionally and globally at coarse spatial scales. Retrievals from almost all of these missions have been of far-red SIF.

7.2. The FLuorescence EXplorer (FLEX): A tandem mission with Sentinel-3

FLEX is the first satellite mission designed specifically for SIF measurement. It will obtain the suite of SIF features and ancillary data types considered necessary for quantification and interpretation of vegetation parameters related to photosynthetic function (Drusch et al., 2017). The overarching scientific objective of FLEX is to achieve an improved understanding of global seasonally variable photosynthetic functioning and efficiency of vegetation, including physiological indicators of plant stress. The five-year global mission will cover terrestrial vegetation and coastal regions, including land areas between 75°N and 56°S, islands > 100 km^2, and coastal zones within 370 km of coastlines. FLEX will produce imagery and maps at 300×300 m^2 spatial resolution, intended for the monitoring of vegetation at scales of local to landscape-scale management unitsand ecosystems (Drusch et al., 2017).

FLEX will be deployed in a tandem mission with Sentinel-3 (Figure 12), a European operational satellite carrying the Ocean and Land Colour Imager (OLCI) and the Sea and Land Surface Temperature Radiometer (SLSTR) sensors. The FLEX mission will carry a single payload, FLORIS, which is a dual-spectrometer imaging system consisting of narrow-band (high SR) and wide-band (low SR) sensors, measuring the spectral range of 500-780 nm to capture the full SIF emission as well as reflectance for vegetation indices. Instruments from S-3 will provide atmospheric and thermal data, geolocation information, and other ancillary data (ESA, 2018).

Unique products from the FLEX/S-3 tandem mission include: (i) total fluorescence emission (F_{tot}, 650-780 nm); (ii) red and far-red fluorescence at the peaks (F_{685}, F_{740}) and at the O_2-B and O_2-A features (F_{687}, F_{760}); (iii) photosynthetic activity estimates; and (iv) biophysical variables and indices derived from reflectance (e.g., surface fractional vegetation cover; canopy chlorophyll content; LAI; the fraction of photosynthetically active radiation absorbed by chlorophyll, $fAPAR_{chl}$; and PRI) (ESA, 2018). These products will be derived from harmonized TOA Synergy data products using FLORIS, OLCI, and SLSTR radiances cross-calibrated, geometrically co-registered, and ortho-rectified to a common 300×300 m^2 grid. Higher-level products include physiological response variables derived from temporal composites and spatial mosaics (e.g., activation/deactivation of photosynthesis; fluorescence quantum efficiency; and PSII and PSI contributions). These data are expected to improve estimation of GPP and surface fluxes at the local scale and to provide indicators of plant stresses that could reduce or compromise productivity and functional resilience. While the spatial resolution of FLEX exceeds existing satellite missions being used for SIF, it is not of the very high spatio-temporal granularity suited to precision agriculture. Also, the monthly repeat cycle (i.e., nadir view of the same area) at low latitude is not geared to applications requiring very frequent sampling – but at high latitudes, FLEX revisits (i.e., off-nadir view) will be more frequent, for example, 1-2 weeks in boreal areas, owing to orbital overlap, but also subject to viewing angle effects (Middleton et al., 2018; Wei et al., 2018). Studies currently underway for FLEX are investigating error analytics for mission products, and refinement of Cal/Val strategies, with fine-tuning of algorithms as required. The FLEX mission design and a conceptual framework for SIF applications have been described in detail elsewhere (e.g., Coppo et al., 2017; Drusch et al., 2017; ESA, 2018, 2015; Mohammed et al., 2014).

7.3. Atmospheric chemistry satellites used for SIF retrieval

Several global SIF datasets have been produced in the last years using spaceborne spectrometers that were originally designed for atmospheric chemistry applications (Table 3). In all cases, retrieval has been based on the utilization of FLs [Section 5.2.2].

The FL in-filling approach was pursued independently by Joiner et al. (2011), Frankenberg et al. (2011a, 2001b), and Guanter et al. (2012), with global application to the Thermal And Near-infrared Sensor for carbon Observation Fourier Transform Spectrometer (TANSO-FTS) on the Japanese satellite, GOSAT. This high-spectral-resolution instrument has a channel covering the O_2-A band. The original purpose of the O_2-A band channel was to quantify the effects of aerosols and clouds on carbon dioxide (CO_2) and methane (CH_4) estimation. Several isolated FLs can be observed within this channel on either side of the O_2-A band, enabling retrieval of SIF. While the first global maps of SIF were generated from TANSO-FTS, its low SNR and relatively low sampling necessitated averaging the data over larger footprints (~2° latitude by 2° longitude) to obtain reliable contiguous coverage.

A similar channel in NASA's OCO-2 includes a high SR grating spectrometer designed to measure CO2. Observations of SIF from OCO-2 (Frankenberg et al., 2014; Sun et al., 2018, 2017), have been compared with SIF results from the airborne CFIS instrument (Frankenberg et al., 2018; Sun et al., 2017. The OCO-2 ground footprint is much smaller

than that of TANSO-FTS and it has denser sampling that enables more precise gridded measurements. But the higher spatial resolution of OCO-2 comes with a trade-off in that it does not provide contiguous orbital collections nor complete global coverage with its 10 km-wide swath.

The higher repeat cycle (on the order of days) afforded by wide-swath satellite sensors designed for global analyses of atmospheric trace gases prompted Joiner et al. (2013) to examine whether those moderate-spectral-resolution sensors could be used reliably to quantify SIF. These include GOME-2 and similar sensors such as SCIAMACHY (which operated onboard the EnviSat satellite until contact was lost in 2012). They do have spectral coverage throughout the SIF emission range, but their ground footprints tend to be large. For example, SCIAMACHY's native footprint is approximately 30 km by 60 km for the nominal nadir mode that applies to red SIF, but due to onboard spectral averaging to reduce data volumes, the resolution is degraded to 30 km by 240 km for far-red SIF observations. GOME-2 spatial footprints are 40 km by 80 km in the nominal wide swath mode, or 40 km by 40 km in a reduced swath mode. There are currently two GOME-2 instruments in orbit: the GOME-2A (on the MetOp-A satellite), which operated in the nominal mode from January 2007 through mid-July 2013 and since then is operating in the small-swath mode; and GOME-2B (on MetOp-B) which has operated in the nominal mode since mid-2013.

Joiner et al. (2013) showed that GOME-2 data could be used for discrimination of far-red SIF and that they produced higher fidelity global monthly maps of the far-red SIF emission as compared with GOSAT. A sample global map for annually integrated far-red SIF is shown in Figure 13. Such retrieval is possible with GOME-2 due to its SR of ~0.5 nm in the SIF emission region, a high SNR (> ~1000), and a wider spectral coverage interval that surrounds the far-red peak (at 740 nm) and enables a fitting window between 712 to 775 nm. Monthly maps of far-red SIF have been produced at higher spatial resolution than was possible with GOSAT (typically ~0.5° latitude by 0.5° longitude); somewhat noisier maps could be made with similar spatial resolution at weekly time scales. [Note also that retrievals of the red SIF have been reported using GOME-2 and SCIAMACHY (Joiner et al., 2016; Wolanin et al., 2015; see also Section 5).]

Europe's S-5P satellite, carrying the TROPOMI, was launched in late 2017 and flies in formation with NASA's Suomi National Polar Partnership satellite timed for an early afternoon overpass. It provides daily SIF observations of similar or better quality as compared to those from GOME-2 and SCIAMACHY but at a much higher spatial resolution of 7 km x 7 km (Köhler et al., 2018a;Guanter et al., 2015) and up to 7 km x 3.5 km in the VNIR (ESA, undated). Preliminary TROPOMI far-red SIF retrievals show that its mapping capabilities far surpass those of its predecessors, offering intriguing opportunities to map SIF at biome scales (Köhler et al., 2018a; Guanter et al., 2015).

Another advance will be from geostationary Earth orbit (GEO) spectrometers. Several planned GEO missions should provide a significant upgrade in temporal resolution of satellite-derived SIF as compared to currently available information, although at variable coarse spatial resolutions. The Tropospheric Emissions Monitoring of Pollution (TEMPO) mission will provide hourly scans over much of North America (Zoogman et al., 2016).

Spectral coverage from the ultraviolet up to the near infrared (~740 nm) – with only one gap near 500 nm – should allow for determination of red and possibly far-red SIF as well as other vegetation indices. The Sentinel-4 GEO spectrometer on the Meteosat Third Generation-Sounder (MTG-S) satellite and the planned Geostationary Carbon Cycle Observatory (GeoCarb) instrument, like GOSAT and OCO-2, will have spectral coverage of the O_2-A band and its shoulders (Meijer et al., 2014; Moore and Crowell, 2018; O'Brien et al., 2016) for Europe and the Americas, respectively. Their SRs of 0.05-0.12 nm are sufficient to retrieve far-red SIF using FL methodology, several times per day.

7.4. Factors affecting SIF retrieval accuracy of satellite data

There are several issues that complicate current satellite SIF retrievals. Large-footprint instruments in particular are affected by clouds and aerosols that contaminate the vast majority of observations. Since the atmosphere modifies the depth of atmospheric absorption features such as O_2 bands that are used in SIF detection, one benefit of using FLs as opposed to O_2 bands for satellite SIF retrieval is that atmospheric effects do not modify the relative depth of the FLs (although the absolute depths are still attenuated by aerosol scattering). The impact of clouds when using far-red FLs has been studied by several research groups (Frankenberg et al., 2012; Köhler et al., 2015; Guanter et al., 2015) who have concluded that a sufficient amount of SIF emitted by the canopy is seen by the satellite even in the presence of optically thin or moderate amounts of broken clouds (optical thicknesses < ~5). However, this is an open topic that requires more study (W. Verhoef, personal communication). Compared to SIF, clouds and aerosols have a greater impact on reflectance-based indices such as the Normalized Difference Vegetation Index (NDVI), as demonstrated with radiative transfer simulations by Guanter et al. (2015).

Another issue that affects all current coarse-spatial-scale sensors is systematic instrument errors. This was first found in GOSAT data, where it was coined 'zero-level offset'. The general problem is that non-zero values for SIF often get retrieved when zero values are expected (such as over the Sahara). These biases – which may have complex dependences on radiance levels and may vary over time – must be accounted for in order to obtain accurate SIF estimates. [The causes of zero-level offset for different types of instrumentation and their mitigation strategies are discussed by Frankenberg et al. (2011b), Guanter et al. (2012), Köhler et al. (2015), Khosravi et al. (2015), and Joiner et al. (2016, 2012).]

Finally, overall sensor degradation occurs at greater or lesser rates in all satellite-based instruments and should be tracked and quantified. Degradation – which might be sudden or discontinuous – can be due to temperature changes, high radiation exposure, mechanical wear and tear, particles adhering to lenses, jolts from space debris, etc. This issue is particularly evident in data acquired by the very high-SR instruments used for atmospheric chemistry. Koren et al. (2018) and Zhang et al. (2018c) have identified possible artefacts in GOME-2 SIF results that may have been due to sensor degradation. This underscores the need for consideration of such effects when using long-term records for analysis of SIF trends over time.

7.5. Challenges and future directions in satellite sensing of SIF

Earth observation from space provides a powerful way to assess and monitor the status of the biosphere. The potential of satellite-based SIF as an indicator of large-scale photosynthetic activity is evident from the growing body of literature on the use of satellite-retrieved SIF to examine global SIF patterns and dynamics (Frankenberg and Berry, 2018) [Section 8].

Although retrieval of SIF using space-based sensors offers an exciting new tool for studying vegetation dynamics, there are a number of challenges to basic understanding of carbon and water cycles at macroscales. The greatest challenge is to develop measurement and modelling approaches that bridge the SIF emission's vertical pathway and profile through the atmosphere, from vegetation at the surface to the observing satellite sensor above the Earth – in other words, we need reliable upscaling and downscaling capabilities in both temporal and spatial dimensions for SIF and carbon/water/energy processes. From basic science, it is known that chlorophyll fluorescence is influenced directly or indirectly by environmental and biological factors and this is not considered in a comprehensive way in the current satellite-based approaches [Section 8]. These factors often are manifested at the local scale, but tend to be overlooked or averaged out in large footprints and/or monthly aggregates (Magnani et al., 2014; Verrelst et al., 2016). Consequently, it is also essential that calibration and validation methods be developed and demonstrated that (i) prove conclusively whether satellite-retrieved SIF measures the same biological processes as ground-based instruments, and (ii) provide reliable quantitative results at local as well as global scales. The atmospheric chemistry satellites all have wide swaths to facilitate global coverage. Thus far, no corrections have been applied to account for the directional effects in the retrieved SIF values due to off-nadir viewing directions, and this definitely should be included in mature versions of the data processing chain for SIF. Also important will be consideration of the surface anisotropy of SIF (Middleton et al., 2018; Verhoef et al., 2018), which has received insufficient attention to date. Therefore, future retrieval schemes will likely be necessary to consider a number of factors not currently addressed, including surface anisotropy, surface reflectance, and aerosol type/amount.

While the atmospheric chemistry missions have provided novel and compelling large-scale information about SIF, the pressing societal applications in agriculture, food security, and forest ecology and management require high spatial resolution (0.5 km) as well as frequent observations, as prescribed by the application. With atmospheric chemistry missions, the observations are frequent but the footprints can be large. Future geostationary missions will provide moderate but variable spatial scale (e.g., 2-5 km^2) observations at several times of day (i.e., diurnally) for specific regions of the world. With FLEX, a higher spatial resolution will be possible globally, but observations will be less frequent. There is an obvious synergy between these different satellite SIF capabilities for achieving global mapping of vegetation health across the Earth's land surfaces. For future operational monitoring of the health of our ecosystems and food sources, we will want to have both aspects: frequent SIF measurements, at local scales.

8.   Applications of remotely sensed SIF

8.1.   Overview of research and application areas

Remotely detected SIF in terrestrial vegetation has been investigated for use in stress detection, estimation of photosynthesis and GPP, and tracking of temporal and phenological changes in terrestrial vegetation types (Table 4) (A et al., 2015; Frankenberg and Berry, 2018; Malenovský et al., 2009; Meroni et al., 2009; Middleton et al., 2018). These efforts have been encouraged significantly by advances in measurement technologies, retrieval methods, and modelling.

Airborne and satellite-based technological developments have stirred considerable interest in SIF usage for research and operational applications. They have also nudged the scientific community back to the basics, including consideration of fundamental drivers and influential factors for SIF to better understand and interpret remote observations. Field and airborne studies are proving essential to interpretation, valuable for ground-truthing of satellite-derived SIF, and helpful for local-to-landscape scale research. Thus, there is a confluence of investigative and developmental efforts that are synergistic and complementary, and which should expedite further progress.

8.2.   Studies performed and lessons learned

8.2.1.   Ground-based canopy studies—Ground-based canopy studies have produced encouraging findings for using SIF to help quantify photosynthesis (Goulas et al., 2017; Pérez-Priego et al., 2015; Rascher et al., 2009; Rossini et al., 2010; Yang et al., 2015), transpiration (Lu et al., 2018b), and stress effects (Daumard et al., 2010; Xu et al., 2018). They have also demonstrated SIF responsiveness to vegetation phenological changes (Daumard et al., 2012; Middleton et al., 2018), diurnal patterns (Rascher et al., 2009), and seasonal adjustments (Meroni et al., 2011; Hu et al., 2018b; Wyber et al., 2017).

Ground-based investigations have afforded insights relevant to the findings of satellite-based studies showing a relationship (even linear) between far-red SIF and GPP. Links to GPP are recognized now to be based in a strong relationship of far-red SIF to APAR (Section 4.6) (Cui et al., 2017a; Miao et al., 2018; Rossini et al., 2010; Wieneke et al., 2018; Yang et al., 2015; Zhang et al., 2016a). (Note: Fluorescence data often are normalized by incident PAR, APAR, or APAR of photosynthetic components of the vegetation, to obtain quantum yield; Damm et al., 2010; Rascher et al., 2009; Rossini et al., 2010.) There are also reports of SIF being associated with LUE – which is another important variable in GPP estimation (Yang et al., 2015; Zhang et al., 2016a) – especially when APAR is constant (Cheng et al., 2013). However, Wohlfahrt et al. (2018) showed that even with constant APAR, the red or far-red SIF accounted for less than 35% of the variability in GPP, whereas air temperature explained 77%. Empirical studies also report a stronger association of far-red SIF to environmental conditions such as high light, vapour pressure deficit, and nitrogen availability than to GPP (Paul-Limoges et al., 2018; Pérez-Priego et al., 2015).

The form of SIF-GPP relationships found can vary, becoming linear with spatio-temporal scaling or aggregation of SIF data (e.g., Damm et al., 2015a, 2015b; Zhang et al., 2016a). Goulas et al. (2017) further showed for wheat that a simple linear SIF-GPP relationship may

apply only under some circumstances, such as when using far-red SIF and in the presence of a high dynamic range of green biomass and a low range of LUE variation. For crops and mixed forests, Paul-Limoges et al. (2018) found that SIF-GPP association was hyperbolic on stress-free days, and linear on days when conditions were stressful, and was attributed to reduced midday SIF values under stress. Liu et al. (2017) emphasized the importance of considering also the photosynthetic pathway (e.g., C_3, C_4) when analyzing far-red SIF-GPP correlations and diurnal patterns.

Improvement in the correlation between SIF with daily GPP has been achieved by upscaling instantaneous far-red SIF to a daily value. Hu et al. (2018a) suggest that a PAR-based correction factor may be more effective than that based on the ratio of instantaneous cos(SZA) to daily integrated cos(SZA) (e.g., Zhang et al., 2018d), as the latter does not account for cloud cover.

Remotely detected SIF has been shown to be responsive to stress effects and to transpiration. The meta-analysis of A et al. (2015) concluded that canopy red or far-red SIF declines with water stress, while the ratio of red to far-red fluorescence increases with nitrogen deficit. Red and far-red SIF can also be early indicators of water stress and of recovery, but red SIF signals tend to be 'noisier' under stress (Daumard et al., 2010; Xu et al., 2018). Far-red SIF has been used to estimate transpiration during the growing season, but this works only in unstressed vegetation and where leaf area is not high (affects scattering and reabsorption of SIF) (Lu et al., 2018b).

Ground-based studies confirm the influence of chlorophyll content, canopy structure and heterogeneity on SIF, factors which can influence re-absorption and scattering within canopies. Scaling from the leaf to the canopy, the ratio of red to far-red SIF (e.g. F687/F760) has been seen to decrease (Daumard et al., 2012; Fournier et al., 2012), likely because of stronger re-absorption of red fluorescence within the canopy (Louis et al., 2005). The ratio also decreases with increasing leaf chlorophyll content (Daumard et al., 2012) and under high light (Fournier et al., 2012). Another factor is leaf inclination in canopies, which can affect light absorption and also detectability of the SIF signal by the remote sensor. A lower far-red SIF signal has been observed with erectophile as compared to either planophile or spherical leaf orientation (Migliavacca et al., 2017b; Pinto et al., 2017). Such factors contribute to differences in SIF emissions among plant functional types or species, resulting in, for example, higher TOC emissions from some crop species than from broadleaf and needleleaf ones (Rossini et al., 2010).

Studies of diurnal behaviour in SIF have shown that far-red SIF measured across days (inter-day) was affected mainly by chlorophyll content, whereas intra-day changes were influenced by photosynthetic activity (Cogliati et al., 2015a; Pinto et al., 2016). Also, when Paul-Limoges et al. (2018) measured far-red SIF in mixed forest or crop canopies during sunny days, they found SIF varied with vegetation type and the presence or absence of stress; midday depression in SIF was evident in a forest canopy and a barley crop, and was associated with increased NPQ (quantified with PRI). Rascher et al. (2009) found a modest reduction in far-red SIF during early afternoon in winter wheat, coincident with maximal light intensity, but red SIF closely followed PPFD. Louis et al. (2005) saw a decline in

fluorescence at leaf level but not in the canopy of a pine forest, and suggested the cause was perhaps a canopy structural effect that moderated the intensity of light penetrating into deeper canopy layers, thereby reducing the need for NPQ.

Understanding possible NPQ effects is important for interpretation of SIF (Cheng et al., 2013; Daumard et al., 2010; Xu et al., 2018). Using PRI (and modified formulations) to estimate NPQ activity has been helpful in short-term assessments (i.e., over hours or a few days) if chlorophyll and structural traits are stable. Combining SIF with PRI also has helped to improve estimation of gross productivity (e.g., Pérez-Priego et al., 2015; Rossini et al., 2010). The caveat is always that PRI is subject to structural, anisotropic, and illumination effects that can confound links to NPQ behaviour (Schickling et al., 2016). Over longer timeframes, boreal evergreen conifers for instance had PRI better affiliated with seasonally changing carotenoid-to-chlorophyll pigment ratios and shifting leaf albedo during periods of deep cold than with NPQ (Wong and Gamon, 2015). Wyber et al. (2017) observed that at seasonal scales, SIF appears principally correlated with increased *constitutive* (rather than *regulated*) heat dissipation along with changes in leaf irradiance and electron transport rate. Measurements of environmental conditions (e.g., incident light intensity, relative humidity and vapour pressure deficit, air temperature, etc.), additional reflectance-based data, and illumination geometry can be helpful for disentangling some of these temporal effects (Goulas et al., 2017; Middleton et al., 2018; Paul-Limoges et al., 2018).

Regarding phenologically associated SIF responses, Daumard et al. (2012) found that during early growth in sorghum, the red SIF (687 nm) increased rapidly then became saturated, even as far-red SIF (760 nm) continued to increase. During growth, they found that the ratio of red to far-red SIF was lower in the canopy than in leaves and decreased with increasing leaf chlorophyll content (likely increasing re-absorption of red SIF). Meroni et al. (2011) found that for grassland, far-red SIF increased in spring, peaked in summer, then declined in late summer, responding primarily to the amount of chlorophyll in the canopy and the intensity of PPFD. Middleton et al.'s (2018) review of their studies on corn point to the combined effects of water stress, phenological state, and anisotropy on red and far-red SIF.

The relative merits of red and far-red SIF have been examined. A et al. (2018) and the review of Middleton et al. (2018) indicate the value of the ratio of red to far-red SIF for identifying nutrient deficiency (notably nitrogen). Modelling exercises using SCOPE (Verrelst et al., 2016, 2015b) also identify benefits to retrieving both emissions, especially in heterogenous canopies. In comparison, Goulas et al. (2017) found far-red SIF to be more informative for GPP in wheat. The complicating factor for red SIF is its susceptibility to re-absorption which can cause substantive reduction in signal strength at the top of the canopy (Rascher et al., 2009).

Overall, ground-based canopy studies offer good prospects for SIF in research and extended applications, but the influence of extraneous factors must be taken into consideration.

8.2.2. Airborne-based studies—Airborne-based deployments for SIF have demonstrated the added value of imaging and mapping of spatial distribution or spatio-temporal trends for stress detection (Rascher et al., 2015; Zarco-Tejada et al., 2013b). Some

have served as pilot studies for early identification of plant disease (Zarco-Tejada et al., 2018), and in validation of satellite-based SIF retrievals (Sun et al., 2017). They have indicated the utility of having both red and far-red SIF (Middleton et al., 2018; Rossini et al., 2015; Wieneke et al., 2016), established natural quantitative ranges in SIF values in different vegetation types (Garzonio et al., 2017), and helped to clarify diurnal as well as canopy functional versus structural influences on SIF (Middleton et al., 2017; Rascher et al., 2015, 2009; Schickling et al., 2016; Sobrino et al., 2011). Hyperspectral imagery of heterogeneous canopies has revealed vegetation age effects, ecosystem type effects, spatio-temporal scaling on SIF-GPP relationships, and surface anisotropic effects (Colombo et al., 2018; Damm et al., 2015a, 2015b; Zarco-Tejada et al., 2013b).

In stress detection, SIF has been used to detect plant diseases (Calderón et al., 2015, 2013; Hernández-Clemente et al., 2017; Zarco-Tejada et al., 2018), water stress (Panigada et al., 2014; Wieneke et al., 2016; Zarco-Tejada et al., 2012), and herbicide stress (Rossini et al., 2015). Zarco-Tejada et al. (2018) were able to identify incipient infection in olive trees by the pathogen *Xylella fastidiosa*, with prediction accuracies exceeding 80%. Their approach combined fluorescence, thermography, and spectral indicators of chlorophyll content and of vegetation structural changes. They suggested the importance of relying on a spectral bandset combination that enables retrieval of the most sensitive host-plant traits linked with a specific disease. For detection of *Phytophthora* infection, advanced modelling strategies have helped to decipher aggregated heterogeneous pixels of complex vegetation systems (Hernández-Clemente et al., 2017).

With herbicide stress, the red and far-red SIF were able to track variations in photosynthetic efficiency caused by a chemical known to inhibit photosynthesis and selectively intensify fluorescence, whereas surface reflectance was almost unaffected (Rossini et al., 2015). This trial demonstrated the capability of SIF to detect herbicide damage before visual symptoms.

For water stress, it has been shown that a helpful index to support interpretation of SIF changes is the temperature difference between the plant canopy and the surrounding air (Calderón et al. 2015; Panigada et al., 2014; Zarco-Tejada et al., 2012). When stress induces stomatal closure, such as in the cases of water deficit or high vapour pressure deficit, evaporative cooling is restricted and foliage can warm to above air temperature, with a concomitant increase in NPQ and decrease in SIF. The temperature differential is a good alternative or complementary index to PRI (Panigada et al., 2014; Schickling et al., 2016).

SIF retrieved from airborne sensors has also been applied for estimation of GPP, although ground-based canopy approaches and satellite-based methods are perhaps the more obvious choices for this purpose owing to the need for continuous or routine monitoring. Zarco-Tejada et al. (2013b) used UAVs to investigate spatio-temporal trends of far-red SIF (and other narrowband physiological and structural indices, and found canopy SIF and indices related to chlorophyll content and LUE (i.e., PRI) had similar seasonal trend as GPP assessed from EC towers at the time of the flights. Wieneke et al. (2016) used a semi-mechanistic approach with far-red SIF to improve forward modelling of GPP, as did Damm et al. (2015a) using SCOPE for mechanistic understanding and scaling, whereby they revealed a linearization of SIF-GPP relationships with leaf-to-canopy and temporal scaling.

To support future operational applications, Garzonio et al. (2017) studied far-red SIF in different vegetation types (crops, meadow, broadleaf species) using the HyUAS system, and found diverse average SIF values, which could have resulted from strong species-related canopy directional effects. They emphasize the existence of potentially complex overlaps and cross-effects among vegetation types and anticipate valuable developments using integrative methods based on combined analysis of reflectance and SIF.

In applications of SIF, age effects should be considered. In different even-aged stands of loblolly pine forest, young stands had a nearly two-fold higher red SIF yield than plantations older than 10-15 years, but the far-red SIF was constant (Colombo et al., 2018). This effect was interpreted as arising mainly from stomatal limitation in the older vegetatation, with possible residual influences from canopy structure with aging and higher re-absorption of the red SIF. Middleton et al. (2017) assessed the same sites and found that temperature difference between the forest canopy and the surrounding air had stronger daily amplitude change for young versus older stands. It was recommended to combine SIF, reflectance, and canopy structural information to help distinguish such functional and structural effects.

8.2.3.   Satellite-based studies—Over the short lifetime of the global satellite SIF data era, a number of papers have reported that far-red SIF from current satellites have the potential to indicate large-scale photosynthetic activity. First trials with GOSAT showed a high correlation of retrieved SIF with data-driven GPP results at coarse global and annual scales (Frankenberg et al., 2011b), although a per-biome dependency in the SIF-to-GPP ratio was also identified (Guanter et al., 2012). Joiner et al. (2014) analyzed time series of SIF retrievals and compared them with GPP estimates from data-driven and process-based models and measurements from eddy covariance flux towers. Those studies found a good correspondence between the temporal trajectories of retrieved far-red SIF and GPP, which performed as well as remote sensing-based vegetation parameters. Initial indications are that far-red SIF might also contain information about LUE, in this case in tundra vegetation, and this aspects warrants further study (Walther et al., 2018).

Global SIF measurements retrieved from GOSAT and GOME-2 satellites for different ecosystem-level vegetation monitoring applications have been published. Space-based far-red SIF data from GOME-2 were shown to have a higher sensitivity to crop photosynthesis than reflectance-based vegetation indices and data-driven GPP models, the latter failing to capture the high GPP levels found in some areas of the US Corn Belt (Guanter et al., 2014). This finding was applied to produce estimates of crop photosynthetic capacity from SIF (Guan et al., 2016; Zhang et al., 2018a; Zhang et al., 2014). Zhang et al. (2014) tuned the maximal carboxylation capacity (Vcmax) in SCOPE to match simulated-to-satellite observed SIF, and found it improved estimates of GPP compared to using an *a priori* Vcmax. In their approach the values of other parameters of SCOPE were obtained from ancillary satellite data. Guan et al. (2016) used a more direct empirical relation to derive the electron transport rate from observed SIF per unit of APAR. The values of GPP they obtained after multiplication of ETR by a photosynthetic-pathway-dependent electron use efficiency, were an improvement over other satellite-derived approaches considered.

Several satellite-based trials have reported the potential of far-red SIF to indicate drought and temperature stress at ecosystem scales (Berkelhammer et al., 2017; Koren et al., 2018; Song et al., 2018; Sun et al., 2015; Wang et al., 2018, 2016; Wu et al., 2018; Yoshida et al., 2015; Zuromski et al., 2018). Other works have used far-red SIF in monitoring the dynamics of photosynthesis in the Amazon forest (e.g., Alden et al., 2016; Guan et al., 2015; Köhler et al., 2018b; Koren et al., 2018; Lee et al., 2013; Parazoo et al., 2013), high latitude forests (Jeong et al., 2017; Walther et al., 2016), tundra ecosystems (Luus et al., 2017; Walther et al., 2018), dryland ecosystems of southwestern North America (Smith et al., 2018; Zhang et al., 2016c) and across Australia (Ma et al., 2016; Sanders et al., 2016). The links between large-scale far-red SIF and GPP (e.g., He et al., 2017; Koffi et al., 2015; Zhang et al., 2018b) have resulted in the use of SIF to analyse the coupling between carbon and water fluxes at regional to global scales (e.g., Alemohammad et al., 2017; Cui et al., 2017b; Green et al., 2017; Madani et al., 2017; Qiu et al., 2018; Wagle et al., 2016; Zhang et al., 2016b) and to benchmark GPP representations and other parameters in global models (e.g., Chang et al., 2016; Lee et al., 2015; MacBean et al., 2018; Parazoo et al., 2014; Thum et al., 2017; Walker et al., 2017).

Methods to downscale SIF spatially from large-pixel instruments such as GOME-2 to smaller scales using higher-resolution imager data also have been developed (Duveiller and Cescatti, 2016; Gentine and Alemohammad, 2018; Joiner et al., 2018). Lately, the advent of higher spatial resolution data from OCO-2 has enabled new possibilities (e.g., Lu et al., 2018a; Sun et al., 2018; Wei et al., 2018; Zhang et al., 2018c, 2018d), including direct comparisons between far-red SIF retrievals and tower-based GPP for the understanding of SIF-GPP relationships (Sun et al., 2017). For instance, Verma et al. (2017) looked at the effect of environmental conditions on the relationship between far-red SIF and GPP at a grassland site and concluded that the linear relationship is more robust at ecosystem scale than the theory based on leaf-level processes might suggest, but that NPQ (besides APAR and LUE) might need to be explicitly factored into GPP estimations in future analyses. Wood et al. (2017) also took advantage of direct comparisons between SIF derived from OCO-2 observations and tower-based estimates of GPP to investigate the effect of different spatial and temporal scales on SIF-GPP relationships. They found a robust linear GPP-SIF scaling that is sensitive to plant physiology but insensitive to the spatial or temporal scale. Li et al. (2018a) performed similar comparisons between OCO-2 SIF retrievals and tower-level GPP to show a linear relationship between SIF and GPP in temperate forests. It was further shown, in a study of the Indo-Gangetic Plans of India, that far-red SIF is related to net primary productivity (NPP) and that SIF values for C_4-crop-dominated areas were higher than for C_3-crop districts during summer and low during winter (Patel et al., 2018). These types of studies are expected to become more comprehensive as further OCO-2 and also TROPOMI results become available (Li et al., 2018b).

8.3. Summary of SIF drivers and influential factors

For applications, correct interpretation of SIF data is a high priority. Daumard et al. (2012) suggested that the modification of leaf level fluorescence emission by canopy structural attributes is one of the major issues that must be addressed to interpret the fluorescence signal in the context of large-scale remote sensing applications. And recently, a historical

review of global-scale assessment of photosynthesis (Ryu et al., 2019) which included a perspective on the potential of SIF for large-scale estimation of GPP, noted that canopy structure effects – which influence, among other parameters, the escape of SIF to the top of the canopy (Yang and Van der Tol, 2018) – might play a more important role in the SIF-GPP relationship than LUE of canopy fluorescence. That review emphasized the need to understand sources of uncertainty in SIF-photosynthesis relationships at a range of scales, which has also been highlighted by others (Malenovský et al., 2009; Porcar-Castell et al., 2014).

We can suggest a consolidated tabulation of SIF drivers and influential factors, and their relevant spatio-temporal scales (Table 5). These factors could influence light absorption, re-absorption, and scattering, as well as PQ, NPQ, and other photoprotective processes. This information is a synthesis of published papers, as well as our own theoretical understanding (chart updated from Mohammed et al., 2016) (see also reviews by Buschmann et al., 2000; Buschmann and Lichtenthaler, 1998; Cerovic et al., 1999; Donaldson and Williams, 2018; García-Plazaola et al., 2015; Lagorio et al., 2015; Lichtenthaler and Rinderle, 1988; Middleton et al., 2018; Moya and Cerovic, 2004; Porcar-Castell et al., 2014; Schreiber, 2004). The matrix serves as a starting point to stimulate thinking and support research planning, development of hypotheses, design of interpretative frameworks, and refinement of process-based models. Not all factors are expected to be influential or equally important in a given situation.

8.4. Challenges and future directions

Several future directions are indicated for remote sensing of SIF. First, planning in SIF satellite-based research should consider more deliberately the types of influential factors and drivers that could confound interpretation of SIF data in a given situation. This will involve consideration of vegetation, site, and environmental factors; possible ancillary data at relevant spatial scales; and application of current modelling capabilities to analyze key drivers in a given situation (Verrelst et al., 2016, 2015a). A trend in satellite-based Earth Observation has been for acquisition of ancillary and complementary data from multiple sensors and missions, which could accelerate in the future as more technologies operating at diverse spatial scales become available (Lausch et al., 2017, 2016; Scholze et al., 2017). Geostationary satellite-based systems for SIF are a further helpful development to acquire high-temporal-resolution data from space.

Second, the capabilities of the remote sensor and the efficacy of retrieval algorithms must be critically appraised in light of the needs of the particular application and the drivers likely to be encountered. Whereas validation of SIF retrievals is more feasible for airborne systems, it has only begun for satellite-based detection (e.g., Sun et al., 2017). Understandably, this has been a challenge for sensors such as GOME-2, and GOSAT, but prospects are improving with the recent higher-spatial-resolution sensors (Frankenberg and Berry, 2018; Guanter et al., 2015). Acquisition of useful ground-truthing information for the satellites can incorporate data from multiple scales at least initially then in a more streamlined way as appropriate. Development of some airborne sensors as demonstrators of satellite counterparts (e.g., *HyPlant* and CFIS for the FLEX and OCO-2 missions, respectively) is a

modern strategy that assists mission preparatory activities and post-launch validation and interpretation – key topics for the coming years. Accuracies of retrieved SIF and achieving satisfactory representativeness for the vegetation of interest are also of key significance, especially in heterogeneous systems with many extraneous factors, or where SIF signals are inherently low (e.g., at high latitudes) which makes those data prone to systematic errors (Thum et al., 2016). Sensor stability is essential to capture real changes in space and time.

Third, routines to ingest diverse and complex data for SIF analytics and applications may be refined and also streamlined for a range of users to apply the information. SIF is already being incorporated into models addressing leaf and canopy SIF and photosynthesis (Van der Tol et al., 2016, 2014), re-absorption phenomena in leaves and canopies (Romero et al., 2018), and 3D vegetation architecture (Gastellu-Etchegorry et al., 2017). Downstream applications geared to non-expert users will eventually require expedited procedures, perhaps involving the use of model emulators (Rivera et al., 2015; Verrelst and Rivera, 2017).

Finally, it is essential that future efforts continue to encompass the full suite of technological options allowing SIF measurement at different spatial and temporal scales. Hand-held devices, stationary and mobile field systems, UAVs and other airborne sensors, and satellite systems offer versatility and flexibility for SIF analysis. It is anticipated that future developments will offer further options for measurement of related photosynthetic and environmental variables. Some systems will serve the requirements of researchers for comprehensive or sophisticated data while others could be tools for non-expert users. Concomitantly, non-expert users also need to be aware of the possibility for artefacts, and so communication between researchers and downstream users is vital. It is an exciting challenge for scientists and R&D professionals to navigate this rather intricate new avenue of remote sensing with diverse users from forestry, agriculture, and environmental domains.

This paper has focused on the progress in remote sensing of fluorescence in terrestrial vegetation. But chlorophyll fluorescence also has been studied remotely in marine systems for decades, with well-established applications addressing estimation of chlorophyll and productivity (Blondeau-Patissier et al., 2014; Gower, 2016). Until recently, satellite options for coastal and inland water bodies lagged behind those for open waters, according to a review by Mouw et al. (2015), who underscored the need for orbital missions sampling on the scales of high variability encountered in coastal and inland water bodies, with the finer spectral, spatial and temporal detail needed for resampling in a variety of applications. Synergies are possible across land and aquatic satellite missions suitable for analyzing these optically complex waters, such as with the Terra/Aqua (MODerate resolution Imaging Spectroradiometer, MODIS), Sentinel-5/5P (TROPOMI), and FLEX/Sentinel-3 missions.

9. Conclusion

Solar-induced chlorophyll fluorescence is a promising optical indicator of photosynthetic status and related stress effects in terrestrial vegetation. In the last few decades, remote detection of SIF has undergone advances in measurement techniques, retrieval algorithms, and modelling of fluorescence-photosynthesis and radiative transfer processes. Assessment

of SIF is now possible across a range of biological, spatial, and temporal scales, with intriguing applications prospects in terrestrial vegetation science. These developments are noteworthy because SIF is not a very simple phenomenon. To fully realize its potential, developments in all subject areas considered in this review will be needed so that researchers and applied users will be able to utilize SIF with confidence. High-priority topics for the future include understanding and addressing of confounding factors, validation of SIF retrievals and related products, provision of user-friendly modelling and data processing options, and availability of technologies to meet the different needs of researchers and non-expert users. Encouraging results in satellite-based detection of SIF have been reported in the last decade which, in concert with ground-based and airborne methods, opens the door to study actual photosynthetic dynamics in canopies, ecosystems, landscapes, and biomes. In the near future, there will be tailored space-based technologies for SIF emphasizing quantifiably high accuracy, availability of multiple SIF metrics, relevant ancillary data, and high spectral, spatial and temporal resolutions. This will allow satellite-derived SIF to be used in local to landscape scale applications – a benefit already evident with field and airborne-based SIF methods. The vision of the early proposers of satellite-based SIF detection was for optimized systems that would reduce uncertainties – and that vision remains strong today. As remote sensing of SIF matures, such systems will allow a more comprehensive appraisal of the capabilities of SIF and will help to shape the trajectory of the *next* 50 years.

Acknowledgements

Acronyms and abbreviations

ACGS	Atmospheric Carbon dioxide Grating Spectroradiometer
APEX	Airborne Prism EXperiment
BEPS	Boreal Ecosystems Productivity Simulator
BESS	Breathing Earth System Simulator
BOA	Bottom of atmosphere
BRDF	Bidirectional reflectance distribution function
CAM	Crassulacean acid metabolism
CASI	Compact Airborne Spectrographic Imager
CF	Chlorophyll fluorescence

CFIS	Chlorophyll Fluorescence Imaging Spectrometer
CLM	Community Land Model
DART	Discrete Anisotropic Radiative Transfer
DOAS	Differential optical absorption spectroscopy
EnviSat	Environmental Satellite
ESA	European Space Agency
EVI	Enhanced Vegetation Index
fAPAR	Fraction of photosynthetically active radiation absorbed
fAPAR$_{chl}$	Fraction of photosynthetically active radiation absorbed by chlorophyll
FIPAM	Frequency Induced Pulse Amplitude Modulation
FL	Fraunhofer line
FLD	Fluoresence line depth
FLEX	FLuorescence EXplorer
FLORIS	FLuORescence Imaging Spectrometer
FSR	Fluorescence Spectrum Reconstruction
FluorWPS	Fluorescence model with Weighted Photon Spread
FRT	Fluorescence–Reflectance–Transmittance
F-SFM	Full-spectrum spectral fitting method
FWHM	Full width at half maximum
GEO	Geostationary Earth orbit
GeoCARB	Geostationary Carbon Cycle Observatory
GEP	Gross ecosystem productivity
GOSAT	Greenhouse gases Observing SATellite
GOME-2	Global Ozone Monitoring Experiment-2
GPP	Gross primary productivity
KMF	Kubelka-Munk Fluorescence
LEAF-NL	Laser Environmental Active Fluorosensor
LIF	Laser-induced fluorescence

LIFT	Laser-Induced (*or* Light-Induced) Fluorescence Transient
LSM	Land surface model
MERIS	MEdium Resolution Imaging Spectrometer
MetOp-A, -B	Meteorological Operational satellite-A or -B
MODIS	MODerate resolution Imaging Spectroradiometer
MODTRAN	MODerate resolution atmospheric TRANsmission
MTCI	MERIS Terrestrial Chlorophyll Index
MTG-S	Meteosat Third Generation-Sounder
NDVI	Normalized Difference Vegetation Index
NPP	Net primary productivity
NPQ	Non-photochemical quenching
OCO	Orbiting Carbon Observatory
OLCI	Ocean and Land Colour Imager
ORCHIDEE	Organising Carbon and Hydrology In Dynamic Ecosystems
PAM	Pulse-amplitude modulation
PCA	Principal Component Analysis
PMFD	Passive Multi-wavelength Fluorescence Detector
PQ	Photochemical quenching
PRI	Photochemical Reflectance Index
PROSPECT	PROpriétés SPECTrales
PSII, PSI	Photosystem II or I
RC	Reaction center
ROSIS	Reflective Optics System Imaging Spectrometer
RTM	Radiative transfer model
SAIL	Scattering of Arbitrarily Inclined Leaves
S-3	Sentinel-3
SCIAMACHY	SCanning Imaging Absorption spectroMeter for Atmospheric CHartographY
SCOPE	Soil-Canopy-Observation of Photosynthesis and Energy fluxes

SEN2FLEX	SENtinel-2 and FLuorescence EXperiment
S-5P	Sentinel-5 Precursor
SiB2	Simple Biosphere Model (2)
SVAT	Soil-Vegetation-Atmosphere-Transfer
SVD	Singular Value Decomposition
SFM	Spectral fitting methods
SLSTR	Sea and Land Surface Temperature Radiometer
SNR	Signal-to-noise ratio
SR	Spectral resolution
TanSat	Carbon Dioxide Observation Satellite
TANSO-FTS	Thermal And Near-infrared Sensor for carbon Observation – Fourier Transform Spectrometer
TEMPO	Tropospheric Emissions: Monitoring of Pollution
TOA	Top of atmosphere
TOC	Top of canopy
TROPOMI	TROPOspheric Monitoring Instrument
UAS	Unmanned aircraft system
UAV	Unmanned aerial vehicle
VIRAF	Visible Infrared Reflectance Absorbance Fluorescence
VNIR	Visible and near-infrared

References

A A, Malenovský Z, Olejní ková J, Gallé A, Rascher U, Mohammed G, 2015 Meta-analysis assessing potential of steady-state chlorophyll fluorescence for remote sensing detection of plant water, temperature and nitrogen stress. Remote Sens. Environ 168, 420–436.

Agati G, Mazzinghi P, Fusi F, Ambrosini I, 1995 The F685/F730 chlorophyll fluorescence ratio as a tool in plant physiology: Response to physiological and environmental factors. J. Plant Physiol 145, 228–238.

Aldea M, Frank TD, DeLucia EH, 2006 A method for quantitative analysis of spatially variable physiological processes across leaf surfaces. Photosynth. Res 90, 161–172. [PubMed: 17211583]

Alden CB, Miller JB, Gatti LV, Gloor MM, Guan K, Michalak AM, Van der Laan-Luijkx IT, Touma D, Andrews A, Basso LS, Correia CSC, Domingues LG, Joiner J, Krol MC, Lyapustin AI, Peters W, Shiga YP, Thoning K, Van der Velde I, Van Leeuwen TT, Yadav V, and Diffenbaugh NS, 2016 Regional atmospheric CO2 inversion reveals seasonal and geographic differences in Amazon net biome exchange. Glob. Change Biol 22, 3427–3443.

Alemohammad SH, Fang B, Konings AG, Aires F, Green JK, Kolassa J, Miralles D, Prigent C, and Gentine P, 2017 Water, Energy, and Carbon with Artificial Neural Networks (WECANN): A

statistically based estimate of global surface turbulent fluxes and gross primary productivity using solar-induced fluorescence. Biogeosciences 14, 4101–4124. [PubMed: 29290755]

Allen WA, Gausman HW, Richardson AJ, Thomas JR, 1969 Interaction of isotropic light with a compact plant leaf. J. Opt. Soc. Am 59, 1376–1379.

Allen WA, Gayle TV, Richardson AJ, 1970 Plant-canopy irradiance specified by the Duntley equations. J. Opt. Soc. Am 60, 372–376.

Alonso L, Gómez-Chova L, Vila-Francés J, Amorós-López J, Guanter L, Calpe J, Moreno J, 2008 Improved Fraunhofer line discrimination method for vegetation fluorescence quantification. IEEE Geosci. Remote Sens. Lett 5, 620–624.

Anderson MC, 1963 Studies of the woodland light climate: I. The photographic computation of light conditions. J. Ecol 52, 27–41.

Atherton J, Nichol CJ, Porcar-Castell A, 2016 Using spectral chlorophyll fluorescence and the photochemical reflectance index to predict physiological dynamics. Remote Sens. Environ 176, 17–30.

Baker NR, Rosenqvist E, 2004 Applications of chlorophyll fluorescence can improve crop production strategies: An examination of future possibilities. J. Exp. Bot 55, 1607–1621. [PubMed: 15258166]

Ball JT, Woodrow IE, Berry JA, 1987 A model predicting stomatal conductance and its contribution to the control of photosynthesis under different environmental conditions, in: Biggins J (Ed.), Progress in Photosynthesis Research. Martinus Nijhoff, Dordrecht, pp. 221–224.

Barón M, Pineda M, Pérez-Bueno ML, 2016 Picturing pathogen infection in plants. Z. Naturforsch C 71, 355–368.

Bendig J, Gautam D, Malenovský Z, Lucieer A, 2018 Influence of cosine corrector and UAS platform dynamics on airborne spectral irradiance measurements, in: Proc. IEEE International Geoscience and Remote Sensing Symposium (IGARSS), 22-27 July 2018, Valencia, Spain, pp. 8826–8829.

Benediktyová Z, Nedbal L, 2009 Imaging of multi-color fluorescence emission from leaf tissues. Photosynth. Res 102, 169. [PubMed: 19784795]

Bennett DIG, Fleming GR, Amarnath K, 2018 Energy-dependent quenching adjusts the excitation diffusion length to regulate photosynthetic light harvesting. Proc. Natl. Acad. Sci. USA 115, E9523–E9531. [PubMed: 30237283]

Berk A, Conforti P, Kennett R, Perkins T, Hawes F, Van den Bosch J, 2014 MODTRAN6: a major upgrade of the MODTRAN radiative transfer code, in: Proc. SPIE 9088, Algorithms and Technologies for Multispectral, Hyperspectral, and Ultraspectral Imagery XX, 90880H, 13 June 2014.

Berkelhammer M, Stefanescu IC, Joiner J, Anderson L, 2017 High sensitivity of gross primary production in the Rocky Mountains to summer rain. Geophys. Res. Lett 44, 3643–3652.

Berni JAJ, Zarco-Tejada PJ, Suárez L, Fereres E, 2009 Thermal and narrowband multispectral remote sensing for vegetation monitoring from an unmanned aerial vehicle. IEEE Trans. Geosci. Remote Sens 47, 722–738.

Bilger W, Björkman O, 1990 Role of the xanthophyll cycle in photoprotection elucidated by measurements of light-induced absorbance changes, fluorescence and photosynthesis in leaves of *Hedera canariensis*. Photosynth. Res 25, 173–185. [PubMed: 24420348]

Blondeau-Patissier D, Gower JFR, Dekker AG, Phinn SR, Brando VE, 2014 A review of ocean color remote sensing methods and statistical techniques for the detection, mapping and analysis of phytoplankton blooms in coastal and open oceans. Prog. Oceanogr 123, 123–144.

Boardman NK, Thorne SW, Anderson JM, 1966 Fluorescence properties of particles obtained by digitonin fragmentation of spinach chloroplasts. Proc. Natl. Acad. Sci. USA 56, 586–593. [PubMed: 5229980]

Bolhàr-Nordenkampf HR, Long SP, Baker NR, Oquist G, Schreiber U, Lechner EG, 1989 Chlorophyll fluorescence as a probe of the photosynthetic competence of leaves in the field: A review of current instrumentation. Funct. Ecol 3, 497–514.

Bonan GB, 1996 A land surface model (LSM version 1.0) for ecological, hydrological, and atmospheric studies: Technical description and user's guide. NCAR Technical Note NCAR/

TN-417-STR. National Center for Atmospheric Research, Boulder, CO (United States) Climate and Global Dynamics Div, doi: 10.5065/D6DF6P5X.

Bonan GB, Lawrence PJ, Oleson KW, Levis S, Jung M, Reichstein M, Lawrence DM, Swenson SC, 2011 Improving canopy processes in the Community Land Model version 4 (CLM4) using global flux fields empirically inferred from FLUXNET data, J. Geophys. Res. Biogeosci 116, G02014, doi: 10.1029/2010JG001593.

Bornman JF, Vogelmann TC, Martin G, 1991 Measurement of chlorophyll fluorescence within leaves using a fibreoptic microprobe. Plant Cell Environ. 14, 719–725.

Bradbury M, Baker NR, 1981 Analysis of the slow phases of the *in vivo* chlorophyll fluorescence induction curve. Changes in redox state of Photosystem II electron acceptors and fluorescence emission from Photosystem I and II. Biochim. Biophys. Acta 635, 542–551. [PubMed: 7236677]

Brewster D, 1834 On the colours of natural bodies. Trans. R. Soc. Edinburgh 12, 538–545.

Brugnoli E, Björkman O, 1992 Chloroplast movements in leaves: Influence on chlorophyll fluorescence and measurements of light-induced absorbance changes related to pH and zeaxanthin formation. Photosynth. Res 32, 23–35. [PubMed: 24408152]

Burkart A, Schickling A, Cendrero Mateo MP, Wrobel TJ, Rossini M, Cogliati S, Julitta T, Rascher U, 2015 A method for uncertainty assessment of passive sun-induced chlorophyll fluorescence retrieval using an infrared reference light. IEEE Sens. J 15, 4603–4611.

Buschmann C, 2007 Variability and application of the chlorophyll fluorescence emission ratio red/far-red of leaves. Photosynth. Res 92, 261–271. [PubMed: 17525834]

Buschmann C, Lichtenthaler HK, 1988 Reflectance and chlorophyll fluorescence signatures in leaves, in: Lichtenthaler HK (Ed.), Applications of Chlorophyll Fluorescence in Photosynthesis Research, Stress Physiology, Hydrobiology and Remote Sensing. Springer, Dordrecht, pp. 325–332.

Buschmann C, Lichtenthaler HK, 1998 Principles and characteristics of multi-colour fluorescence imaging of plants. J. Plant Physiol 152, 297–314.

Buschmann C, Langsdorf G, Lichtenthaler HK, 2000 Imaging of the blue, green, and red fluorescence emission of plants: An overview. Photosynthetica 38, 483–491.

Buschmann C, Langsdorf G, Lichtenthaler HK, 2009 Blue, green, red, and far-red fluorescence signatures of plant tissues, their multicolor fluorescence imaging, and application for agrofood assessment, in: Zude M (Ed.), Optical Monitoring of Fresh and Processed Agricultural Crops. Taylor & Francis / CRC Press, Boca Raton, pp. 272–319.

Buurman EP, Sanders R, Draaijer A, Gerritsen HC, Van Veen JJF, Houpt PM, Levine YK, 1992 Fluorescence lifetime imaging using a confocal laser scanning microscope. Scanning 14, 155–159.

Calatayud A, Roca D, Martinez PF, 2006 Spatio-temporal variations in rose leaves under water stress conditions studied by chlorophyll fluorescence imaging. Plant Physiol. Biochem 44, 564–573. [PubMed: 17064922]

Calderón R, Navas-Cortés JA, Lucena C, Zarco-Tejada PJ, 2013 High-resolution airborne hyperspectral and thermal imagery for early detection of *Verticillium* wilt of olive using fluorescence, temperature and narrow-band spectral indices. Remote Sens. Environ 139, 231–245.

Calderón R, Navas-Cortés JA, Zarco-Tejada PJ, 2015 Early detection and quantification of *Verticillium* wilt in olive using hyperspectral and thermal imagery over large areas. Remote Sens. 7, 5584–5610.

Campbell PKE, Middleton EM, McMurtrey JE, Corp LA, Chappelle EW, 2007 Assessment of vegetation stress using reflectance or fluorescence measurements. J. Environ. Qual 36, 832–845. [PubMed: 17485715]

Campbell PKE, Middleton EM, Corp LA, Kim MS, 2008 Contribution of chlorophyll fluorescence to the apparent vegetation reflectance. Sci. Total Environ 404, 433–439. [PubMed: 18164750]

Carter GA, Jones JH, Mitchell RJ, Brewer CH, 1996 Detection of solar-excited chlorophyll *a* fluorescence and leaf photosynthetic capacity using a Fraunhofer line radiometer. Remote Sens. Environ 55, 89–92.

Carter GA, Theisen AF, Mitchell RJ, 1990 Chlorophyll fluorescence measured using the Fraunhofer line-depth principle and relationship to photosynthetic rate in the field. Plant Cell Environ. 13, 79–83.

Cazzaniga S, Dall'Osto L, Kong S-G, Wada M, Bassi R, 2013 Interaction between avoidance of photon absorption, excess energy dissipation and zeaxanthin synthesis against photooxidative stress in Arabidopsis. Plant J. 76, 568–579. [PubMed: 24033721]

Cecchi G, Mazzinghi P, Pantani L, Valentini R, Tirelli D, De Angelis P, 1994 Remote sensing of chlorophyll *a* fluorescence of vegetation canopies. 1. Near and far field measurement techniques. Remote Sens. Environ 47, 18–28.

Celesti M, Van der Tol C, Cogliati S, Panigada C, Yang P, Pinto F, Rascher U, Miglietta F, Colombo R, Rossini M, 2018 Exploring the physiological information of sun-induced chlorophyll fluorescence through radiative transfer model inversion. Remote Sens. Environ 215, 97–108.

Cendrero-Mateo MP, Moran MS, Papuga SA, Thorp KR, Alonso L, Moreno J, Ponce-Campos G, Rascher U, Wang G, 2016 Plant chlorophyll fluorescence: Active and passive measurements at canopy and leaf scales with different nitrogen treatments. J. Exp. Bot 67, 275–286. [PubMed: 26482242]

Cerovic ZG, Goulas Y, Gorbunov M, Briantais J-M, Camenen L, Moya I, 1996 Fluorosensing of water stress in plants: Diurnal changes of the mean lifetime and yield of chlorophyll fluorescence, measured simultaneously and at a distance with a τ-LIDAR and a modified PAM-fluorimeter, in maize, sugar beet, and kalanchoe. Remote Sens. Environ 58, 311–321.

Cerovic ZG, Samson G, Morales F, Tremblay N, Moya I, 1999 Ultraviolet-induced fluorescence for plant monitoring: Present state and prospects. Agronomie 19, 543–578.

Chaerle L, Leinonen I, Jones HG, Van der Straeten D, 2007 Monitoring and screening plant populations with combined thermal and chlorophyll fluorescence imaging. J. Exp. Bot 58, 773–784. [PubMed: 17189594]

Chang J, Ciais P, Herrero M, Havlik P, Campioli M, Zhang X, Bai Y, Viovy N, Joiner J, Wang X, Peng S, Yue C, Piao S, Wang T, Hauglustaine DA, Soussana J-F, Peregon A, Kosykh N, Mironycheva-Tokareva N, 2016 Combining livestock production information in a process-based vegetation model to reconstruct the history of grassland management. Biogeosciences, 13, 3757–3776.

Chappelle EW, Williams DL, 1987 Laser-induced fluorescence (LIF) from plant foliage. IEEE Trans. Geosci. Remote Sens, GE-25, 726–736.

Chekalyuk AM, Hoge FE, Wright CW, Swift RN, 2000 Short-pulse pump-and-probe technique for airborne laser assessment of Photosystem II photochemical characteristics. Photosynth. Res 66, 33–44. [PubMed: 16228408]

Chen JM, Liu J, Cihlar J, Goulden ML, 1999 Daily canopy photosynthesis model through temporal and spatial scaling for remote sensing applications. Ecol. Modell 124, 99–119.

Chen JM, Leblanc SG, 1997 A four-scale bidirectional reflectance model based on canopy architecture. IEEE Trans. Geosci. Remote Sens 35, 1316–1337.

Cheng Y-B, Middleton EM, Zhang Q, Huemmrich KF, Campbell PKE, Corp LA, Cook BD, Kustas WP, Daughtry CS, 2013 Integrating solar induced fluorescence and the photochemical reflectance index for estimating gross primary production in a cornfield. Remote Sens. 5, 6857–6879.

Cogliati S, Colombo R, Celesti M, Tagliabue G, Rascher U, Schickling A, Rademske P, Alonso L, Sabater N, Schuettemeyer D, Drusch M, 2018 Red and far-red fluorescence emission retrieval from airborne high-resolution spectra collected by the Hyplant-Fluo sensor, in: Proc. IEEE International Geoscience and Remote Sensing Symposium (IGARSS), 22-27 July 2018, Valencia, Spain, pp. 3935–3938.

Cogliati S, Rossini M, Julitta T, Meroni M, Schickling A, Burkart A, Pinto F, Rascher U, Colombo R, 2015a Continuous and long-term measurements of reflectance and sun-induced chlorophyll fluorescence by using novel automated field spectroscopy systems. Remote Sens. Environ 164, 270–281.

Cogliati S, Verhoef W, Kraft S, Sabater N, Alonso L, Vicent J, Moreno J, Drusch M, Colombo R, 2015b Retrieval of sun-induced fluorescence using advanced spectral fitting methods. Remote Sens. Environ 169, 344–357.

Collatz GJ, Ball JT, Grivet C, Berry JA, 1991 Physiological and environmental regulation of stomatal conductance, photosynthesis and transpiration: A model that includes a laminar boundary layer. Agric. For. Meteorol 54, 107–136.

Colombo R, Celesti M, Bianchi R, Campbell PKE, Cogliati S, Cook BD, Corp LA, Damm A, Domec J-C, Guanter L, Julitta T, Middleton EM, Noormets A, Panigada C, Pinto F, Rascher U, Rossini M, Schickling A, 2018 Variability of sun-induced chlorophyll fluorescence according to stand age-related processes in a managed loblolly pine forest. Glob. Change Biol 24, 2980–2996.

Coppo P, Taiti A, Pettinato L, Francois M, Taccola M, Drusch M, 2017 Fluorescence Imaging Spectrometer (FLORIS) for ESA FLEX mission. Remote Sens. 9, 649.

Corp LA, McMurtrey JE, Middleton EM, Mulchi CL, Chappelle EW, Daughtry CST, 2003 Fluorescence sensing systems: In vivo detection of biophysical variations in field corn due to nitrogen supply. Remote Sens. Environ 86, 470–479.

Cui T, Sun R, Qiao C, Zhang Q, Yu T, Liu G, Liu Z, 2017a Estimating diurnal courses of gross primary production for maize: A comparison of sun-induced chlorophyll fluorescence, light-use efficiency and process-based models. Remote Sens. 9, 1267.

Cui Y, Xiao X, Zhang Y, Dong J, Qin Y, Doughty RB, Zhang G, Wang J, Wu X, Qin Y, Zhou S, Joiner J, Moore B III, 2017b Temporal consistency between gross primary production and solar-induced chlorophyll fluorescence in the ten most populous megacity areas over years. Sci. Rep 7, 14963. [PubMed: 29097731]

Dai Y, Dickinson RE, Wang Y-P, 2004 A Two-Big-Leaf Model for Canopy Temperature, Photosynthesis, and Stomatal Conductance, Journal of Climate 17, 2281–2299.

Dall'Osto L, Cassaniga S, Wada M, Bassi R, 2014 On the origin of a slowly reversible fluorescence decay component in the *Arabidopsis npq4* mutant. Phil. Trans. R. Soc. B 369, 20130221. [PubMed: 24591708]

Damm A, Elbers JA, Erler A, Giolis B, Hamdi K, Hutjes RWA, Kosvancova M, Meroni M, Miglietta F, Moersch A, Moreno J, Schickling A, Sonnenschein R, Udelhoven T, Van der Linden S, Hostert P, Rascher U, 2010 Remote sensing of sun-induced fluorescence to improve modeling of diurnal courses of gross primary production (GPP). Glob. Change Biol 16, 171–186.

Damm A, Erler A, Hillen W, Meroni M, Schaepman ME, Verhoef W, Rascher U, 2011 Modeling the impact of spectral sensor configurations on the FLD retrieval accuracy of sun-induced chlorophyll fluorescence. Remote Sens. Environ 115, 1882–1892.

Damm A, Guanter L, Laurent VCE, Schaepman ME, Schickling A, Rascher U, 2014 FLD-based retrieval of sun-induced chlorophyll fluorescence from medium spectral resolution airborne spectroscopy data. Remote Sens. Environ 147, 256–266.

Damm A, Guanter L, Paul-Limoges E, Van der Tol C, Hueni A, Buchmann N, Eugster W, Ammann C, Schaepman ME, 2015a Far-red sun-induced chlorophyll fluorescence shows ecosystem-specific relationships to gross primary production: An assessment based on observational and modeling approaches. Remote Sens. Environ 166, 91–105.

Damm A, Guanter L, Verhoef W, Schläpfer D, Garbari S, Schaepman ME, 2015b Impact of varying irradiance on vegetation indices and chlorophyll fluorescence derived from spectroscopy data. Remote Sens. Environ 156, 202–215.

Daumard F, Champagne S, Fournier A, Goulas Y, Ounis A, Hanocq J-F, Moya I, 2010 A field platform for continuous measurement of canopy fluorescence. IEEE Trans. Geosci. Remote Sens 48, 3358–3368.

Daumard F, Goulas Y, Champagne S, Fournier A, Ounis A, Olioso A, Moya I, 2012 Continuous monitoring of canopy level sun-induced chlorophyll fluorescence during the growth of a sorghum field. IEEE Trans. Geosci. Remote Sens 50, 4292–4300.

DeEll JR, Toivonen PMA (Eds.), 2003 Practical Applications of Chlorophyll Fluorescence in Plant Biology. Kluwer/Springer, Dordrecht.

Demmig-Adams B, 1990 Carotenoids and photoprotection in plants: A role for the xanthophyll zeaxanthin. Biochim. Biophys. Acta 1020, 1–24.

Demmig-Adams B, Adams WW III, Heber U, Neimanis S, Winter K, Krüger A, Czygan F-C, Bilger W, Björkman O, 1990 Inhibition of zeaxanthin formation and of rapid changes in radiationless energy dissipation by dithiothreitol in spinach leaves and chloroplasts. Plant Physiol. 92, 293–301. [PubMed: 16667274]

Demmig-Adams B, Cohu CM, Muller O, Adams WW III, 2012 Modulation of photosynthetic energy conversion efficiency in nature: From seconds to seasons. Photosynth. Res 113, 75–88. [PubMed: 22790560]

De Pury DGG, Farquhar GD, 1997 Simple scaling of photosynthesis from leaves to canopies without the errors of big-leaf models. Plant Cell Environ. 20, 537–557.

De Wit CT, 1965 Photosynthesis of leaf canopies Agricultural Research Report No. 663. PUDOC, Wageningen.

Disney M, 2016 Remote sensing of vegetation: Potentials, limitations, developments and applications, in: Hikosaka K, Niinemets Ü, Anten NPR (Eds.), Canopy Photosynthesis: From Basics to Applications. Springer, Dordrecht, pp. 289–331.

Disney MI, Lewis P, North PRJ, 2000 Monte Carlo ray tracing in optical canopy reflectance modelling. Remote Sensing Reviews 18, 163–196.

D'Odorico P, Alberti E, Schaepman ME, 2010 In-flight spectral performance monitoring of the Airborne Prism Experiment. Appl. Opt 49, 3082–3091. [PubMed: 20517379]

Dobrowski SZ, Pushnik JC, Zarco-Tejada PJ, Ustin SL, 2005 Simple reflectance indices track heat and water stress-induced changes in steady-state chlorophyll fluorescence at the canopy scale. Remote Sens. Environ 97, 403–414.

Donaldson L, Williams N, 2018 Imaging and spectroscopy of natural fluorophores in pine needles. Plants 7, 10.

Drusch M, Moreno J, Del Bello U, Franco R, Goulas Y, Huth A, Kraft S, Middleton EM, Miglietta F, Mohammed G, Nedbal L, Rascher U, Schüttemeyer D, Verhoef W, 2017 The FLuorescence EXplorer mission concept - ESA's Earth Explorer 8. IEEE Trans. Geosci. Remote Sens 55, 1273–1284.

Du S, Liu L, Liu X, Zhang X, Zhang X, Bi Y, Zhang L, 2018 Retrieval of global terrestrial solar-induced chlorophyll fluorescence from TanSat satellite. Sci. Bull 63, 1502–1512.

Duveiller G, Cescatti A, 2016 Spatially downscaling sun-induced chlorophyll fluorescence leads to an improved temporal correlation with gross primary productivity. Remote Sens. Environ 182, 72–89.

Duysens LNM, 1963 Role of two photosynthetic pigment systems in cytochrome oxidation, pyridine nucleotide reduction, and fluorescence. Proc. R. Soc. Lond. B. 157, 301–313.

Duysens LNM, Sweers HE, 1963 Mechanism of two photochemical reactions in algae as studied by means of fluorescence, in: Japanese Society of Plant Physiologists (Eds.), Studies on Microalgae and Photosynthetic Bacteria. A collection of papers. University of Tokyo Press, Tokyo, Japan, pp. 353–372.

ESA (European Space Agency), undated. Sentinel-5P: TROPOMI. https://www.esa.int/Our_Activities/Observing_the_Earth/Copernicus/Sentinel-5P/Tropomi (accessed 03 February 2019).

ESA (European Space Agency), 2018 FLEX Earth Explorer 8 Mission Requirements Document, Version 3.0, Issue date 05/06/2018, ESA Earth and Mission Science Division, Ref: ESAEOP-SM/2221/MDru-md.

ESA (European Space Agency), 2015 Report for Mission Selection: FLEX. ESA SP-1330/2 (2 volume series), 197 pp., Noordwijk (The Netherlands) https://esamultimedia.esa.int/docs/EarthObservation/SP1330-2_FLEX.pdf

Evain S, Camenen L, Moya I, 2001 Three channels detector for remote sensing of chlorophyll fluorescence and reflectance from vegetation, in: Proc. 8th International Symposium: Physical Measurements and Signatures in Remote Sensing, 8-12 January 2001, Aussois, France, pp. 395–400.

Evain S, Flexas J, Moya I, 2004 A new instrument for passive remote sensing: 2. Measurement of leaf and canopy reflectance changes at 531 nm and their relationship with photosynthesis and chlorophyll fluorescence. Remote Sens. Environ 91, 175–185.

Farquhar GD, Von Caemmerer S, Berry JA, 1980 A biochemical model of photosynthetic CO_2 assimilation in leaves of C_3 species. Planta 149, 78–90. [PubMed: 24306196]

Fawcett D, Verhoef W, Schläpfer D, Schneider FD, Schaepman ME, Damm A, 2018 Advancing retrievals of surface reflectance and vegetation indices over forest ecosystems by combining imaging spectroscopy, digital object models, and 3D canopy modelling. Remote Sens. Environ 204, 583–595.

Fernandez-Jaramillo AA, Duarte-Galvan C, Contreras-Medina LM, Torres-Pacheco I, Romero-Troncoso RJ, Guevara-Gonzalez RG, Millan-Almaraz JR, 2012 Instrumentation in developing chlorophyll fluorescence biosensing: A review. Sensors 12, 11853–11869. [PubMed: 23112686]

Flexas J, Escalona JM, Evain S, Gulías J, Moya I, Osmond CB, Medrano H, 2002 Steady-state chlorophyll fluorescence (Fs) measurements as a tool to follow variations of net CO_2 assimilation and stomatal conductance during water-stress in C_3 plants. Physiol. Plant 114, 231–240. [PubMed: 11903970]

Flexas J, Briantais J-M, Cerovic Z, Medrano H, Moya I, 2000 Steady-state and maximum chlorophyll fluorescence responses to water stress in grapevine leaves: A new remote sensing system. Remote Sens. Environ 73, 283–297.

Fournier A, Daumard F, Champagne S, Ounis A, Goulas Y, Moya I, 2012 Effect of canopy structure on sun-induced chlorophyll fluorescence. ISPRS J. Photogramm. Remote Sens 68, 112–120.

Fournier A, Daumard F, Champagne S, Ounis A, Moya I, Goulas Y, 2014 Effects of vegetation directional reflectance on sun-induced fluorescence retrieval in the oxygen absorption bands, in: Proc. 5th International Workshop on Remote Sensing of Vegetation Fluorescence, 22-24 April 2014, Paris, France.

Franck F, Juneau P, Popovic R, 2002 Resolution of the photosystem I and photosystem II contributions to chlorophyll fluorescence of intact leaves at room temperature. Biochim. Biophys. Acta 1556, 239–246. [PubMed: 12460682]

Franck J, French CS, Puck TT, 1941 The fluorescence of chlorophyll and photosynthesis. J. Phys. Chem 45, 1268–1300.

Franck J, Herzfeld KF, 1941 Contribution to a theory of photosynthesis. J. Phys. Chem 45, 978–1025.

Frankenberg C, Berry J, 2018 Solar induced chlorophyll fluorescence: Origins, relation to photosynthesis and retrieval Reference Module in Earth Systems and Environmental Sciences, Vol. 3, 143–162. Elsevier DOI: 10.1016/B978-0-12-409548-9.10632-3.

Frankenberg C, Butz A, Toon GC, 2011a Disentangling chlorophyll fluorescence from atmospheric scattering effects in O_2 A-band spectra of reflected sun-light. Geophys. Res. Lett 38, L03801.

Frankenberg C, Fisher JB, Worden J, Badgley G, Saatchi SS, Lee J-E, Toon GC, Butz A, Jung M, Kuze A, Yokota T, 2011b New global observations of the terrestrial carbon cycle from GOSAT: Patterns of plant fluorescence with gross primary productivity. Geophys. Res. Lett 38, L17706.

Frankenberg C, Köhler P, Magney TS, Geier S, Lawson P, Schwochert M, McDuffie J, Drewry DT, Pavlick R, Kuhnert A, 2018 The Chlorophyll Fluorescence Imaging Spectrometer (CFIS), mapping far red fluorescence from aircraft. Remote Sens. Environ 217, 523–536.

Frankenberg C, O'Dell C, Berry J, Guanter L, Joiner J, Köhler P, Pollack R, Taylor TE, 2014 Prospects for chlorophyll fluorescence remote sensing from the Orbiting Carbon Observatory-2. Remote Sens. Environ 147, 1–12.

Frankenberg C, O'Dell C, Guanter L, McDuffie J, 2012 Remote sensing of near-infrared chlorophyll fluorescence from space in scattering atmospheres: Implications for its retrieval and interferences with atmospheric CO_2 retrievals. Atmospheric Meas. Tech 5, 2081–2094.

Gamon JA, Field CB, Bilger W, Björkman O, Fredeen AL, Peñuelas J, 1990 Remote sensing of the xanthophyll cycle and chlorophyll fluorescence in sunflower leaves and canopies. Oecol. 85, 1–7.

Gamon JA, Peñuelas J, Field CB, 1992 A narrow-waveband spectral index that tracks diurnal changes in photosynthetic efficiency. Remote Sens. Environ 41, 35–44.

Gamon JA, Serrano L, Surfus JS, 1997 The photochemical reflectance index: An optical indicator of photosynthetic radiation use efficiency across species, functional types, and nutrient levels. Oecol. 112, 492–501.

Gamon JA, Surfus JS, 1999 Assessing leaf pigment content and activity with a reflectometer. New. Phytol 143, 105–117.

Garbulsky MF, Filella I, Peñuelas J, 2014a Recent advances in the estimation of photosynthetic stress for terrestrial ecosystem services related to carbon uptake, in: Alcaraz-Segura D, Di Bella CM, Straschnoy JV (Eds.), Earth Observation of Ecosystem Services. CRC Press, Boca Raton, pp. 39–62.

Garbulsky MF, Filella I, Verger A, Peñuelas J, 2014b Photosynthetic light use efficiency from satellite sensors: From global to Mediterranean vegetation. Environ. Exp. Bot 103, 3–11.

García-Plazaola JI, Fernández-Marín B, Duke SO, Hernández A, López-Arbeloa F, Becerril JM, 2015 Autofluorescence: Biological functions and technical applications. Plant Sci. 236, 136–145. [PubMed: 26025527]

Garzonio R, Di Mauro B, Colombo R, Cogliati S, 2017 Surface reflectance and sun-induced fluorescence spectroscopy measurements using a small hyperspectral UAS. Remote Sens. 9, 472.

Gastellu-Etchegorry JP, Demarez V, Pinel V, Zagolski F, 1996 Modeling radiative transfer in heterogeneous 3-D vegetation canopies. Remote Sens. Environ 58, 131–156.

Gastellu-Etchegorry J-P, Lauret N, Yin T, Landier L, Kallel A, Malenovský Z, Al Bitar A, Aval J, Benhmida S, Qi J, Medjdoub G, Guilleux J, Chavanon E, Cook B, Morton D, Chrysoulakis N, Mitraka Z, 2017 DART: Recent advances in remote sensing data modeling with atmosphere, polarization, and chlorophyll fluorescence. IEEE J. Sel. Top. Appl. Earth Obs. Remote Sens 10, 2640–2649.

Gastellu-Etchegorry J-P, Yin T, Lauret N, Cajgfinger T, Gregoire T, Grau E, Feret J-B, Lopes M, Guilleux J, Dedieu G, Malenovský Z, Cook BD, Morton D, Rubio J, Durrieu S, Cazanave G, Martin E, Ristorcelli T, 2015 Discrete anisotropic radiative transfer (DART 5) for modeling airborne and satellite spectroradiometer and LIDAR acquisitions of natural and urban landscapes. Remote Sens. 7, 1667–1701.

Gautam D, Watson C, Lucieer A, Malenovský Z, 2018 Error budget for geolocation of spectroradiometer point observations from an unmanned aircraft system. Sensors 18, 3465.

Gentine P, Alemohammad SH, 2018 Reconstructed solar-induced fluorescence: A machine learning vegetation product based on MODIS surface reflectance to reproduce GOME-2 solar-induced fluorescence. Geophys. Res. Lett 45, 3136–3146. [PubMed: 30034047]

Genty B, Briantais J-M, Baker NR, 1989 The relationship between the quantum yield of photosynthetic electron transport and quenching of chlorophyll fluorescence. Biochim. Biophys. Acta 990, 87–92.

Genty B, Meyer S, 1995 Quantitative mapping of leaf photosynthesis using chlorophyll fluorescence imaging. Aust. J. Plant Physiol 22, 277–284.

Genty B, Wonders J, Baker NR, 1990 Non-photochemical quenching of F0 in leaves is emission wavelength dependent: Consequences for quenching analysis and its interpretation. Photosynth. Res 26, 133–139. [PubMed: 24420466]

Gerhards M, Schlerf M, Rascher U, Udelhoven T, Juszczak R, Alberti G, Miglietta F, Inoue Y, 2018 Analysis of airborne optical and thermal imagery for detection of water stress symptoms. Remote Sens. 10, 1139.

Gitelson AA, Buschmann C, Lichtenthaler HK, 1999 The chlorophyll fluorescence ratio F_{735}/F_{700} as an accurate measure of the chlorophyll content in plants. Remote Sens. Environ 69, 296–302.

Gitelson AA, Buschmann C, Lichtenthaler HK, 1998 Leaf chlorophyll fluorescence corrected for re-absorption by means of absorption and reflectance measurements. J. Plant Physiology 152, 283–296.

Gómez-Chova L, Alonso-Chorda L, Amoros-Lopez J, Vila-Frances J, Del Valle-Tascon S, Calpe J, Moreno J, 2006 Solar induced fluorescence measurements using a field spectroradiometer. AIP Conference Proceedings 852, 274–281.

Gorbe E, Calatayud A, 2012 Applications of chlorophyll fluorescence imaging technique in horticultural research: A review. Sci. Hort 138, 24–35.

Goss R, Lepetit B, 2015 Biodiversity of NPQ. J. Plant Physiol 172, 13–32. [PubMed: 24854581]

Goudriaan J, 1977 Crop micrometeorology: A simulation study Simulation Monograph. PUDOC, Wageningen.

Goulas Y, Fournier A, Daumard F, Champagne S, Ounis A, Marloie O, Moya I, 2017 Gross primary production of a wheat canopy relates stronger to far red than to red solar-induced chlorophyll fluorescence. Remote Sens. 9, 97.

Govindjee, 1995 Sixty-three years since Kautsky: Chlorophyll *a* fluorescence. Aust. J. Plant Physiol 22, 131–160.

Govindjee, 2004 Chlorophyll *a* fluorescence: A bit of basics and history, in: Papageorgiou GC, Govindjee (Eds.), Chlorophyll Fluorescence: A Signature of Photosynthesis. Kluwer, Dordrecht, pp. 1–41.

Gower J, 2016 On the use of satellite-measured chlorophyll fluorescence for monitoring coastal waters. Int. J. Remote Sens 37, 2077–2086.

Gower JFR and Borstad GA, 1990 Mapping of phytoplankton by solar-stimulated fluorescence using an imaging spectrometer. Int. J. Remote Sens 11, 313–320.

Green JK, Konings AG, Alemohammad SH, Berry J, Entekhabi D, Kolassa J, Lee J-E, Gentine P, 2017 Regionally strong feedbacks between the atmosphere and terrestrial biosphere. Nat. Geosci 10, 410–414. [PubMed: 31709007]

Grossmann K, Frankenberg C, Magney TS, Hurlock SC, Seibt U, Stutz J, 2018 PhotoSpec: A new instrument to measure spatially distributed red and far-red solar-induced chlorophyll fluorescence. Remote Sens. Environ 216, 311–327.

Guan K, Berry JA, Zhang Y, Joiner J, Guanter L, Badgley G, Lobell DB, 2016 Improving the monitoring of crop productivity using spaceborne solar-induced fluorescence. Glob. Change Biol 22, 716–726.

Guan K, Pan M, Li H, Wolf A, Wu J, Medvigy D, Caylor KK, Sheffield J, Wood EF, Malhi Y, Liang M, Kimball JS, Saleska SR, Berry J, Joiner J, Lyapustin AI, 2015 Photosynthetic seasonality of global tropical forests constrained by hydroclimate. Nat. Geosci 8, 284–289.

Guanter L, Aben I, Tol P, Krijger JM, Hollstein A, Köhler P, Damm A, Joiner J, Frankenberg C, Landgraf J, 2015 Potential of the TROPOspheric Monitoring Instrument (TROPOMI) onboard the Sentinel-5 Precursor for the monitoring of terrestrial chlorophyll fluorescence. Atmospheric Meas. Tech 8, 1337–1352.

Guanter L, Alonso L, Gómez-Chova L, Amorós-López J, Vila J, Moreno J, 2007 Estimation of solar-induced vegetation fluorescence from space measurements. Geophys. Res. Lett 34, L08401.

Guanter L, Alonso L, Gómez-Chova L, Meroni M, Preusker R, Fischer J, Moreno J, 2010 Developments for vegetation fluorescence retrieval from spaceborne high-resolution spectrometry in the O_2-A and O_2-B absorption bands. J. Geophys. Res. Atmos 115(D19), 303, D19303.10.1029/2009JD013716.

Guanter L, Frankenberg C, Dudhia A, Lewis PE, Gómez-Dans J, Kuze A, Suto H, Grainger RG, 2012 Retrieval and global assessment of terrestrial chlorophyll fluorescence from GOSAT space measurements. Remote Sens. Environ 121, 236–251.

Guanter L, Zhang Y, Jung M, Joiner J, Voigt M, Berry JA, Frankenberg C, Huete AR, Zarco-Tejada P, Lee J-E, Moran MS, Ponce-Campos G, Beer C, Camps-Valls G, Buchmann N, Dianelle D, Klumpp K, Cescatti A, Baker JM, Griffis TJ, 2014 Global and time-resolved monitoring of crop photosynthesis with chlorophyll fluorescence. Proc. Natl. Acad. Sci. USA 111, E1327–E1333. [PubMed: 24706867]

He L, Chen JM, Liu J, Mo G, Joiner J, 2017 Angular normalization of GOME-2 sun-induced chlorophyll fluorescence observation as a better proxy of vegetation productivity. Geophys. Res. Lett 44, 5691–5699.

Hemphill WR, Watson RD, Bigelow RC, Hessen TD, 1977 Measurement of luminescence of geochemically stressed trees and other materials. U.S. Geological Survey Professional Paper 1015, 93–112.

Hendrickson L, Chow WS, Furbank RT, 2004 A simple alternative approach to assessing the fate of absorbed light energy using chlorophyll fluorescence. Photosynth. Res 82, 73–81. [PubMed: 16228614]

Hernández-Clemente R, North PRJ, Hornero A, Zarco-Tejada PJ, 2017 Assessing the effects of forest health on sun-induced chlorophyll fluorescence using the FluorFLIGHT 3-D radiative transfer model to account for forest structure. Remote Sens. Environ 193, 165–179.

Herwitz SR, Johnson LF, Dunagan SE, Higgins RG, Sullivan DV, Zheng J, Lobitz BM, Leung JG, Gallmeyer BA, Aoyagi M, Slye RE, Brass JA, 2004 Imaging from an unmanned aerial vehicle: Agricultural surveillance and decision support. Comput. Electron. Agr 44, 49–61.

Hoge FE, Swift RN, 1981 Airborne simultaneous spectroscopic detection of laser-induced water Raman backscatter and fluorescence from chlorophyll *a* and other naturally-occurring pigments. Appl. Opt 20, 3197–3205. [PubMed: 20333121]

Hu J, Liu L, Guo J, Du S, Liu X, 2018a Upscaling solar-induced chlorophyll fluorescence from an instantaneous to daily scale gives an improved estimation of the gross primary productivity. Remote Sens. 10, 1663.

Hu J, Liu X, Liu L, Guan L, 2018b Evaluating the performance of the SCOPE model in simulating canopy solar-induced chlorophyll fluorescence. Remote Sens. 10, 250.

Ireland CR, Long SP, Baker NR, 1984 The relationship between carbon dioxide fixation and chlorophyll *a* fluorescence during induction of photosynthesis in maize leaves at different temperatures and carbon dioxide concentrations. Planta 160, 550–558. [PubMed: 24258783]

Jacquemoud S, 1993 Inversion of the PROSPECT + SAIL canopy reflectance model from AVIRIS equivalent spectra: Theoretical study. Remote Sens. Environ 44, 281–292.

Jacquemoud S, Baret F, 1990 PROSPECT: A model of leaf optical properties spectra. Remote Sens. Environ 34, 75–91.

Jacquemoud S, Verhoef W, Baret F, Bacour C, Zarco-Tejada PJ, Asner GP, François C, Ustin SL, 2009 PROSPECT + SAIL models: A review of use for vegetation characterization. Remote Sens. Environ 113, Suppl. 1, S56–S66.

Jeong S-J, Schimel D, Frankenberg C, Drewry DT, Fisher JB, Verma M, Berry JA, Lee J-E, Joiner J, 2017 Application of satellite solar-induced chlorophyll fluorescence to understanding large-scale variations in vegetation phenology and function over northern high latitude forests. Remote Sens. Environ 190, 178–187.

Johnson LF, Herwitz S, Dunagan S, Lobitz B, Sullivan D, Slye R, 2003 Collection of ultra high spatial and spectral resolution image data over California vineyards with a small UAV, in: Proc. 30th International Symposium on Remote Sensing of Environment, 10-14 November 2003, Honolulu (HI), USA, pp. 663–665.

Joiner J, Guanter L, Lindstrot R, Voigt M, Vasilkov AP, Middleton EM, Huemmrich KF, Yoshida Y, Frankenberg C, 2013 Global monitoring of terrestrial chlorophyll fluorescence from moderate spectral resolution near-Infrared satellite measurements: Methodology, simulations, and application to GOME-2. Atmospheric Meas. Tech, 6, 2803–2823.

Joiner J, Yoshida Y, Guanter L, Middleton EM, 2016 New methods for retrieval of chlorophyll red fluorescence from hyperspectral satellite instruments: Simulations and application to GOME-2 and SCIAMACHY. Atmospheric Meas. Tech 9, 3939–3967.

Joiner J, Yoshida Y, Vasilkov AP, Middleton EM, Campbell PKE, Yoshida Y, Kuze A, Corp LA, 2012 Filling-in of near-infrared solar lines by terrestrial fluorescence and other geophysical effects: Simulations and space-based observations from SCIAMACHY and GOSAT. Atmospheric Meas. Tech 5, 809–829.

Joiner J, Yoshida Y, Vasilkov AP, Schaefer K, Jung M, Guanter L, Zhang Y, Garrity S, Middleton EM, Huemmrich KF, Gu L, Belelli Marchesini L, 2014 The seasonal cycle of satellite chlorophyll fluorescence observations and its relationship to vegetation phenology and ecosystem atmosphere carbon exchange. Remote Sens. Environ 152, 375–391.

Joiner J, Yoshida Y, Vasilkov AP, Yoshida Y, Corp LA, Middleton EM, 2011 First observations of global and seasonal terrestrial chlorophyll fluorescence from space. Biogeosciences 8, 637–651.

Joiner J, Yoshida Y, Zhang Y, Duveiller G, Jung M, Lyapustin A, Wang Y, Tucker CJ, 2018 Estimation of terrestrial global gross primary production (GPP) with satellite data-driven models and eddy covariance flux data. Remote Sens. 10, 1346.

Julitta T, Burkart A, Colombo R, Rossini M, Schickling A, Migliavacca M, Cogliati S, Wutzler T, Rascher U, 2017 Accurate measurements of fluorescence in the O_2A and O_2B band using the FloX spectroscopy system - Results and prospects, in: Proc. Potsdam GHG Flux Workshop: From Photosystems to Ecosystems, 24-26 October 2017, Potsdam, Germany https://www.potsdam-flux-workshop.eu/

Julitta T, Corp LA, Rossini M, Burkart A, Cogliati S, Davies N, Hom M, Mac Arthur A, Middleton EM, Rascher U, Schickling A, Colombo R, 2016 Comparison of sun-induced chlorophyll fluorescence estimates obtained from four portable field spectroradiometers. Remote Sens. 8, 122.

Kalaji HM, Goltsev V, Bosa K, Allakhverdiev SI, Strasser RJ, Govindjee, 2012 Experimental *in vivo* measurements of light emission in plants: A perspective dedicated to David Walker. Photosynth. Res 114, 69–96. [PubMed: 23065335]

Kalaji HM, Schansker G, Ladle RJ, Goltsev V, Bosa K, Allakhverdiev SI, Brestic M, Bussotti F, Calatayud A, Dabrowski P, Elsheery NI, Ferroni L, Guidi L, Hogewoning SW, Jajoo A, Misra AN, Nebauer SG, Pancaldi S, Penella C, Poli D, Pollastrini M, Romanowska-Duda ZB, Rutkowska B, Serôdio J, Suresh K, Szulc W, Tambussi E, Yanniccari M, Zivcak M, 2014 Frequently asked questions about *in vivo* chlorophyll fluorescence: Practical issues. Photosynth. Res 122, 121–158. [PubMed: 25119687]

Kalma JD, McVicar TR, McCabe MF, 2008 Estimating land surface evaporation: A review of methods using remotely sensed surface temperature data. Surv. Geophys 29, 421–469.

Kancheva R, Borisova D, Iliev I, Yonova P, 2007 Chlorophyll fluorescence as a quantitative measure of plant stress, in: Bochenek Z (Ed.), New Developments and Challenges in Remote Sensing. Millpress, Rotterdam, pp. 37–43.

Kautsky H, Hirsch A, 1931 Neue versuche zur kohlensäureassimilation. Die Naturwissenschaften 19, 964–964.

Kebabian PL, Theisen AF, Kallelis S, Freedman A, 1999 A passive two-band sensor of sunlight-excited plant fluorescence. Rev. Sci. Instrum 70, 4386–4393.

Keller B, Vass I, Matsubara S, Paul K, Jedmowski C, Pieruschka R, Nedbal L, Rascher U, Muller O, 2018 Maximum fluorescence and electron transport kinetics determined by light induced fluorescence transients (LIFT) for photosynthesis phenotyping. Photosynth. Res, doi: 10.1007/s11120-018-0594-9.

Khosravi N, Vountas M, Rozanov VV, Bracher A, Wolanin A, Burrows JP, 2015 Retrieval of terrestrial plant fluorescence based on the in-filling of far-red Fraunhofer lines using SCIAMACHY observations. Front. Environ. Sci 3, doi: 10.3389/fenvs.2015.00078.

Kim HH, 1973 New algae mapping technique by the use of an airborne laser fluorosensor. Appl. Opt 12, 1454–1459. [PubMed: 20125547]

Kitajima M, Butler WL, 1975 Quenching of chlorophyll fluorescence and primary photochemistry in chloroplasts by dibromothymoquinone. Biochim. Biophys. Acta 376, 105–115. [PubMed: 1125215]

Koffi EN, Rayner PJ, Norton AJ, Frankenberg C, Scholze M, 2015 Investigating the usefulness of satellite-derived fluorescence data in inferring gross primary productivity within the carbon cycle data assimilation system. Biogeosciences 12, 4067–4084.

Köhler P, Guanter L, Joiner J, 2015 A linear method for the retrieval of sun-induced chlorophyll fluorescence from GOME-2 and SCIAMACHY data. Atmospheric Meas. Tech 8, 2589–2608.

Köhler P, Frankenberg C, Magney TS, Guanter L, Joiner J, Landgraf J, 2018a Global retrievals of solar-induced chlorophyll fluorescence with TROPOMI: First results and intersensor comparison to OCO-2. Geophys. Res. Lett, 10.1029/2018GL079031.

Köhler P, Guanter L, Kobayashi H, Walther S, Yang W, 2018b Assessing the potential of sun-induced fluorescence and the canopy scattering coefficient to track large-scale vegetation dynamics in Amazon forests. Remote Sens. Environ 204, 769–785.

Kolber Z, Falkowski PG, 1993 Use of active fluorescence to estimate phytoplankton photosynthesis *in situ*. Limnol. Oceanogr 38, 1646–1665.

Kolber Z, Klimov D, Ananyev G, Rascher U, Berry J, Osmond B, 2005 Measuring photosynthetic parameters at a distance: Laser induced fluorescence transient (LIFT) method for remote measurements of photosynthesis in terrestrial vegetation. Photosynth. Res 84, 121–129. [PubMed: 16049764]

Kolber ZS, Prášil O, Falkowski PG, 1998 Measurements of variable chlorophyll fluorescence using fast repetition rate techniques: Defining methodology and experimental protocols. Biochim. Biophys. Acta 1367, 88–106. [PubMed: 9784616]

Koren G, Van Schaik E, Araújo AC, Boersma KF, Gärtner A, Killaars L, Kooreman ML, Kruijt B, Van der Laan-Luijkx IT, Von Randow C, Smith NE, Peters W, 2018 Widespread reduction in sun-induced fluorescence from the Amazon during the 2015/2016 El Niño. Phil. Trans. R. Soc. B. 373, 20170408. [PubMed: 30297473]

Kotchenova SY, Vermote EF, Levy R, Lyapustin A, 2008 Radiative transfer codes for atmospheric correction and aerosol retrieval: Intercomparison study. Appl. Opt 47, 2215–2226. [PubMed: 18449285]

Krause GH, Weis E, 1991 Chlorophyll fluorescence and photosynthesis: The basics. Annu. Rev. Plant Physiol. Plant Mol. Biol 42, 313–349.

Krause GH, Weis E, 1984 Chlorophyll fluorescence as a tool in plant physiology. II. Interpretation of fluorescence signals. Photosynth. Res 5, 139–157. [PubMed: 24458602]

Krinner G, Viovy N, De Noblet-Ducoudré N, Ogée J, Polcher J, Friedlingstein P, Ciais P, Sitch S, Prentice IC, 2005 A dynamic global vegetation model for studies of the coupled atmosphere-biosphere system. Global Biogeochem. Cycles 19, GB1015.

Kubelka P, Munk F, 1931 An article on optics of paint layers. Z. Tech. Phys 12, 593–601.

Kuckenberg J, Tartachnyk I, Noga G, 2009 Detection and differentiation of nitrogen-deficiency, powdery mildew and leaf rust at wheat leaf and canopy level by laser-induced chlorophyll fluorescence. Biosyst. Eng 103, 121–128.

Kückenbrink D, Hueni A, Schneider F, Damm A, Gastellu-Etchegorry JP, Schaepman ME, Morsdorf F, (in press). Mapping the irradiance field of a single tree: Quantifying vegetation induced adjacency effects. IEEE Trans. Geosci. Remote Sens

Lagorio MG, Cordon GB, Iriel A, 2015 Reviewing the relevance of fluorescence in biological systems. Photochem. Photobiol. Sci 14, 1538–1559. [PubMed: 26103563]

Lang M, Lichtenthaler HK, Sowinska M, Heisel F, Miehé JA, 1996 Fluorescence imaging of water and temperature stress in plant leaves. J. Plant Physiol 148, 613–621.

Lausch A, Bannehr L, Beckmann M, Boehm C, Feilhauer H, Hacker JM, Heurich M, Jung A, Klenke R, Neumann C, Pause M, Rocchini D, Schaepman ME, Schmidtlein S, Schulz K, Selsam P, Settele J, Skidmore AK, Cord AF, 2016 Linking Earth Observation and taxonomic, structural and functional biodiversity: Local to ecosystem perspectives. Ecol. Indic 70, 317–339.

Lausch A, Erasmi S, King DJ, Magdon P, Heurich M, 2017 Understanding forest health with remote sensing-Part II--A review of approaches and data models. Remote Sens. 9, 129.

Lawson T, 2009 Guard cell photosynthesis and stomatal function. New Phytol. 181, 13–34. [PubMed: 19076715]

Lee J-E, Berry JA, Van der Tol C, Yang X, Guanter L, Damm A, Baker I, Frankenberg C, 2015 Simulations of chlorophyll fluorescence incorporated into the Community Land Model version 4. Glob. Chang. Biol 21, 3469–3477. [PubMed: 25881891]

Lee J-E, Frankenberg C, Van der Tol C, Berry JA, Guanter L, Boyce CK, Fisher JB, Morrow E, Worden JR, Asefi S, Badgley G, Saatchi S, 2013 Forest productivity and water stress in Amazonia: Observations from GOSAT chlorophyll fluorescence. Proc. R. Soc. London B Biol. Sci 280, 20130171.

Leuning R, 1995 A critical appraisal of a combined stomatal-photosynthesis model for C_3 plants. Plant Cell Environ. 18, 339–355.

Li X, Xiao J, He B, 2018a Chlorophyll fluorescence observed by OCO-2 is strongly related to gross primary productivity estimated from flux towers in temperate forests. Remote Sens. Environ 204, 659–671.

Li X, Xiao J, He B, Arain MA, Beringer J, Desai AR, Emmel C, Hollinger DY, Krasnova A, Mammarella I, Noe SM, Ortiz PS, Rey-Sanchez AC, Rocha AV, Varlagin A, 2018b Solar-induced chlorophyll fluorescence is strongly correlated with terrestrial photosynthesis for a wide variety of biomes: First global analysis based on OCO-2 and flux tower observations. Glob. Change Biol 24, 3990–4008.

Lichtenthaler HK (Ed.), 1989 Applications of Chlorophyll Fluorescence in Photosynthesis Research, Stress Physiology, Hydrobiology and Remote Sensing. Kluwer, Dordrecht.

Lichtenthaler HK, Rinderle U, 1988 The role of chlorophyll fluorescence in the detection of stress conditions in plants. Crit. Rev. Anal. Chem 19, Suppl. 1, S29–S85.

Liu J, Chen JM, Cihlar J, Park WM, 1997 A process-based boreal ecosystem productivity simulator using remote sensing inputs. Remote Sens. Environ 62, 158–175.

Liu L, Guan L, Liu X, 2017 Directly estimating diurnal changes in GPP for C3 and C4 crops using far-red sun-induced chlorophyll fluorescence. Agric. For. Meteorol 232, 1–9.

Liu L, Zhang Y, Wang J, Zhao C, 2005 Detecting solar-induced chlorophyll fluorescence from field radiance spectra based on the Fraunhofer line principle. IEEE Trans. Geosci. Remote Sens 43, 827–832.

Liu X, Guanter L, Liu L, Damm A, Malenovský Z, Rascher U, Peng D, Du S, Gastellu-Etchegorry J-P, (in press). Downscaling of solar-induced chlorophyll fluorescence from canopy level to photosystem level using a random forest model. Remote Sens. Environ 10.1016/j.rse.2018.05.035.

Liu X, Liu L, 2018 Influence of the canopy BRDF characteristics and illumination conditions on the retrieval of solar-induced chlorophyll fluorescence. Int. J. Remote Sens 39, 1782–1799.

Liu X, Liu L, Zhang S, Zhou X, 2015 New spectral fitting method for full-spectrum solar-induced chlorophyll fluorescence retrieval based on principal components analysis. Remote Sens. 7, 10626–10645.

Louis J, Cerovic ZG, Moya I, 2006 Quantitative study of fluorescence excitation and emission spectra of bean leaves. J. Photochem. Photobiol 85, 65–71.

Louis J, Ounis A, Ducruet J-M, Evain S, Laurila T, Thum T, Aurela M, Wingsle G, Alonso L, Pedrós R, Moya I, 2005 Remote sensing of sunlight-induced chlorophyll fluorescence and reflectance of Scots pine in the boreal forest during spring recovery. Remote Sens. Environ 96, 37–48.

Lu X, Cheng X, Li X, Tang J, 2018a Opportunities and challenges of applications of satellite-derived sun-induced fluorescence at relatively high spatial resolution. Sci. Total Environ 619-620, 649–653. [PubMed: 29156283]

Lu X, Liu Z, An S, Miralles DG, Maes W, Liu Y, Tang J, 2018b Potential of solar-induced chlorophyll fluorescence to estimate transpiration in a temperate forest. Agric. For. Meteorol 252, 75–87.

Lucieer A, Malenovský Z, Veness T, Wallace L, 2014 HyperUAS—Imaging spectroscopy from a multirotor unmanned aircraft system. J. Field Robot 31, 571–590.

Luus KA, Commane R, Parazoo NC, Benmergui J, Euskirchen ES, Frankenberg C, Joiner J, Lindaas J, Miller CE, Oechel WC, Zona D, Wofsy S, Lin JC, 2017 Tundra photosynthesis captured by satellite-observed solar-induced chlorophyll fluorescence. Geophys. Res. Lett 44, 1564–1573.

Ma X, Huete A, Cleverly J, Eamus D, Chevallier F, Joiner J, Poulter B, Zhang Y, Guanter L, Meyer W, Xie Z, Ponce-Campos G, 2016 Drought rapidly diminishes the large net CO_2 uptake in 2011 over semi-arid Australia. Sci. Rep 6, 37747. [PubMed: 27886216]

Mac Arthur A, Robinson I, Rossini M, Davies N, McDonald K, 2014 A dual-field-of-view spectrometer system for reflectance and fluorescence measurements (Piccolo Doppio) and correction of etaloning, in: Proc. 5th International Workshop on Remote Sensing of Vegetation Fluorescence, 22-24 April 2014, Paris, France.

MacBean N, Maignan F, Bacour C, Lewis P, Peylin P, Guanter L, Köhler P, Gomez-Dans J, Disney M, 2018 Strong constraint on modelled global carbon uptake using solar-induced chlorophyll fluorescence data. Sci. Rep 8, 1973. [PubMed: 29386626]

Madani N, Kimball JS, Jones LA, Parazoo NC, Guan K, 2017 Global analysis of bioclimatic controls on ecosystem productivity using satellite observations of solar-induced chlorophyll fluorescence. Remote Sens. 9, 530.

Magnani F, Olioso A, Demarty J, Germain V, Verhoef W, Moya I, Goulas Y, Cecchi G, Agati G, Zarco-Tejada P, Mohammed G, Van der Tol C, 2009 Assessment of Vegetation Photosynthesis Through Observation of Solar Induced Fluorescence From Space, Final Report. ESA/ESTEC Contract No. 20678/07/NL/HE. 256 p.

Magnani F, Raddi S, Mohammed G, Middleton EM, 2014 Let's exploit available knowledge on vegetation fluorescence. Proc. Natl. Acad. Sci. USA 111, E2510. [PubMed: 24927587]

Magney TS, Frankenberg C, Fisher JB, Sun Y, North GB, Davis TS, Kornfeld A, Siebke K, 2017 Connecting active to passive fluorescence with photosynthesis: A method for evaluating remote sensing measurements of Chl fluorescence. New Phytol. 215, 1594–1608. [PubMed: 28664542]

Maier SW, 2002 Remote sensing and modelling of solar induced fluorescence, in: Proc. FLEX Workshop, 19-20 June 2002, Noordwijk, Netherlands European Space Agency, (Special Publication) ESA SP, Issue 527.

Maier SW, Günther KP, Stellmes M, 2003 Sun-induced fluorescence: A new tool for precision farming, in: Schepers J, VanToai T (Eds.), Digital Imaging and Spectral Techniques: Applications

to Precision Agriculture and Crop Physiology. ASA Spec. Publ. 66. ASA, CSSA, and SSSA; Madison (Wisconsin), USA, pp. 209–222.

Malenovský Z, Lucieer A, King DH, Turnbull JD, Robinson SA, 2017 Unmanned aircraft system advances health mapping of fragile polar vegetation. Methods Ecol. Evol 8, 1842–1857.

Malenovský Z, Mishra KB, Zemek F, Rascher U, Nedbal L, 2009 Scientific and technical challenges in remote sensing of plant canopy reflectance and fluorescence. J. Exp. Bot 60, 2987–3004. [PubMed: 19465688]

Matsubara S, Morosinotto T, Osmond CB, Bassi R, 2007 Short- and long-term operation of the lutein-epoxide cycle in light-harvesting antenna complexes. Plant Physiol. 144, 926–941. [PubMed: 17384157]

Maxwell K, Johnson GN, 2000 Chlorophyll fluorescence -- a practical guide. J. Exp. Bot 51, 659–668. [PubMed: 10938857]

Mazzoni M, Falorni P, Del Bianco S, 2008 Sun-induced leaf fluorescence retrieval in the O_2-B atmospheric absorption band. Opt. Express 16, 7014–7022. [PubMed: 18545405]

Mazzoni M, Falorni P, Verhoef W, 2010 High-resolution methods for fluorescence retrieval from space. Opt. Express 18, 15649–15643. [PubMed: 20720947]

Mazzoni M, Meroni M, Fortunato C, Colombo R, Verhoef W, 2012 Retrieval of maize canopy fluorescence and reflectance by spectral fitting in the O_2-A absorption band. Remote Sens. Environ 124, 72–82.

McAlister ED, Myers J, 1940 Time course of photosynthesis and fluorescence. Science 92, 241–243. [PubMed: 17814310]

McFarlane JC, Watson RD, Theisen AF, Jackson RD, Ehrler WL, Pinter PJ, Idso SB, Reginato RJ, 1980 Plant stress detection by remote measurement of fluorescence. Appl. Opt 19, 3287–3289. [PubMed: 20234608]

Meijer Y, Ingmann P, Langen J, Veihelmann B, Zehner C, 2014 Potential of current and future Copernicus satellite missions for low spatial resolution fluorescence monitoring, in: Proceedings 5th International Workshop on Remote Sensing of Vegetation Fluorescence, 22-24 April 2014, Paris, France, http://www.congrexprojects.com/2014-events/14c04/proceedings.

Meroni M, Barducci A, Cogliati S, Castagnoli F, Rossini M, Busetto L, Migliavacca M, Cremonese E, Galvagno M, Colombo R, Morra di Cella U, 2011 The hyperspectral irradiometer, a new instrument for long-term and unattended field spectroscopy measurements. Rev. Sci. Instrum 82, 043106. [PubMed: 21528994]

Meroni M, Busetto L, Colombo R, Guanter L, Moreno J, Verhoef W, 2010 Performance of Spectral Fitting Methods for vegetation fluorescence quantification. Remote Sens. Environ 114, 363–374.

Meroni M, Colombo R, 2006 Leaf level detection of solar induced chlorophyll fluorescence by means of a subnanometer resolution spectroradiometer. Remote Sens. Environ 103, 438–448.

Meroni M, Colombo R, 2009 3S: A novel program for field spectroscopy. Comput. Geosci 35, 1491–1496.

Meroni M, Rossini M, Guanter L, Alonso L, Rascher U, Colombo R, Moreno J, 2009 Remote sensing of solar-induced chlorophyll fluorescence: Review of methods and applications. Remote Sens. Environ 113, 2037–2051.

Meroni M, Rossini M, Picchi V, Panigada C, Cogliati S, Nali C, Colombo R, 2008 Assessing steady-state fluorescence and PRI from hyperspectral proximal sensing as early indicators of plant stress: The case of ozone exposure. Sensors 8, 1740–1754. [PubMed: 27879790]

Miao G, Guan K, Yang X, Bernacchi CJ, Berry JA, DeLucia EH, Wu J, Moore CE, Meacham K, Cai Y, Peng B, Kimm H, Masters MD, 2018 Sun-induced chlorophyll fluorescence, photosynthesis, and light use efficiency of a soybean field from seasonally continuous measurements. J. Geophys. Res. Biogeosci 123, 610–623.

Middleton EM, Chappelle EW, Cannon TA, Adamse P, Britz SJ, 1996 Initial assessment of physiological response to UV-B irradiation using fluorescence measurements. J. Plant Physiol 148, 69–77.

Middleton EM, Corp LA, Campbell PKE, 2008 Comparison of measurements and FluorMOD simulations for solar-induced chlorophyll fluorescence and reflectance of a corn crop under nitrogen treatments. Int. J. Remote Sens 29, 5193–5213.

Middleton EM, Huemmrich KF, Zhang Q, Campbell PKE, Landis DR, 2018 Spectral bioindicators of photosynthetic efficiency and vegetation stress, Chap. 5 in: Thenkabail PS, Lyon JG, Huete A (Eds.), Hyperspectral Remote Sensing of Vegetation (2nd Edition), Vol. III: Biophysical and Biochemical Characterization and Plant Species Studies. Taylor & Francis, New York, 133–179

Middleton EM, Kim MS, Krizek DT, Bajwa RK, 2005 Evaluating UV-B effects and EDU protection in soybean leaves using fluorescence. Photochem. Photobiol 81, 1075–1085. [PubMed: 16022558]

Middleton EM, Rascher U, Corp LA, Huemmrich KF, Cook BD, Noormets A, Schickling A, Pinto F, Alonso L, Damm A, Guanter L, Colombo R, Campbell PKE, Landis DR, Zhang Q, Rossini M, Schuettemeyer D, Bianchi R, 2017 The 2013 FLEX–US airborne campaign at the Parker Tract loblolly pine plantation in North Carolina, USA. Remote Sens. 9, 612.

Migliavacca M, El Madany T, Perez-Priego O, Carrara A, Hammer T, Henkel K, Kolle O, Luo Y, Moreno G, Morris K, Nair R, Schrumpf M, Wutzler T, Reichstein M, 2017a Effects of a large scale nitrogen and phosphorus fertilization on the ecosystem functioning of a Mediterranean tree-grass ecosystem, in: Proc. 19th EGU General Assembly, EGU2017, 23-28 April 2017, Vienna, Austria, p. 11586.

Migliavacca M, Perez-Priego O, Rossini M, El-Madany TS, Moreno G, Van der Tol C, Rascher U, Berninger A, Bessenbacher V, Burkart A, Carrara A, Fava F, Guan J-H, Hammer TW, Henkel K, Juarez-Alcalde E, Julitta T, Kolle O, Martin MP, Musavi T, Pacheco-Labrador J, Pérez-Burgueño A, Wutzler T, Zaehle S, Reichstein M, 2017b Plant functional traits and canopy structure control the relationship between photosynthetic CO_2 uptake and far-red sun-induced fluorescence in a Mediterranean grassland under different nutrient availability. New Phytol. 214, 1078–1091. [PubMed: 28181244]

Miller J, Berger M, Goulas Y, Jacquemoud S, Louis J, Mohammed G, Noise N, Moreno J, Moya I, Pédros R, Verhoef W, Zarco-Tejada P, 2005 Development of a Vegetation Fluorescence Canopy Model, Final Report. ESA/ESTEC Contract No. 16365/02/NL/FF. 138 p.

Mohammed GH, Binder WD, Gillies SL, 1995 Chlorophyll fluorescence: A review of its practical forestry applications and instrumentation. Scandinavian Journal of Forest Research 10, 383–410.

Mohammed GH, Colombo R, Moreno J, Van der Tol C, Rascher U, A A, Alonso L, Celesti M, Cogliati S, Damm A, Fawcett D, Gomez-Dans J, Henry C, Lewis P, MacBean N, Magnani F , Malaprade J, Matveeva M, Olejní ková J, Pernokis D, Pinto F, Raddi S, Rajh Vilfan N, Rivera JP, Rossini M, Sabater N, Schickling A, Tenjo C, Verhoef W, Verrelst J, Vicent Servera J, Drusch M, 2016 FLEX Bridge Study, Final Report. ESA/ESTEC Contract No. 4000112341/14/NL/FF/gp. 187 p.

Mohammed GH, Goulas Y, Magnani F, Moreno J, Olejní ková J, Rascher U, Van der Tol C, Verhoef W, A A, Daumard F, Gallé A, Malenovský Z, Pernokis D, Rivera JP, Verrelst J, Drusch M, 2014 FLEX/Sentinel-3 Tandem Mission Photosynthesis Study, Final Report. ESA/ESTEC Contract No. 4000106396/12/NL/AF. 159 p.

Mohammed GH, Zarco-Tejada P, Miller JR, 2003 Applications of chlorophyll fluorescence in forestry and ecophysiology, in: DeEll JR, Toivonen PMA (Eds.), Practical Applications of Chlorophyll Fluorescence in Plant Biology. Kluwer/Springer, Dordrecht, pp. 79–124.

Mohanty P, Braun BZ, Govindjee, Thornber JP, 1972 Chlorophyll fluorescence characteristics of system I chlorophyll *a*-protein complex and system II particles at room and liquid nitrogen temperatures. Plant Cell Physiol. 13, 81–91.

Moore B III, Crowell S, 2018 The GeoCarb mission, in: Proc. 98th Amer. Meteor. Soc. Annual meeting, 7-11 January 2018, Austin, TX.

Moreno J, Asner GP, Bach H, Belenguer T, Bell A, Buschmann C, Calera A, Calpe J, Campbell P, Cecchi G, Colombo R, Corp LA, Court A, Cutter MA, Disney M, Dudelzak A, D'Urso G, Fernandes R, Flexas J, Gege P, Gielen B, Gitelson A, Gloor EU, Gower J, Green RO, Hill J, Jacquemoud S, Jia L, Kneubühler M, Laurila T, Lewis P, Lobb D, Magnani F, Maier SW, Marek MV, Martinez A, Martinez-Cobo P, Mazzinghi P, Menenti M, Merton R, Middleton E, De Miguel E, Miller J, Mohammed G, Milton EJ, Morales F, Moya I, Nedbal L, Knorr W, Ottlé C, Olioso A, Pace S, Palucci A, Pedros R, Peltoniemi J, Peñuelas J, Plaza A, Polcher J, Rascher U, Reuter R, Rosema A, Roujean J-L, Saito Y, Saugier B, Schaepman M, Serrano JB, Settle JJ, Sierra M, Sobrino J, Stoll M-P, Su ZB, Tobehn C, Tremblay N, Valcke R, Verhoef W, Veroustraete F, Verstraete M, Zarco-Tejada P, 2006 FLuorescence EXplorer (FLEX): An optimised payload to

map vegetation photosynthesis from space, in: Proc. 57th International Astronautical Congress, 2-6 October 2006, Valencia, Spain.

Moreno J, Rascher U, Goulas Y, Colombo R, Verhoef W, Damm A, Alonso L, Cogliati S, Daumard F, Rivera JP, Sabater N, Schickling A, Tenjo C, Timmermans J, Verrelst J, Drusch M, 2014 FLEX/S3 Tandem Mission Performance Analysis and Requirements Consolidation Study (PARCS), Final Report. ESA/ESTEC Contract No. 4000105078/11/NL/AF. 141 p.

Morris JM, Fleming GR, 2018 Quantitative modeling of energy dissipation in *Arabidopsis thaliana*. Environ. Exp. Bot 154, 99–109.

Mouw CB, Greb S, Aurin D, DiGiacomo PM, Lee Z, Twardowski M, Binding C, Hu C, Ma R, Moore T, Moses W, Craig SE, 2015 Aquatic color radiometry remote sensing of coastal and inland waters: Challenges and recommendations for future satellite missions. Remote Sens. Environ 160, 15–30.

Moya I, Camenen L, Evain S, Goulas Y, Cerovic ZG, Latouche G, Flexas J, Ounis A, 2004 A new instrument for passive remote sensing. 1. Measurements of sunlight-induced chlorophyll fluorescence. Remote Sens. Environ 91, 186–197.

Moya I, Cerovic ZG, 2004 Remote sensing of chlorophyll fluorescence: Instrumentation and analysis, in: Papageorgiou GC, Govindjee (Eds.), Chlorophyll *a* Fluorescence: A Signature of Photosynthesis. Springer, Dordrecht, pp. 429–445.

Moya I, Daumard F, Moise N, Ounis A, Goulas Y, 2006 First airborne multiwavelength passive chlorophyll fluorescence measurements over La Mancha (Spain) fields, in: Proc. 2nd International Symposium on Recent Advances In Quantitative Remote Sensing, 25-29 September 2006, Torrent (Valencia), Spain, pp. 820–825.

Moya I, Goulas Y, Morales F, Camenen L, Guyot G, Schmuck G, 1995 Remote sensing of time-resolved chlorophyll fluorescence and back-scattering of the laser excitation by vegetation. EARSeL Advances in Remote Sensing 3, 188–197.

Moya I, Guyot G, Goulas Y, 1992 Remotely sensed blue and red fluorescence emission for monitoring vegetation. ISPRS J. Photogram. Remote Sens 47, 205–231.

Müller NJC, 1874 Beziehungen zwischen assimilation, absorption und fluoreszenz im chlorophyll des lebenden blattes. Jahrbücher für Wissenchaftliche Botanik 9, 42–49.

Murata N, Nishimura M, Tamiya A, 1966 Fluorescence of chlorophyll in photosynthetic systems. III. Emission and action spectra of fluorescence—Three emission bands of chlorophyll *a* and the energy transfer between two pigment systems. Biochim. Biophys. Acta 126, 234–243. [PubMed: 5971849]

Murchie EH, Lawson T, 2013 Chlorophyll fluorescence analysis: A guide to good practice and understanding some new applications. J. Exp. Bot 64, 3983–3998. [PubMed: 23913954]

Nedbal L, Trtílek M, Kaftan D, 1999 Flash fluorescence induction: A novel method to study regulation of photosystem II. J. Photochem. Photobiol. B 48, 154–157.

Nedbal L, Soukupová J, Kaftan D, Whitmarsh J, Trtílek M, 2000 Kinetic imaging of chlorophyll fluorescence using modulated light. Photosynth. Res 66, 3–12. [PubMed: 16228406]

Nedbal L, Whitmarsh J, 2004 Chlorophyll fluorescence imaging of leaves and fruits, in: Papageorgiou GC, Govindjee (Eds.), Chlorophyll *a* Fluorescence: A Signature of Photosynthesis. Springer, Dordrecht, pp. 389–407.

Neville RA, Gower JFR, 1977 Passive remote-sensing of phytoplankton via chlorophyll *a* fluorescence. J. Geophys. Res 82, 3487–3493.

Ni-Meister W, Yang W, Kiang NY, 2010 A clumped-foliage canopy radiative transfer model for a global dynamic terrestrial ecosystem model. I: Theory. Agric. For. Meteorol 150, 881–894.

Norman JM, 1979 Modeling the complete crop canopy, in: Barfield BJ Gerber JF (Eds.), Modification of the Aerial Environment of Plants Am. Soc. Agric. Eng, St Joseph, MI, pp. 249–277.

North PRJ, 1996 Three-dimensional forest light interaction model using a Monte Carlo method. IEEE Trans. Geosci. Remote Sens 34, 946–956.

Norton AJ, Rayner PJ, Koffi EN, Scholze M, 2018 Assimilating solar-induced chlorophyll fluorescence into the terrestrial biosphere model BETHY-SCOPE v1.0: Model description and information content. Geosci. Model Dev 11, 1517–1536.

O'Brien DM, Polonsky IN, Utembe SR, Rayner PJ, 2016 Potential of a geostationary geoCARB mission to estimate surface emissions of CO_2, CH_4 and CO in a polluted urban environment: Case study Shanghai. Atmospheric Meas. Tech 9, 4633–4654.

Omasa K, Hosoi F, Konishi A, 2007 3D lidar imaging for detecting and understanding plant responses and canopy structure. J. Exp. Bot 58, 881–898. [PubMed: 17030540]

Öquist G, Wass R, 1988 A portable, microprocessor operated instrument for measuring chlorophyll fluorescence kinetics in stress physiology. Physiol. Plant 73, 211–217.

Osmond B, Schwartz O, Gunning B, 1999 Photoinhibitory printing on leaves, visualised by chlorophyll fluorescence imaging and confocal microscopy, is due to diminished fluorescence from grana. Aust. J. Plant Physiol 26, 717–724.

Ounis A, Bach J, Mahjoub A, Daumard F, Moya I, Goulas Y, 2016 Combined use of LIDAR and hyperspectral measurements for remote sensing of fluorescence and vertical profile of canopies. Revista de Teledetección 45, Special Issue, 87–94.

Ounis A, Cerovic ZG, Briantais JM, Moya I, 2001 Dual-excitation FLIDAR for the estimation of epidermal UV absorption in leaves and canopies. Remote Sens. Environ 76, 33–48.

Oxborough K, 2004 Imaging of chlorophyll *a* fluorescence: Theoretical and practical aspects of an emerging technique for the monitoring of photosynthetic performance. J. Exp. Bot 55, 1195–1205. [PubMed: 15107453]

Palombi L, Cecchi G, Lognoli D, Raimondi V, Toci G, Agati G, 2011 A retrieval algorithm to evaluate the Photosystem I and Photosystem II spectral contributions to leaf chlorophyll fluorescence at physiological temperatures. Photosynth. Res 108, 225–239. [PubMed: 21866392]

Panigada C, Rossini M, Meroni M, Cilia C, Busetto L, Amaducci S, Boschetti M, Cogliati S, Picchi V, Pinto F, Marchesi A, Colombo R, 2014 Fluorescence, PRI and canopy temperature for water stress detection in cereal crops. Int. J. Appl. Earth Obs. Geoinf 30, 167–178.

Paul-Limoges E, Damm A, Hueni A, Liebische F, Eugster W, Schaepman ME, Buchmann N, 2018 Effect of environmental conditions on sun-induced fluorescence in a mixed forest and a cropland. Remote Sens. Environ 219, 310–323.

Papageorgiou G, 1975 Chlorophyll fluorescence: An intrinsic probe of photosynthesis, in: Govindjee (Ed.), Bioenergetics of photosynthesis. Academic Press, New York, pp. 319–371.

Papageorgiou G, Govindjee (Eds.), 2004 Chlorophyll *a* Fluorescence: A Signature of Photosynthesis. Springer, Dordrecht.

Parazoo NC, Bowman K, Fisher JB, Frankenberg C, Jones DBA, Cescatti A, Pérez-Priego O, Wohlfahrt G, Montagnani L, 2014 Terrestrial gross primary production inferred from satellite fluorescence and vegetation models. Glob. Change Biol 20, 3103–3121.

Parazoo NC, Bowman K, Frankenberg C, Lee J-E, Fisher JB, Worden J, Jones DBA, Berry J, Collatz GJ, Baker IT, Jung M, Liu J, Osterman G, O'Dell C, Sparks A, Butz A, Guerlet S, Yoshida Y, Chen H, Gerbig C, 2013 Interpreting seasonal changes in the carbon balance of southern Amazonia using measurements of XCO_2 and chlorophyll fluorescence from GOSAT. Remote Sens. Environ 40, 2829–2833.

Patel NR, Padalia H, Devadas R, Huete A, Kumar AS, Krishna Murthy YVN, 2018 Estimating net primary productivity of croplands in Indo-Gangetic Plains using GOME-2 sun-induced fluorescence and MODIS NDVI. Curr. Sci 114, 1333–1337.

Pedrós R, Goulas Y, Jacquemoud S, Louis J, Moya I, 2010 FluorMODleaf: A new leaf fluorescence emission model based on the PROSPECT model. Remote Sens. Environ 114, 155–167.

Pedrós R, Moya I, Goulas Y, Jacquemoud S, 2008 Chlorophyll fluorescence emission spectrum inside a leaf. Photochem. Photobiol. Sci 7, 498–502. [PubMed: 18385895]

Peñuelas J, Llusia J, Piñol J, Filella I, 1997 Photochemical reflectance index and leaf photosynthetic radiation-use-efficiency assessment in Mediterranean trees. Int. J. Remote Sens 18, 2863–2868.

Peñuelas J, Filella I, Llusià J, Siscart D, Piñol J, 1998 Comparative field study of spring and summer leaf gas exchange and photobiology of the Mediterranean trees *Quercus ilex* and *Phillyrea latifolia*. J. Exp. Bot 49, 229–238.

Pérez-Priego O, Guan J, Rossini M, Fava F, Wutzler T, Moreno G, Carvalhais N, Carrara A, Kolle O, Julitta T, Schrumpf M, Reichstein M, Migliavacca M, 2015 Sun-induced chlorophyll fluorescence and photochemical reflectance index improve remote-sensing gross primary

production estimates under varying nutrient availability in a typical Mediterranean savanna ecosystem. Biogeosciences 12, 6351–6367.

Pérez-Priego O, Zarco-Tejada PJ, Miller JR, Sepulcre-Cantó G, Fereres E, 2005 Detection of water stress in orchard trees with a high-resolution spectrometer through chlorophyll fluorescence *infilling* of the O_2-A band. IEEE Trans. Geosci. Remote Sens 43, 2860–2869.

Pfündel E, 1998 Estimating the contribution of Photosystem I to total leaf chlorophyll fluorescence. Photosynth. Res 56, 185–195.

Pingle VS, 2017 Detection of change in chlorophyll fluorescence using low spectral resolution spectrometer - A study for temperature induced stress detection. MSc thesis, University of Twente, Enschede, The Netherlands https://webapps.itc.utwente.nl/librarywww/papers_2017/msc/wrem/pingle.pdf

Pinto F, Damm A, Schickling A, Panigada C, Cogliati S, Müller-Linow M, Balvora A, Rascher U, 2016 Sun-induced chlorophyll fluorescence from high-resolution imaging spectroscopy data to quantify spatio-temporal patterns of photosynthetic function in crop canopies. Plant Cell Environ. 39, 1500–1512. [PubMed: 26763162]

Pinto F, Müller-Linow M, Schickling A, Cendrero-Mateo MP, Ballvora A, Rascher U, 2017 Multiangular observation of canopy sun-induced chlorophyll fluorescence by combining imaging spectroscopy and stereoscopy. Remote Sens. 9, 415.

Pitman AJ, 2003 The evolution of, and revolution in, land surface schemes designed for climate models. Int. J. Climatol 23, 479–510.

Plascyk JA, 1975 The MK II Fraunhofer Line Discriminator (FLD-II) for airborne and orbital remote sensing of solar-stimulated luminescence. Opt. Eng 14, 144339.

Plascyk JA, Gabriel FC, 1975 The Fraunhofer Line Discriminator MKII – An airborne instrument for precise and standardized ecological luminescence measurement. IEEE Trans. Instrum. Meas 24, 306–313.

Porcar-Castell A, Tyystjärvi E, Atherton J, Van der Tol C, Flexas J, Pfündel EE, Moreno J, Frankenberg C, Berry JA, 2014 Linking chlorophyll *a* fluorescence to photosynthesis for remote sensing applications: Mechanisms and challenges. J. Exp. Bot 65, 4065–4095. [PubMed: 24868038]

Qiu B, Xue Y, Fisher JB, Guo W, Berry JA, Zhang Y, 2018 Satellite chlorophyll fluorescence fluorescence and soil moisture observations lead to advances in the predictive understanding of global terrestrial coupled carbon-water cycles. Global Biogeochem. Cycles 32, 360–375.

Rascher U, Agati G, Alonso L, Cecchi G, Champagne S, Colombo R, Damm A, Daumard F, De Miguel E, Fernandez G, Franch B, Franke J, Gerbig C, Gioli B, Gómez JA, Goulas Y, Guanter L, Gutiérrez-de-la-Cámara Ó, Hamdi K, Hostert P, Jiménez M, Kosvancova M, Lognoli D, Meroni M, Miglietta F, Moersch A, Moreno J, Moya I, Neininger B, Okujeni A, Ounis A, Palombi L, Raimondi V, Schickling A, Sobrino JA, Stellmes M, Toci G, Toscano P, Udelhoven T, Van der Linden S, Zaldei A, 2009 CEFLES2: The remote sensing component to quantify photosynthetic efficiency from the leaf to the region by measuring sun-induced fluorescence in the oxygen absorption bands. Biogeosciences 6, 1181–1198.

Rascher U, Alonso L, Burkart A, Cilia C, Cogliati S, Colombo R, Damm A, Drusch M, Guanter L, Hanus J, Hyvírinen T, Julitta T, Jussila J, Kataja K, Kokkalis P, Kraft S, Kraska T, Matveeva M, Moreno J, Muller O, Panigada C, Pikl M, Pinto F, Prey L, Pude R, Rossini M, Schickling A, Schurr U, Schüttemeyer D, Verrelst J, Zemek F, 2015 Sun-induced fluorescence - a new probe of photosynthesis: First maps from the imaging spectrometer *HyPlant*. Glob. Change Biol 21, 4673–4684.

Rascher U, Gioli B, Miglietta F, 2008 FLEX – Fluorescence Explorer: A remote sensing approach to quantify spatio-temporal variations of photosynthetic efficiency from space, in: Allen JF, Gantt E, Golbeck JH, Osmond B (Eds.), Photosynthesis. Energy from the Sun. Springer, Dordrecht, pp. 1387–1390.

Rascher U, Hütt M-T, Siebke K, Osmond B, Beck F. Lüttge U, 2001 Spatiotemporal variation of metabolism in a plant circadian rhythm: The biological clock as an assembly of coupled individual oscillators. Proc. Natl. Acad. Sci. USA 98, 11801–11805. [PubMed: 11573013]

Rascher U, Lüttge U, 2002 High-resolution chlorophyll fluorescence imaging serves as a non-invasive indicator to monitor the spatio-temporal variations of metabolism during the day-night cycle and

during the endogenous rhythm in continuous light in the CAM plant *Kalanchoä daigremontiana*. Plant Biology 4, 671–681.

Rivera JP, Verrelst J, Gómez-Dans J, Muñoz-Marí J, Moreno J, Camps-Valls G, 2015 An emulator toolbox to approximate radiative transfer models with statistical learning. Remote Sens. 7, 9347–9370.

Rohá ek K, Soukupová J, Barták M, 2008 Chlorophyll fluorescence: A wonderful tool to study plant physiology and plant stress, in: Schoefs B (Ed.), Plant Cell Compartments – Selected Topics. Kerala India, Research Signpost, pp. 41–104.

Romero JM, Cordon GB, Lagorio MG, 2018 Modeling re-absorption of fluorescence from the leaf to the canopy level. Remote Sens. Environ 204, 138–146.

Rosema A, Snel JFH, Zahn H, Buurmeijer WF, Van Hove LWA, 1998 The relation between laser-induced chlorophyll fluorescence and photosynthesis. Remote Sens. Environ 65, 143–154.

Rosema A, Verhoef W, Noorbergen H, Borgesius JJ, 1992 A new forest light interaction model in support of forest monitoring. Remote Sens. Environ 42, 23–41.

Rosema A, Verhoef W, Schroote J, Snel JFH, 1991 Simulating fluorescence light-canopy interaction in support of laser-induced fluorescence measurements. Remote Sens. Environ 37, 117–130.

Rossini M, Meroni M, Celesti M, Cogliati S, Julitta T, Panigada C, Rascher U, Van der Tol C, Colombo R, 2016 Analysis of red and far-red sun-induced chlorophyll fluorescence and their ratio in different canopies based on observed and modeled data. Remote Sens. 8, 412.

Rossini M, Meroni M, Migliavacca M, Manca G, Cogliati S, Busetto L, Picchi V, Cescatti A, Seufert G, Colombo R, 2010 High resolution field spectroscopy measurements for estimating gross ecosystem production in a rice field. Agric. For. Meteorol 150, 1283–1296.

Rossini M, Nedbal L, Guanter L, A A, Alonso L, Burkart A, Cogliati S, Colombo R, Damm A, Drusch M, Hanus J, Janoutova R, Julitta T, Kokkalis P, Moreno J, Novotny J, Panigada C, Pinto F, Schickling A, Schuttemeyer D, Zemek F, Rascher U, 2015 Red and far-red sun-induced chlorophyll fluorescence as a measure of plant photosynthesis. Geophys. Res. Lett 42, 1632–1639.

Ryu Y, Baldocchi DD, Kobayashi H, van Ingen C, Li J, Black TA, Beringer J, van Gorsel E, Knohl A, Law BE, Roupsard O, 2011 Integration of MODIS land and atmosphere products with a coupled-process model to estimate gross primary productivity and evapotranspiration from 1 km to global scales. Global Biogeochemical Cycles 25, doi: 10.1029/2011GB004053.

Ryu Y, Berry JA, Baldocchi DD, 2019 What is global photosynthesis? History, uncertainties and opportunities. Remote Sens. Environ 223, 95–114.

Sabater N, Alonso L, Cogliati S, Vicent J, Tenjo C, Verrelst J, Moreno J, 2015 A sun-induced vegetation fluorescence retrieval method from top of atmosphere radiance for the FLEX/Sentinel-3 tandem mission, in: Proc. IEEE International Geoscience and Remote Sensing Symposium (IGARSS), 26-31 July 2015, Milan, Italy, pp. 2669–2672.

Sabater N, Vicent J, Alonso L, Cogliati S, Verrelst J, Moreno J, 2017 Impact of atmospheric inversion effects on solar-induced chlorophyll fluorescence: Exploitation of the apparent reflectance as a quality indicator. Remote Sens. 9, 622.

Sabater N, Vicent J, Alonso L, Verrelst J, Middleton EM, Porcar–Castell A, Moreno J, 2018 Compensation of oxygen transmittance effects for proximal sensing retrieval of canopy-leaving sun-induced chlorophyll fluorescence. Remote Sens. 10, 1551.

Sanders AFJ, Verstraeten WW, Kooreman ML, Van Leth TC, Beringer C, Joiner J, 2016 Spaceborne sun-induced vegetation fluorescence time series from 2007 to 2015 evaluated with Australian flux tower measurements. Remote Sens. 8, 895.

Schickling A, Matveeva M, Damm A, Schween JH, Wahner A, Graf A, Crewell S, Rascher U, 2016 Combining sun-induced chlorophyll fluorescence and photochemical reflectance index improves diurnal modeling of gross primary productivity. Remote Sens. 8, 574.

Schlapfer D, Nieke J, Itten KI, 2007 Spatial PSF nonuniformity effects in airborne pushbroom imaging spectrometry data. IEEE Trans. Geosci. Remote Sens 45, 458–468.

Schmuck G, Moya I, 1994 Time-resolved chlorophyll fluorescence spectra of intact leaves. Remote Sens. Environ 47, 72–76.

Scholze M, Buchwitz M, Dorigo W, Guanter L, Quegan S, 2017 Reviews and syntheses: Systematic Earth observations for use in terrestrial carbon cycle data assimilation systems. Biogeosciences 14, 3401–3429.

Schreiber U, 2004 Pulse-amplitude-modulation (PAM) fluorometry and saturation pulse method: An overview, in: Papageorgiou GC, Govindjee (Eds.), Chlorophyll *a* Fluorescence: A Signature of Photosynthesis. Springer, Dordrecht, pp. 279–319.

Schreiber U, Bilger W, Neubauer C, 1995 Chlorophyll fluorescence as a nonintrusive indicator for rapid assessment of *in vivo* photosynthesis, in: Schulze E-D, Caldwell MM (Eds.) Ecophysiology of Photosynthesis. Springer, Berlin/Heidelberg, pp. 49–70.

Schreiber U, Schliwa U, Bilger W, 1986 Continuous recording of photochemical and nonphotochemical chlorophyll fluorecence quenching with a new type of modulation fluorometer. Photosynth. Res 10, 51–62. [PubMed: 24435276]

Sellers PJ, Tucker CJ, Collatz GJ, Los SO, Justice CO, Dazlich DA, Randall DA, 1996 A revised land surface parameterization (SiB$_2$) for atmospheric GCMs. Part II: The generation of global fields of terrestrial biophysical parameters from satellite data. Journal of Climate 9, 706–737.

Simmer C, Thiele-Eich I, Masbou M, Amelung W, Bogena H, Crewell S, Diekkrüger B, Ewert F, Hendricks Franssen H-J, Huisman JA, Kemna A, Klitzsch N, Kollet S, Langensiepen M, Löhnert U, Rahman ASMM, Rascher U, Schneider K, Schween J, Shao Y, Shrestha P, Stiebler M, Sulis M, Vanderborght J, Vereecken H, Van der Kruk J, Waldhoff G, Zerenner T, 2015 Monitoring and modeling the terrestrial system from pores to catchments: The Transregional Collaborative Research Center on Patterns in the Soil–Vegetation–Atmosphere System. Bull. Am. Meteorol. Soc 96, 1765–1787.

Smith WK, Biederman JA, Scott RL, Moore DJP, He M, Kimball JS, Yan D, Hudson A, Barnes ML, MacBean N, Fox AM, Litvak ME, 2018 Chlorophyll fluorescence better captures seasonal and interannual gross primary productivity dynamics across dryland ecosystems of southwestern North America. Geophys. Res. Lett 45, 748–757.

Sobrino JA, Franch B, Jimenez-Muñoz JC, Hidalgo V, Soria G, Julien Y, Oltra-Carrio R, Mattar C, Ruescas A, Daumard F, Champagne S, Fournier A, Goulas Y, Ounis A, Moya I, 2011 Fluorescence estimation in the framework of the CEFLES2 campaign. Int. J. Remote Sens 32, 5875–5889.

Song L, Guanter L, Guan K, You L, Huete A, Ju W, Zhang Y, 2018 Satellite sun-induced chlorophyll fluorescence detects early response of winter wheat to heat stress in the Indian Indo-Gangetic Plains. Glob. Change Biol 2018, 1–15.

Soukupová J, Cséfalvay L, Urban O, Košvancovñ M, Marek M, Rascher U, Nedbal L, 2008 Annual variation of the steady-state chlorophyll fluorescence emission of evergreen plants in temperate zone. Funct. Plant Biol 35, 63–76. [PubMed: 32688757]

Srivastava P, Pandey J, 2012 LICF spectrum as a fast detector of chlorophyll damage in safflower growing under mutagenic stress. World Journal of Agricultural Sciences 8, 322–325.

Stober F, Lang M, Lichtenthaler HK, 1994 Blue, green, and red fluorescence emission signatures of green, etiolated, and white leaves. Remote Sens. Environ 47, 65–71.

Stokes GG, 1852 On the change of refrangibility of light. Trans. R. Soc. Lond 142, 463–562.

Stoll M-P, Laurila T, Cunin B, Gitelson AA, Lichtenthaler HK, Häme T 1999 FLEX: Fluorescence Explorer – a space mission for screening vegetated areas in the Fraunhofer lines, in: Proc. SPIE 3868, Remote Sensing for Earth Science, Ocean, and Sea Ice Applications, 20-24 September 1999, Florence, Italy, pp. 108–119.

Strand M, Öquist G, 1988 Effects of frost hardening, dehardening and freezing stress on in vivo chlorophyll fluorescence of seedlings of Scots pine (*Pinus sylvestris* L.). Plant Cell Environ. 11, 231–238.

Strasser RJ, Srivastava A, Govindjee, 1995 Polyphasic chlorophyll a fluorescence transient in plants and cyanobacteria. Photochem. Photobiol 61, 32–42.

Subhash N, 1995 Detection of vegetation stress from laser-induced fluorescence signatures. International Centre for Theoretical Physics (Trieste, Italy), LAMP Series Report, LAMP/95/4, June 1995.

Subhash N, Mohanan CN, 1997 Curve-fit analysis of chlorophyll fluorescence spectra: Application to nutrient stress detection in sunflower. Remote Sens. Environ 60, 347–356.

Suits GH, 1972 The calculation of the directional reflectance of a vegetative canopy. Remote Sens. Environ 2, 117–125.

Sun Y, Frankenberg C, Jung M, Joiner J, Guanter L, Köhler P, Magney TS, 2018 Overview of solar-induced chlorophyll fluorescence (SIF) from the Orbiting Carbon Observatory-2: Retrieval, cross-mission comparison, and global monitoring for GPP. Remote Sens. Environ 209, 808–823.

Sun Y, Frankenberg C, Wood JD, Schimel DS, Jung M, Guanter L, Drewry DT, Verma M, Porcar-Castell A, Griffis TJ, Gu L, Magney TS, Köhler P, Evans B, Yuen K, 2017 OCO-2 advances photosynthesis observation from space via solar-induced chlorophyll fluorescence. Science 358, eaam5747, doi: 10.1126/science.aam5747. [PubMed: 29026013]

Sun Y, Fu R, Dickinson R, Joiner J, Frankenberg C, Gu L, Xia Y, Fernando N, 2015 Drought onset mechanisms revealed by satellite solar-induced chlorophyll fluorescence: Insights from two contrasting extreme events. J. Geophys. Res. Biogeosci 120, 2427–2440.

Sylak-Glassman EJ, Zaks J, Amarnath K, Leuenberger M, Fleming GR, 2016 Characterizing nonphotochemical quenching in leaves through fluorescence lifetime snapshots. Photosynth. Res 127, 69–76. [PubMed: 25762378]

Szabó K, Lichtenthaler HK, Kocsányi L, Richter P, 1992 A CCD-OMA device for the measurement of complete chlorophyll fluorescence emission spectra of leaves during the fluorescence induction kinetics. Radiat. Environ. Biophys 31, 153–160. [PubMed: 1609060]

Terjung F, 1998 Reabsorption of chlorophyll fluorescence and its effects on the spectral distribution and the picosecond decay of higher plant leaves. Z. Naturforsch C 53, 924–926.

Thum T, Zaehle S, Köhler P, Aalto T, Aurela M, Guanter L, Kolari P, Laurila T, Lohila A, Magnani F, Van Der Tol C, Markkanen T, 2017 Modelling sun-induced fluorescence and photosynthesis with a land surface model at local and regional scales in northern Europe. Biogeosciences 14, 1969–1987.

Toivonen P, Vidaver W, 1984 Integrating fluorometer for the measurement of chlorophyll fluorescence induction in intact plants. Rev. Sci. Instrum 55, 1687–1690.

Turner D, Lucieer A, Malenovský Z, King DH, Robinson SA, 2014 Spatial co-registration of ultra-high resolution visible, multispectral and thermal images acquired with a micro-UAV over Antarctic moss beds. Remote Sens. 6, 4003–4024.

Vácha F, Sarafis V, Benediktyový Z, Bumba L, Valenta J, Vácha M, Sheue Ch.-R., Nedbal L, 2007 Identification of Photosystem I and Photosystem II enriched regions of thylakoid membrane by optical microimaging of cryo-fluorescence emission spectra and of variable fluorescence. Micron 38, 170–175. [PubMed: 16962333]

Valentini R, Cecchi G, Mazzinghi P, Scarascia Mungnozza G, Agati G, Bazzani M, De Angelis P, Fusi F, Matteucci G, Raimondi V, 1994 Remote sensing of chlorophyll *a* fluorescence of vegetation canopies: 2. Physiological significance of fluorescence signal in response to environmental stresses. Remote Sens. Environ 47, 29–35.

Van de Hulst HC, 1981 Light scattering by small particles. Dover Publications, New York.

Van de Hulst HC, 1957 Light scattering by small particles. John Wiley & Sons, New York.

Van der Tol C, Berry JA, Campbell PKE, Rascher U, 2014 Models of fluorescence and photosynthesis for interpreting measurements of solar-induced chlorophyll fluorescence. J. Geophys. Res. Biogeosci 119, 2312–2327. [PubMed: 27398266]

Van der Tol C, Rossini M, Cogliati S, Verhoef W, Colombo R, Rascher U, Mohammed G, 2016 A model and measurement comparison of diurnal cycles of sun-induced chlorophyll fluorescence of crops. Remote Sens. Environ 186, 663–677.

Van der Tol C, Verhoef W, Rosema A, 2009a A model for chlorophyll fluorescence and photosynthesis at leaf scale. Agric. For. Meteorol 149, 96–105.

Van der Tol C, Verhoef W, Timmermans J, Verhoef A, Su Z, 2009b An integrated model of soil-canopy spectral radiances, photosynthesis, fluorescence, temperature and energy balance. Biogeosciences 6, 3109–3129.

Van Kooten O, Snel JFH, 1990 The use of chlorophyll fluorescence nomenclature in plant stress physiology. Photosynth. Res 25, 147–150. [PubMed: 24420345]

Van Wittenberghe S, Alonso L, Verrelst J, Hermans I, Delegido J, Veroustraete F, Valcke R, Moreno J, Samson R, 2013 Upward and downward solar-induced chlorophyll fluorescence yield indices of four tree species as indicators of traffic pollution in Valencia. Environ. Pollut 173, 29–37. [PubMed: 23202634]

Van Wittenberghe S, Alonso L, Verrelst J, Hermans I, Valcke R, Veroustraete F, Moreno J, Samson R, 2014 A field study on solar-induced chlorophyll fluorescence and pigment parameters along a vertical canopy gradient of four tree species in an urban environment. Sci. Total Environ 466-467, 185–194. [PubMed: 23895782]

Van Wittenberghe S, Alonso L, Verrelst J, Moreno J, Samson R, 2015 Bidirectional sun-induced chlorophyll fluorescence emission is influenced by leaf structure and light scattering properties – A bottom-up approach. Remote Sens. Environ 158, 169–179.

Verhoef W, 1984 Light scattering by leaf layers with application to canopy reflectance modeling: The SAIL model. Remote Sens. Environ 16, 125–141.

Verhoef W, 1985 Earth observation modeling based on layer scattering matrices. Remote Sens. Environ 17, 165–178.

Verhoef W, Van der Tol C, Middleton EM, 2014 Vegetation canopy fluorescence and reflectance retrieval by model inversion using optimization, in: Proc. 5th International Workshop on Remote Sensing of Vegetation Fluorescence, 22-24 April 2014, Paris, France.

Verhoef W, Van der Tol C, Middleton EM, 2018 Hyperspectral radiative transfer modeling to explore the combined retrieval of biophysical parameters and canopy fluorescence from FLEX – Sentinel-3 tandem mission multi-sensor data. Remote Sens. Environ 204, 942–963.

Verma M, Schimel D, Evans B, Frankenberg C, Beringer J, Drewry DT, Magney T, Marang I, Hutley L, Moore C, Eldering A, 2017 Effect of environmental conditions on the relationship between solar-induced fluorescence and gross primary productivity at an OzFlux grassland site. J. Geophys. Res. Biogeosci 122, 716–733.

Verrelst J, Camps-Valls G, Muñoz-Marí J, Rivera JP, Veroustraete F, Clevers JGPW, Moreno J, 2015a Optical remote sensing and the retrieval of terrestrial vegetation bio-geophysical properties – A review. ISPRS J. Photogramm. Remote Sens 108, 273–290.

Verrelst J, Rivera JP, 2017 A global sensitivity analysis toolbox to quantify drivers of vegetation radiative transfer models, in: Petropoulos G, Srivastava P (Eds.) Sensitivity Analysis in Earth Observation Modelling. Elsevier, pp. 319–339.

Verrelst J, Van der Tol C, Magnani F, Sabater N, Rivera JP, Mohammed G, Moreno J, 2016 Evaluating the predictive power of sun-induced chlorophyll fluorescence to estimate net photosynthesis of vegetation canopies: A SCOPE modeling study. Remote Sens. Environ 176, 139–151.

Verrelst J, Rivera JP, Van der Tol C, Magnani F, Mohammed G, Moreno J, 2015b Global sensitivity analysis of the SCOPE model: What drives simulated canopy-leaving sun-induced fluorescence? Remote Sens. Environ 166, 8–21.

Vicent J, Sabater N, Tenjo C, Acarreta JR, Manzano M, Rivera JP, Jurado P, Franco R, Alonso L, Verrelst J, Moreno J, 2016 FLEX end-to-end mission performance simulator. IEEE Trans. Geosci. Remote Sens 54, 4215–4223.

Vilfan N, Van der Tol C, Muller O, Rascher U, Verhoef W, 2016 Fluspect-B: A model for leaf fluorescence, reflectance and transmittance spectra. Remote Sens. Environ 186, 596–615.

Vilfan N, Van der Tol C, Yang P, Wyber R, Malenovský Z, Robinson SA, Verhoef W, 2018 Extending Fluspect to simulate xanthophyll driven leaf reflectance dynamics. Remote Sens. Environ 211, 345–356.

Vogelmann TC, Bornman JF, Yates DJ, 1996 Focusing of light by leaf epidermal cells. Physiol. Plant 98, 43–56.

Vogelmann TC, Evans JR, 2002 Profiles of light absorption and chlorophyll within spinach leaves from chlorophyll fluorescence. Plant Cell Environ. 25, 1313–1323.

Von Hebel C, Matveeva M, Verweij E, Rademske P, Kaufmann MS, Brogi C, Vereecken H, Rascher U, Van der Kruk J, 2018 Understanding soil and plant interaction by combining ground-based quantitative electromagnetic induction and airborne hyperspectral data. Geophys. Res. Lett 45, 7571–7579.

Wagle P, Zhang Y, Jin C, Xiao X, 2016 Comparison of solar-induced chlorophyll fluorescence, light-use efficiency, and process-based GPP models in maize. Ecol. Appl 26, 1211–1222. [PubMed: 27509759]

Walker AP, Quaife T, Van Bodegom PM, De Kauwe MG, Keenan TF, Joiner J, Lomas MR, MacBean N, Xu C, Yang X, Woodward FI, 2017 The impact of alternative trait-scaling hypotheses for the maximum photosynthetic carboxylation rate (V_{cmax}) on global gross primary production. New Phytol. 215, 1370–1386. [PubMed: 28643848]

Walther S, Guanter L, Heim B, Jung M, Duveiller G, Wolanin A, Sachs T, 2018 Assessing the dynamics of vegetation productivity in circumpolar regions with different satellite indicators of greenness and photosynthesis. Biogeosciences 15, 6221–6255.

Walther S, Voigt M, Thum T, Gonsamo A, Zhang Y, Köhler P, Jung M, Varlagin A, Guanter L, 2016 Satellite chlorophyll fluorescence measurements reveal large-scale decoupling of photosynthesis and greenness dynamics in boreal evergreen forests. Glob. Change Biol 22, 2979–2996.

Wang S, Huang C, Zhang L, Lin Y, Cen Y, Wu T, 2016 Monitoring and assessing the 2012 drought in the Great Plains: Analyzing satellite-retrieved solar-induced chlorophyll fluorescence, drought indices, and gross primary production. Remote Sens. 8, 61.

Watson RD, Hemphill WR, 1976 Use of an airborne Fraunhofer line discriminator for the detection of solar stimulated luminescence. U.S. Geological Survey Open-File Report 76-202, 109 p., 10.3133/ofr76202.

Wei X, Wang X, Wei W, Wan W, 2018 Use of sun-induced chlorophyll fluorescence obtained by OCO-2 and GOME-2 for GPP estimates of the Heihe River Basin, China. Remote Sens 10, 2039.

Weis E, Berry JA, 1987 Quantum efficiency of Photosystem II in relation to 'energy'-dependent quenching of chlorophyll fluorescence. Biochim. Biophys. Acta 894, 198–208.

Wieneke S, Burkart A, Cendrero-Mateo MP, Julitta T, Rossini M, Schickling A, Schmidt M, Rascher U, 2018 Linking photosynthesis and sun-induced fluorescence at sub-daily to seasonal scales. Remote Sens. Environ 219, 247–258.

Wieneke S, Ahrends H, Damm A, Pinto F, Stadler A, Rossini M, Rascher U, 2016 Airborne based spectroscopy of red and far-red sun-induced chlorophyll fluorescence: Implications for improved estimates of gross primary productivity. Remote Sens. Environ 184, 654–667.

Wohlfahrt G, Gerdel K, Migliavacca M, Rotenberg E, Tatarinov F, Müller J, Hammerle A, Julitta T, Spielmann FM, Yakir D 2018 Sun-induced fluorescence and gross primary productivity during a heat wave. Sci. Rep 8, 14169. [PubMed: 30242255]

Wolanin A, Rozanov VV, Dinter T, Nöel S, Vountas M, Burrows JP, Bracher A, 2015 Global retrieval of marine and terrestrial chlorophyll fluorescence at its red peak using hyperspectral top of atmosphere radiance measurements: Feasibility study and first results. Remote Sens. Environ 166, 243–261.

Wong CY, Gamon JA, 2015 Three causes of variation in the photochemical reflectance index (PRI) in evergreen conifers. New Phytol. 206, 187–195. [PubMed: 25408288]

Wood JD, Griffis TJ, Baker JM, Frankenberg C, Verma M, Yuen K, 2017 Multiscale analyses of solar-induced fluorescence and gross primary production. Geophys. Res. Lett 44, 533–541.

Wu X, Xiao X, Zhang Y, He W, Wolf S, Chen J, He M, Gough CM, Qin Y, Zhou Y, Doughty R, Blanken PD, 2018 Spatiotemporal consistency of four gross primary production products and solar-induced chlorophyll fluorescence in response to climate extremes across CONUS in 2012. J. Geophys. Res. Biogeosci 123, 10.1029/2018JG004484.

Wyber R, Malenovský Z, Ashcroft MB, Osmond B, Robinson SA, 2017 Do daily and seasonal trends in leaf solar induced fluorescence reflect changes in photosynthesis, growth or light exposure? Remote Sens. 9, 604.

Xu S, Liu Z, Zhao L, Zhao H, Ren S, 2018 Diurnal response of sun-induced fluorescence and PRI to water stress in maize using a near-surface remote sensing platform. Remote Sens. 10, 1510.

Yang J, Tian H, Pan S, Chen G, Zhang B, Dangal S, 2018a Amazon drought and forest response: Largely reduced forest photosynthesis but slightly increased canopy greenness during the extreme drought of 2015/2016. Glob. Change Biol 24, 1919–1934.

Yang K, Ryu Y, Dechant B, Berry JA, Hwang Y, Jiang C, Kang M, Kim J, Kimm H, Kornfeld A, Yang X, 2018b Sun-induced chlorophyll fluorescence is more strongly related to absorbed light than to photosynthesis at half-hourly resolution in a rice paddy. Remote Sens. Environ 216, 658–673.

Yang P, Van der Tol C, 2018 Linking canopy scattering of far-red sun-induced chlorophyll fluorescence with reflectance. Remote Sens. Environ 209, 456–467.

Yang P, Van der Tol C, Verhoef W, Damm A, Schickling A, Kraska T, Muller O, Rascher U (in press). Using reflectance to explain vegetation biochemical and structural effects on sun-induced chlorophyll fluorescence. Remote Sens. Environ, doi 10.1016/j.rse.2018.11.039.

Yang P, Verhoef W, Van der Tol C, 2017 The mSCOPE model: A simple adaptation to the SCOPE model to describe reflectance, fluorescence and photosynthesis of vertically heterogeneous canopies. Remote Sens. Environ 201, 1–11.

Yang X, Tang J, Mustard JF, Lee J-E, Rossini M, Joiner J, Munger JW, Kornfeld A, Richardson AD, 2015 Solar-induced chlorophyll fluorescence that correlates with canopy photosynthesis on diurnal and seasonal scales in a temperate deciduous forest. Geophys. Res. Lett 42, 2977–2987.

Yang X, Shi H, Stovall A, Guan K, Miao G, Zhang Y, Zhang Y, Xiao X, Ryu Y, Lee J-E, 2018c FluoSpec 2—An automated field spectroscopy system to monitor canopy solar-induced fluorescence. Sensors 18, 2063.

Yoshida Y, Joiner J, Tucker C, Berry J, Lee J-E, Walker G, Reichle R, Koster R, Lyapustin A , Wang Y, 2015 The 2010 Russian drought impact on satellite measurements of solar-induced chlorophyll fluorescence: Insights from modeling and comparisons with parameters derived from satellite reflectances. Remote Sens. Environ 166, 163–177.

Zaks J, Amarnath K, Kramer DM, Niyogi KK, Fleming GR, 2012 A kinetic model of rapidly reversible nonphotochemical quenching. Proc. Natl. Acad. Sci. USA 109, 15757–15762. [PubMed: 22891305]

Zarco-Tejada PJ, Camino C, Beck PSA, Calderon R, Hornero A, Hernández-Clemente R, Kattenborn T, Montes-Borrego M, Susca L, Morelli M, Gonzalez-Dugo V, North PRJ, Landa BB, Boscia D, Saponari M, Navas-Cortes JA, 2018 Previsual symptoms of *Xylella fastidiosa* infection revealed in spectral plant-trait alterations. Nat. Plants 4, 432–439. [PubMed: 29942047]

Zarco-Tejada PJ, Catalina A, González MR, Martin P, 2013a Relationships between net photosynthesis and steady-state chlorophyll fluorescence retrieved from airborne hyperspectral imagery. Remote Sens. Environ 136, 247–258.

Zarco-Tejada PJ, González-Dugo V, Bemi JAJ, 2012 Fluorescence, temperature and narrow-band indices acquired from a UAV platform for water stress detection using a micro-hyperspectral imager and a thermal camera. Remote Sens. Environ 117, 322–337.

Zarco-Tejada PJ, Miller JR, Mohammed GH, Noland TL, Sampson PH, 1999a Canopy optical indices from infinite reflectance and canopy reflectance models for forest condition monitoring: Application to hyperspectral CASI data, in: Proc. IEEE International Geoscience and Remote Sensing Symposium (IGARSS), 28 June-2 July 1999, Hamburg, Germany, Vol. 3, pp. 1878–1881.

Zarco-Tejada PJ, Miller JR, Mohammed GH, Noland TL, Sampson PH, 1999b Optical indices as bioindicators of forest condition from hyperspectral CASI data, in: Proceedings 19th EARSeL Symposium on Remote Sensing in the 21st Century, 31 May-2 June 1999, Valladolid, Spain.

Zarco-Tejada PJ, Miller JR, Mohammed GH, Noland TL, 2000a Chlorophyll fluorescence effects on vegetation apparent reflectance: I. Leaf-level measurements and model simulation. Remote Sens. Environ 74, 582–595.

Zarco-Tejada PJ, Miller JR, Mohammed GH, Noland TL, Sampson PH, 2000b Chlorophyll fluorescence effects on vegetation apparent reflectance: II. Laboratory and airborne canopy-level measurements with hyperspectral data. Remote Sens. Environ74, 596–608.

Zarco-Tejada PJ, Miller JR, Mohammed GH, Noland TL, Sampson PH, 2001 Estimation of chlorophyll fluorescence under natural illumination from hyperspectral data. Int. J. Appl. Earth Obs. Geoinf. (Special Issue on Applications of Imaging Spectroscopy) 3, 321–327.

Zarco-Tejada PJ, Miller JR, Mohammed GH, Noland TL, Sampson PH, 2002 Vegetation stress detection through chlorophyll a+b estimation and fluorescence effects on hyperspectral imagery. J. Environ. Qual 31, 1433–1441. [PubMed: 12371159]

Zarco-Tejada PJ, Miller JR, Pedrós R, Verhoef W, Berger M, 2006 FluorMODgui V3.0: A graphic user interface for the spectral simulation of leaf and canopy chlorophyll fluorescence. Computers & Geosciences 32, 577–591.

Zarco-Tejada PJ, Morales A, Testi L, Villalobos FJ, 2013b Spatio-temporal patterns of chlorophyll fluorescence and physiological and structural indices acquired from hyperspectral imagery as compared with carbon fluxes measured with eddy covariance. Remote Sens. Environ 133, 102–115.

Zarco-Tejada PJ, Pushnik JC, Dobrowski S, Ustin SL, 2003 Steady-state chlorophyll a fluorescence detection from canopy derivative reflectance and *double-peak* red-edge effects. Remote Sens. Environ 84, 283–294.

Zhang Y, Guanter L, Berry JA, Joiner J, Van der Tol C, Huete A, Gitelson A, Voigt M, Kohler P, 2014 Estimation of vegetation photosynthetic capacity from space-based measurements of chlorophyll fluorescence for terrestrial biosphere models. Glob. Chang. Biol 20, 3727–3742. [PubMed: 24953485]

Zhang Y, Guanter L, Berry JA, Van der Tol C, Yang X, Tang J, Zhang F, 2016a Model-based analysis of the relationship between sun-induced chlorophyll fluorescence and gross primary production for remote sensing applications. Remote Sens. Environ 187, 145–155.

Zhang Y, Guanter L, Joiner J, Song L, Guan K, 2018a Spatially-explicit monitoring of crop photosynthetic capacity through the use of space-based chlorophyll fluorescence data. Remote Sens. Environ 210, 362–374.

Zhang Y, Joiner J, Alemohammad SH, Zhou S, Gentine P, 2018b A global spatially Continuous Solar Induced Fluorescence (CSIF) dataset using neural networks. Biogeosciences 15, 5779–5800.

Zhang Y, Joiner J, Gentine P, Zhou S, 2018c Reduced solar-induced chlorophyll fluorescence from GOME-2 during Amazon drought caused by dataset artifacts. Glob. Change Biol 24, 10.1111/gcb.14134.

Zhang Y, Xiao X, Guanter L, Zhou S, Ciais P, Joiner J, Sitch S, Wu X, Nabel J, Dong J, Kato E, Jain AK, Wiltshire A, Stocker BD, 2016b Precipitation and carbon-water coupling jointly control the interannual variability of global land gross primary production. Sci. Rep 6, 39748. [PubMed: 28008960]

Zhang Y, Xiao X, Jin C, Dong J, Zhou S, Wagle P, Joiner J, Guanter L, Zhang Y, Zhang G, Qin Y, Wang J, Moore B III, 2016c Consistency between sun-induced chlorophyll fluorescence and gross primary production of vegetation in North America. Remote Sens. Environ 183, 154–169.

Zhang Y, Xiao X, Zhang Y, Wolf S, Zhou S, Joiner J, Guanter L, Verma M, Sun Y, Yang X, Paul-Limoges E, Gough CM, Wohlfahrt G, Gioli B, Van der Tol C, Yann N, Lund M, De Grandcourt A, 2018d On the relationship between sub-daily instantaneous and daily total gross primary production: Implications for interpreting satellite-based SIF retrievals. Remote Sens. Environ 205, 276–289.

Zhang YJ, Liu LY, Hou MY, Liu LT, Li CD, 2009 Progress in remote sensing of vegetation chlorophyll fluorescence. Journal of Remote Sensing 13, 963–978.

Zhang Z, Zhang Y, Joiner J, Migliavacca M, 2018e Angle matters: Bidirectional effects impact the slope of relationship between gross primary productivity and sun-induced chlorophyll fluorescence from Orbiting Carbon Observatory-2 across biomes. Glob. Change Biol 24, 5017–5020.

Zhao F, Dai X, Verhoef W, Guo Y, Van der Tol C, Li Y, Huang Y, 2016 FluorWPS: A Monte Carlo ray-tracing model to compute sun-induced chlorophyll fluorescence of three-dimensional canopy. Remote Sens. Environ 187, 385–399.

Zhao F, Guo Y, Verhoef W, Gu X, Liu L, Yang G, 2014 A method to reconstruct the solar-induced canopy fluorescence spectrum from hyperspectral measurements. Remote Sens. 6, 10171–10192.

Zhao F, Li R, Verhoef W, Cogliati S, Liu X, Huang Y, Guo Y, Huang J, 2018 Reconstruction of the full spectrum of solar-induced chlorophyll fluorescence: Intercomparison study for a novel method. Remote Sens. Environ 219, 233–246.

Zhou X, Liu Z, Xu S, Zhang W, Wu J, 2016 An automated comparative observation system for sun-induced chlorophyll fluorescence of vegetation canopies. Sensors 16, 775.

Zoogman P, Liu X, Suleiman RM, Pennington WF, Flittner DE, Al-Saadi JA, Hilton BB, Nicks DK, Newchurch MJ, Carr JL, Janz SJ, Andraschko MR, Arola A, Baker BD, Canova BP, Miller CC, Cohen RC, Davis JE, Dussault ME, Edwards DP, Fishman J, Ghulam A, González Abad G, Grutter M, Herman JR, Houck J, Jacob DJ, Joiner J, Kerridge BJ, Kim J, Krotkov NA, Lamsal L, Li C, Lindfors A, Martin RV, McElroy CT, McLinden C, Natraj V, Neil DO, Nowlan CR, O'Sullivan EJ, Palmer PI, Pierce RB, Pippin MR, Saiz-Lopez A, Spurr RJD, Szykman JJ, Torres O, Veefkind JP, Veihelmann B, Wang H, Wang J, Chance K, 2016 Tropospheric emissions: Monitoring of pollution (TEMPO). J. Quant. Spectrosc. Radiat. Transfer 186, 17–39.

Zuromski LM, Bowling DR, Köhler P, Frankenberg C, Goulden ML, Blanken PD, Lin JC, 2018 Solar-induced fluorescence detects interannual variation in gross primary production of coniferous forests in the western United States. Geophys. Res. Lett 45, 7184–7193.
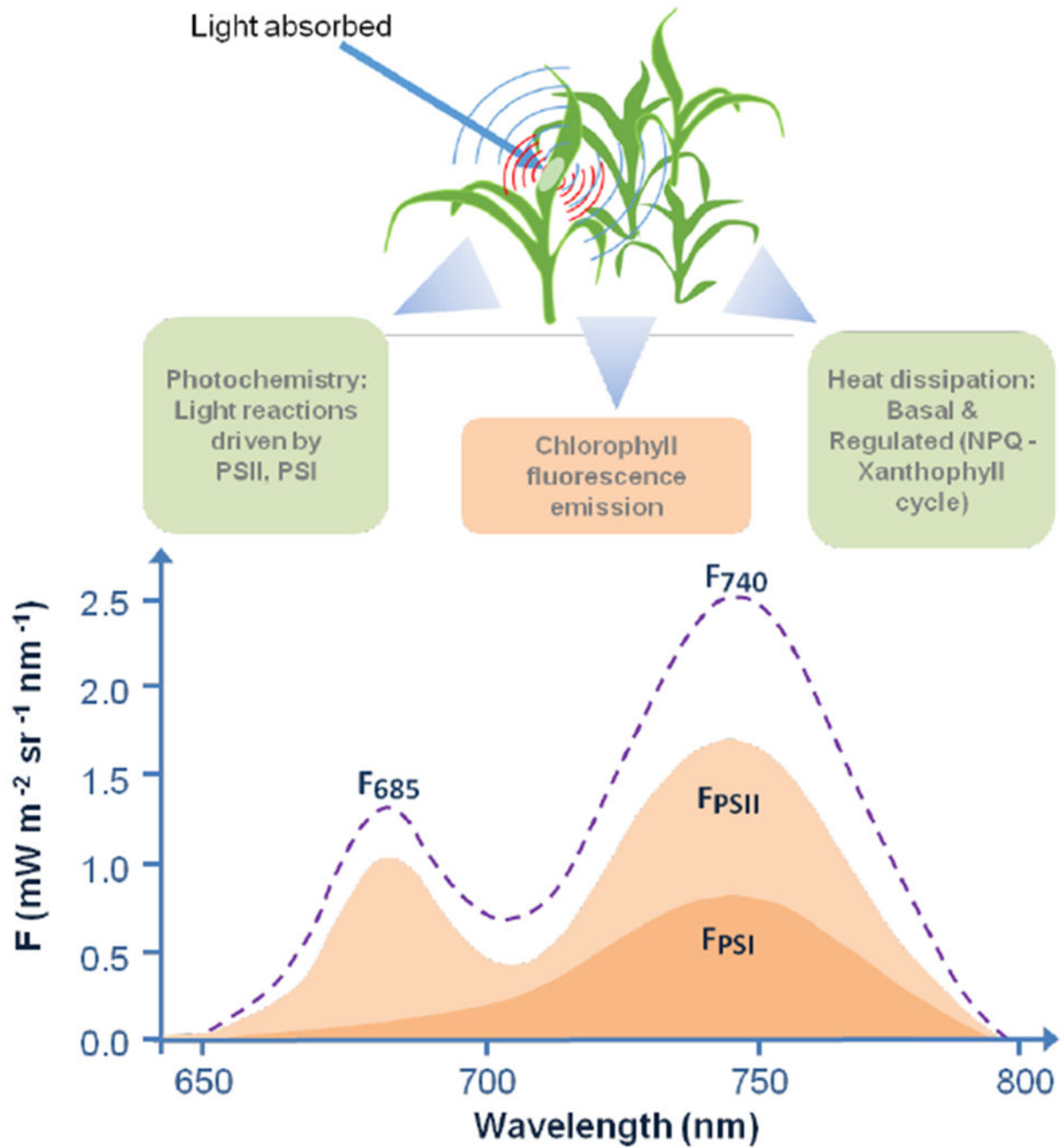
Figure 1.
Distribution of absorbed light energy in leaves under steady-state conditions. Absorbed light may be used for photochemistry, dissipated thermally, or re-emitted as chlorophyll fluorescence. Lower graph: Conceptual figure of leaf fluorescence emission, with maxima in the red and far-red spectral regions, and arising from photosystems PSII and PSI. PSII contributes to both red and far-red emissions, and PSI mainly to the far-red region. In healthy green leaves the red peak typically is lower than the far-red one, due to greater re-absorption of red fluorescence by chlorophyll during the transit of fluorescence to the leaf

surface. (Plant drawing courtesy of C. van der Tol; lower graph courtesy of U. Rascher, and adapted.)
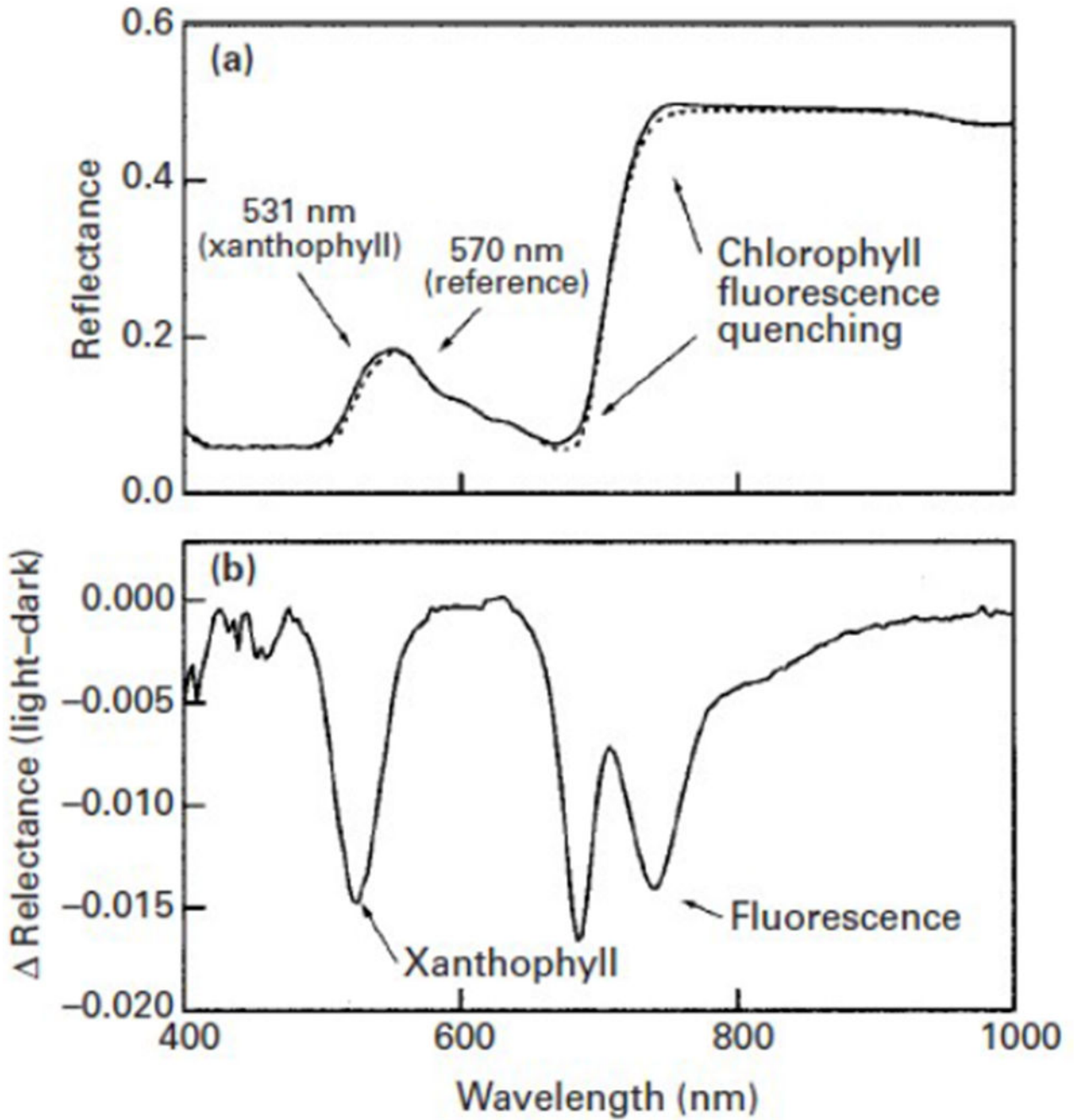
Figure 2.
Leaf reflectance spectra of *Helianthus annuus* (sunflower), (a) in the dark state (solid line) and after 10 minutes of exposure to light (dotted line); (b) reflectance-difference calculation (dark-state minus light-state), showing the effects due to xanthophyll pigment de-epoxidation in the green region, and chlorophyll fluorescence quenching in the red-edge region. (Source: Gamon and Surfus, 1999.)
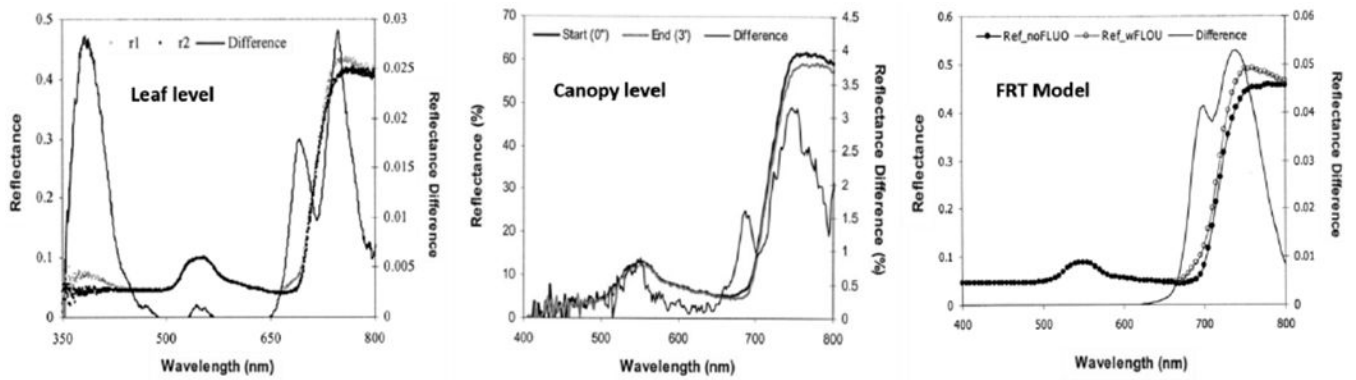
Figure 3.
Reflectance differences between a dark-adapted and light-adapted leaf of *Acer saccharum* (sugar maple) showing the spectral differences in the blue region, in the green region due to the xanthophyll pigment dynamics, and in the red edge region due to the fluorescence emission (**left**). Canopy level reflectance of dark-adapted seedlings after illumination with white light, showing the fluorescence signal extracted by spectral subtraction using the CASI imager after three minutes (**centre**). First attempts of fluorescence simulation by radiative transfer with the Fluorescence–Reflectance–Transmittance model to simulate leaf reflectance accounting for the fluorescence emission (**right**). (Source: Zarco-Tejada et al., 2000a, 2000b.)
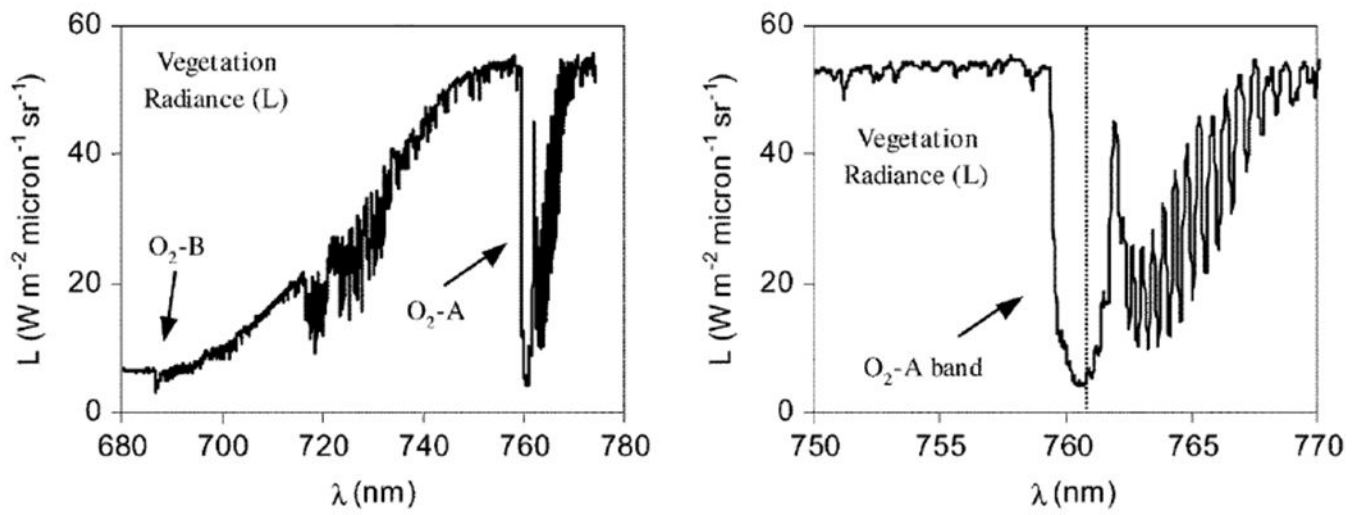
Figure 4.
Canopy radiance measured from *Olea europea* (olive) trees under water stress levels using a sub-nanometer spectrometer covering the O_2-B and O_2-A regions (left) and the detailed absorption features observed (right). (Source: Pérez-Priego et al., 2005.)
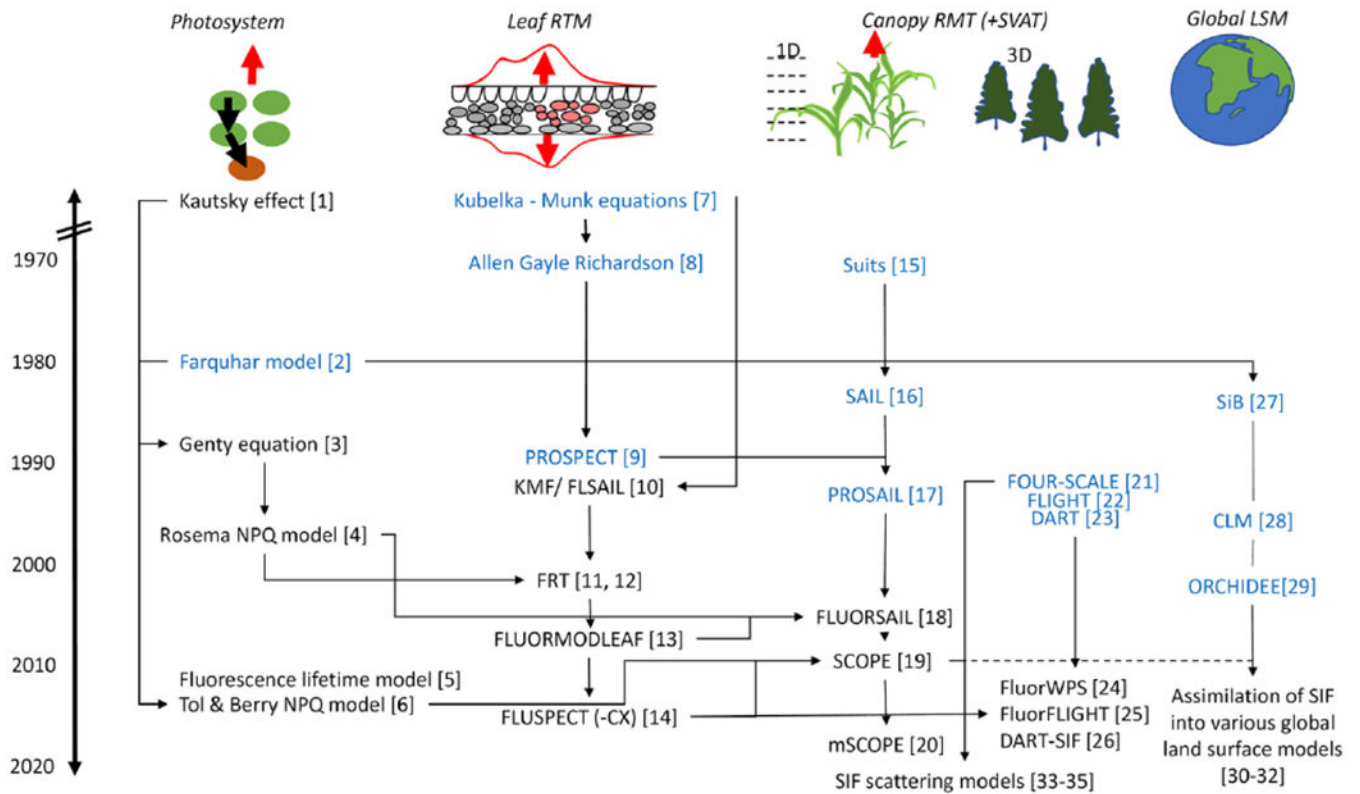
Figure 5.
History of leaf physiological and radiative transfer models of leaves and canopy for fluorescence. Relevant models that do not include fluorescence are shown in blue. **[1]** Kautsky and Hirsch, 1931. **[2]** Farquhar et al., 1980. **[3]** Genty et al., 1989. **[4]** Rosema et al., 1998. **[5]** Zaks et al., 2012. **[6]** Van der Tol et al., 2014. **[7]** Kubelka and Munk, 1931. **[8]** Allen et al., 1970. **[9]** Jacquemoud and Baret, 1990. **[10]** Rosema et al., 1991. **[11]** Zarco-Tejada et al., 2000a. **[12]** Zarco-Tejada et al., 2000b. **[13]** Pedrós et al., 2010. **[14]** Vilfan et al., 2016. **[15]** Suits, 1972. **[16]** Verhoef, 1984. **[17]** Jacquemoud, 1993. **[18]** Miller et al., 2005. **[19]** Van der Tol et al., 2009b. **[20]** Yang et al., 2017. **[21]** North, 1996. **[22]** Gastellu-Etchegorry et al., 1996. **[23]** Zhao et al., 2014. **[24]** Hernández-Clemente et al., 2017. **[25]** Gastellu-Echegorry et al., 2017. **[26]** Sellers et al., 1996. **[27]** Bonan, 1996. **[28]** Krinner et al., 2005. **[29]** Lee et al., 2015. **[30]** Lee et al., 2015. **[31]** MacBean et al., 2018. **[32]** Norton et al., 2018. **[33]** He et al., 2017. **[34]** Yang and Van der Tol., 2018. **[35]** Köhler et al., 2018b.
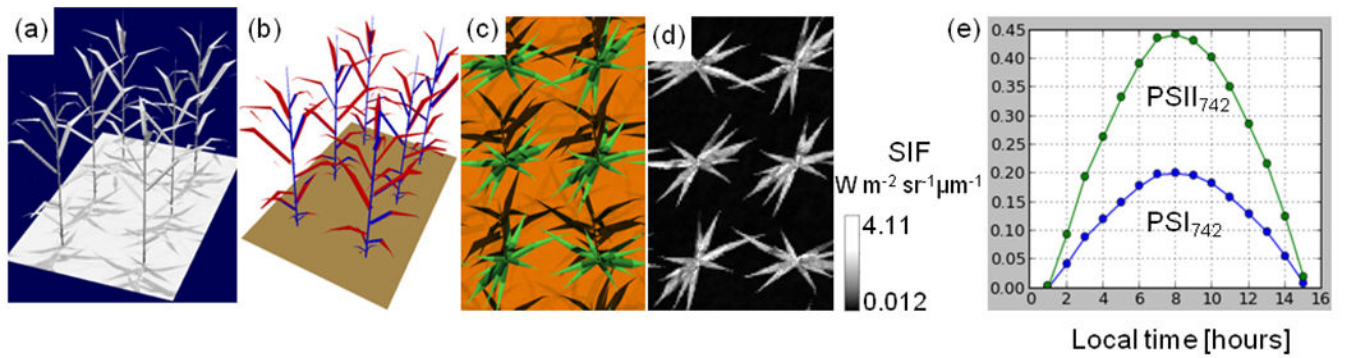
Figure 6.
Simulation of BOA fluorescence in maize by DART: (a) Intensity of solar irradiance for a maize field in an early growth stage (39°N, 76.8°E; June 21, 2015; 13h local time); (b) 3D representation of sun- (red) and shade-adapted (blue) leaves; (c) DART true colour composite of the nadir reflectance image; (d) DART simulated PSII fluorescence radiance image; and (e) hourly evolution of the maize canopy BOA PSI and PSII fluorescence radiance at the wavelength of 742.5 nm for clear sky conditions (atmosphere characterized by the USSTD 76 gas model and the Rural V23 aerosols model according to the MODTRAN gas and aerosol databases (see Berk et al., 2014).
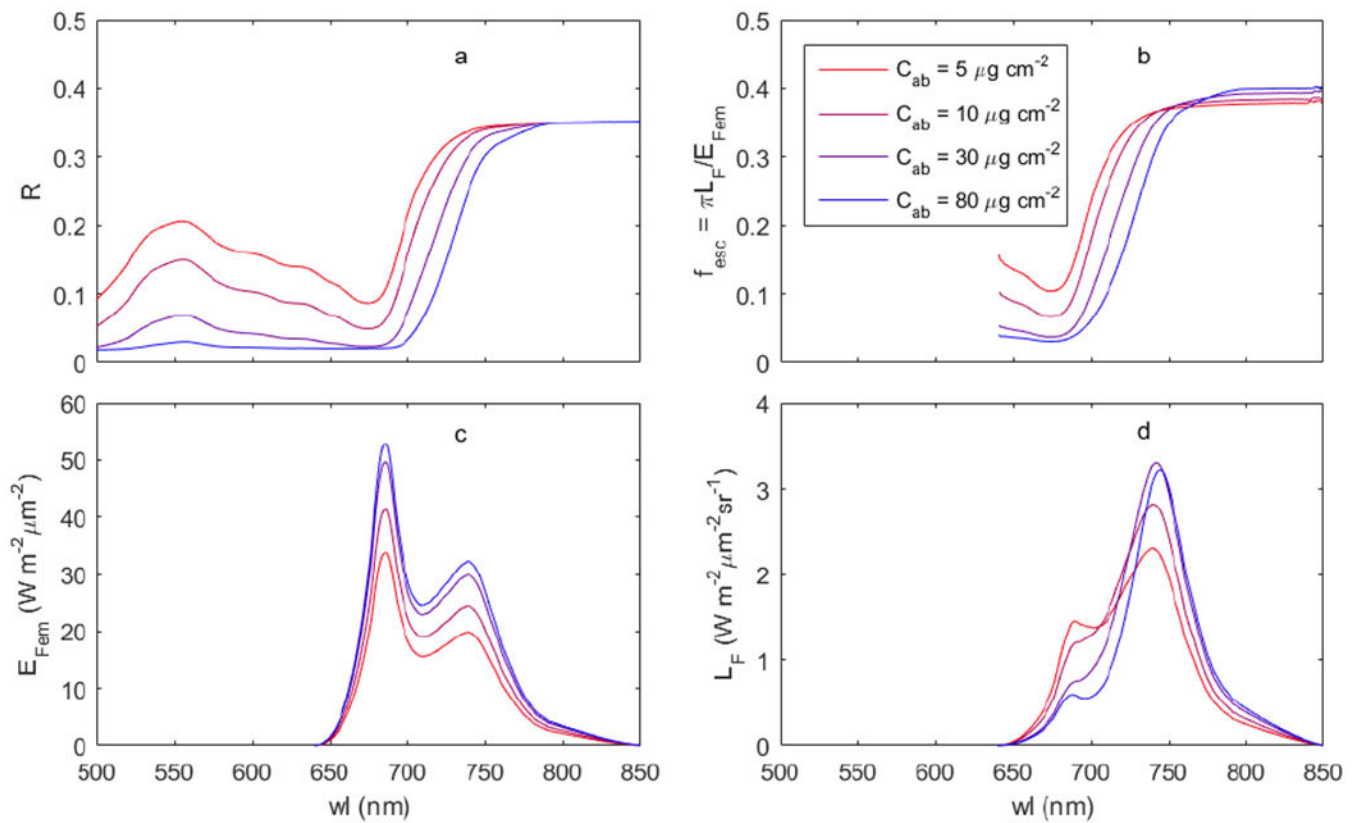
Figure 7.
SCOPE model simulation of (a) reflectance R, (b) fluorescence escape probability f_{esc}, (c) the fluorescence irradiance emitted by all photosystems E_{Fem}, and (d) the fluorescence radiance in nadir direction L_F – for four values of leaf chlorophyll content and a leaf area index of 3. Note the changes in fluorescence spectral shape as chlorophyll(a+b) mass per unit leaf surface (C_{ab}) increases, and the similarity between the fluorescence escape probability and the reflectance.
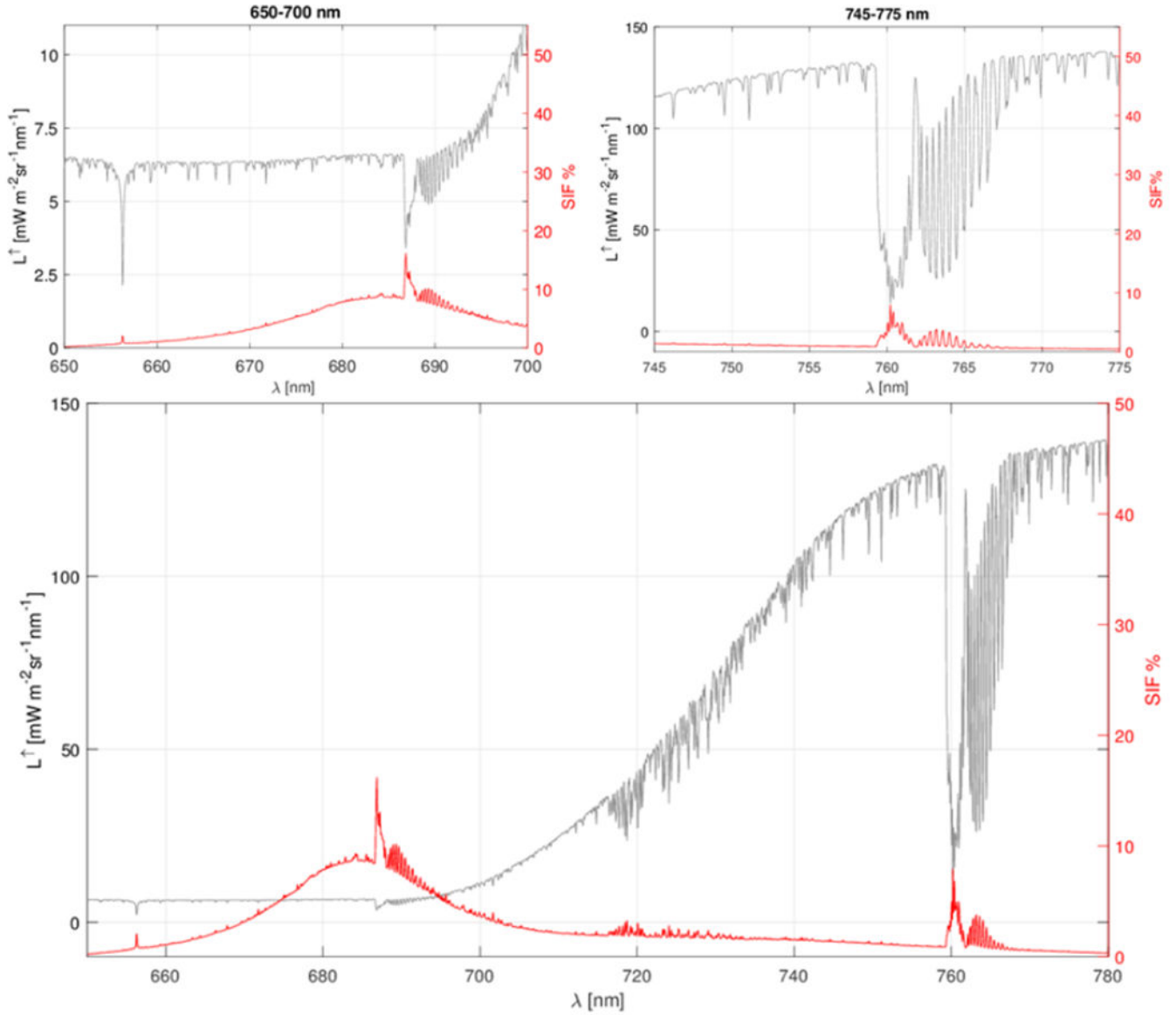
Figure 8.
Relative contribution of solar-induced fluorescence (red curves and right axes) with respect to the total emerging radiance at top-of-canopy (grey curves and left axes) at spectral resolution of 0.1 nm, considering typical dense vegetation during summer conditions. The figure on the bottom shows the spectral range of fluorescence emission; whereas the figures on top show O_2-B (left) and O_2-A (right) details. Note the difference in radiance scales for plots.
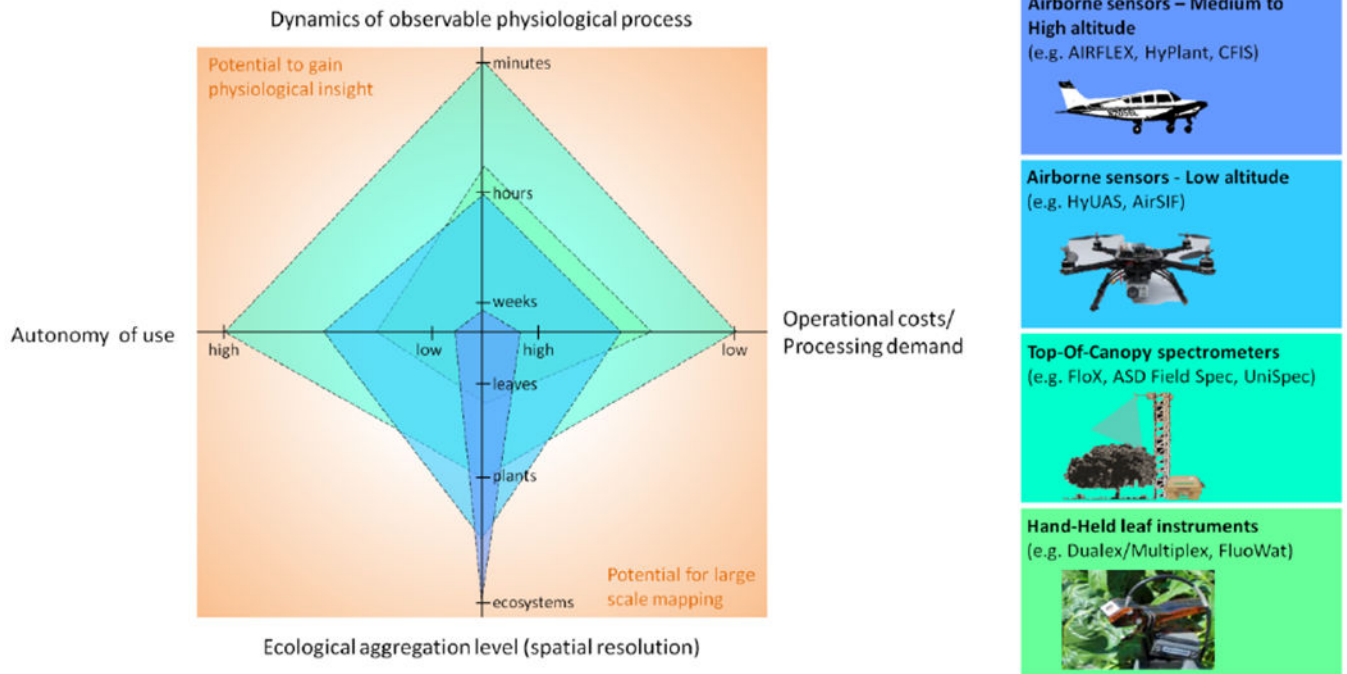
Figure 9.
Comparison and complementarity of hand-held, top-of-canopy, and airborne instrumentation to gain insight into the information content of fluorescence and facilitate mapping. (Colours on the left panel correspond to those on the right.)
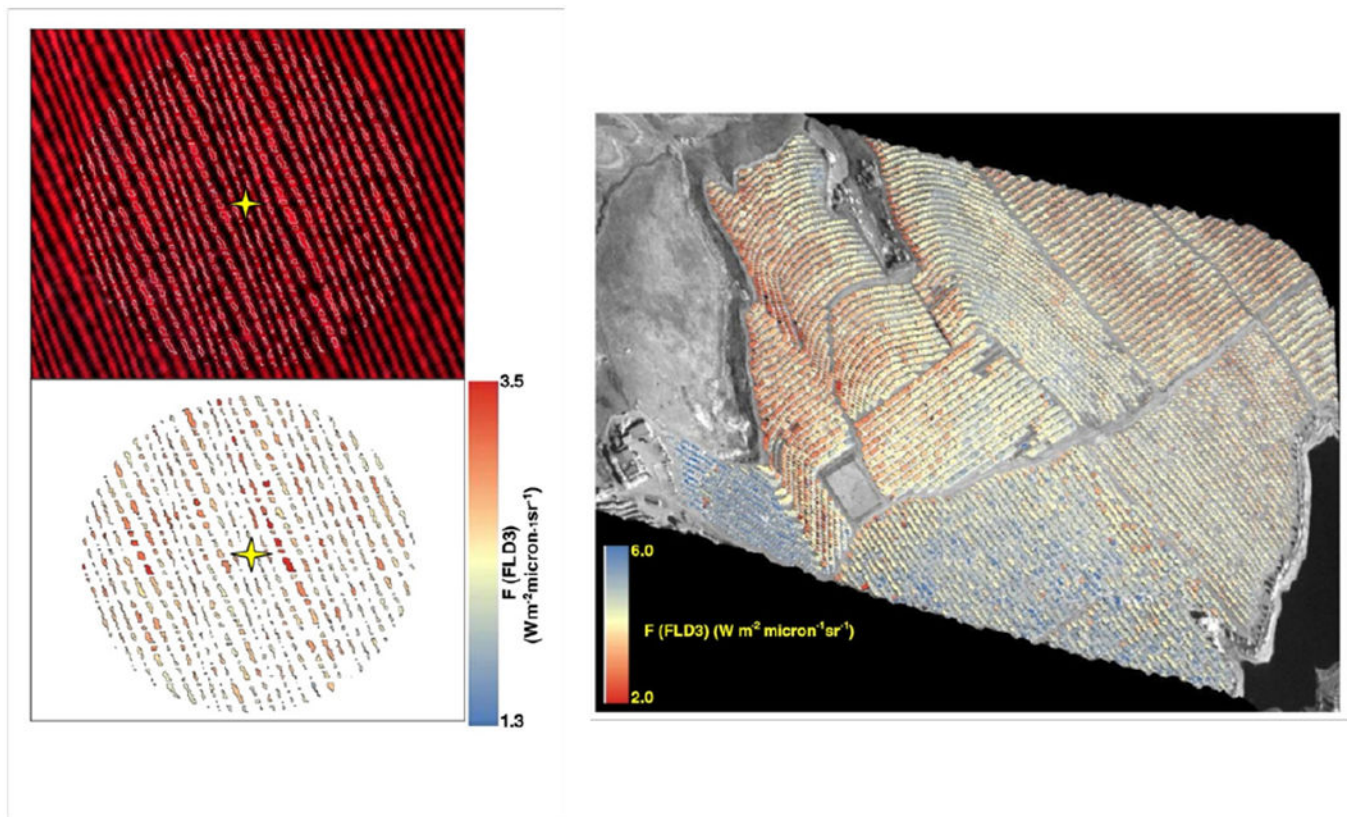
Figure 10.
High (30- or 40-cm) resolution SIF retrievals from hyperspectral imagery acquired from an unmanned aerial vehicle flown over an eddy covariance flux tower in an olive orchard (left, false colour composite) (Source: Zarco-Tejada et al., 2013b), and over a citrus field subjected to water stress treatments (right) (Source: Zarco-Tejada et al., 2012). The high resolution imagery acquired by the micro-hyperspectral camera enabled the quantification of SIF (O_2-A band) on pure tree crowns, removing the large effects caused by shadows and background in heterogeneous canopies.
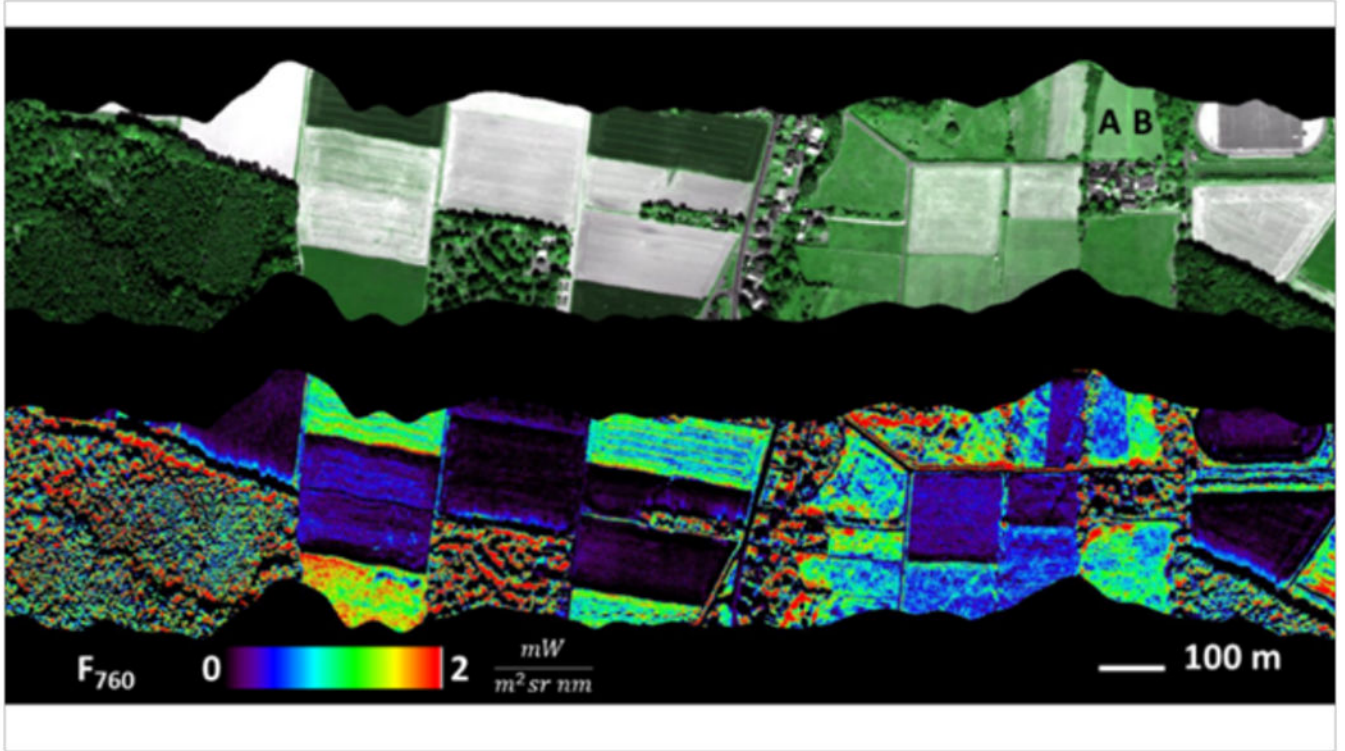
Figure 11.
Reflectance (upper panel) and canopy SIF (lower panel) maps obtained with the *HyPlant* airborne sensor over an agricultural research site in Klein Altendorf, Germany. Lower SIF is evident in forests (left in lower panel) and higher SIF in dense agricultural fields (middle and right in lower panel). Fluorescence emission reveals information on vegetation status which is not visible in the reflectance domain. For example, the two fields denoted as A and B display almost identical reflectance (upper panel), whereas their fluorescence emission is very different (lower panel). (Source: U. Rascher/Forschungszentrum Jülich)
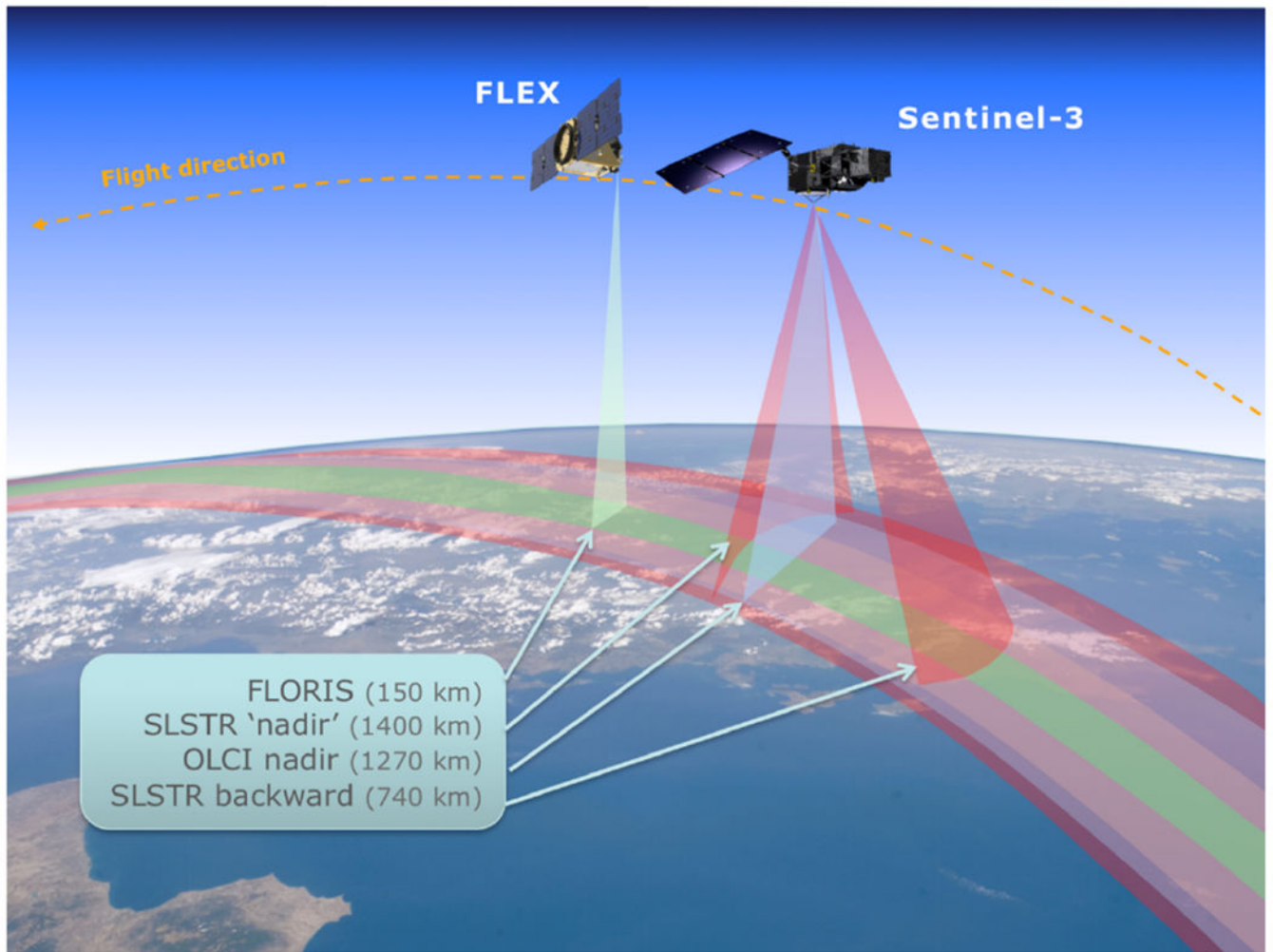
Figure 12.
Schematic of the FLEX two-satellite tandem mission combining the FLORIS free-flyer with an operational Sentinel-3 satellite having a 10:00 am equatorial overpass time. FLEX's 150 km nadir swath (green track) lies within the wider swath of the nadir OLCI camera (blue track, 1270 km). The SLSTR (red tracks) has a back-looking swath (740 km, 500 x 500 m^2 pixels) and a nadir swath (1400 km, 1000 x 1000 m^2 pixels). (Source: European Space Agency.)
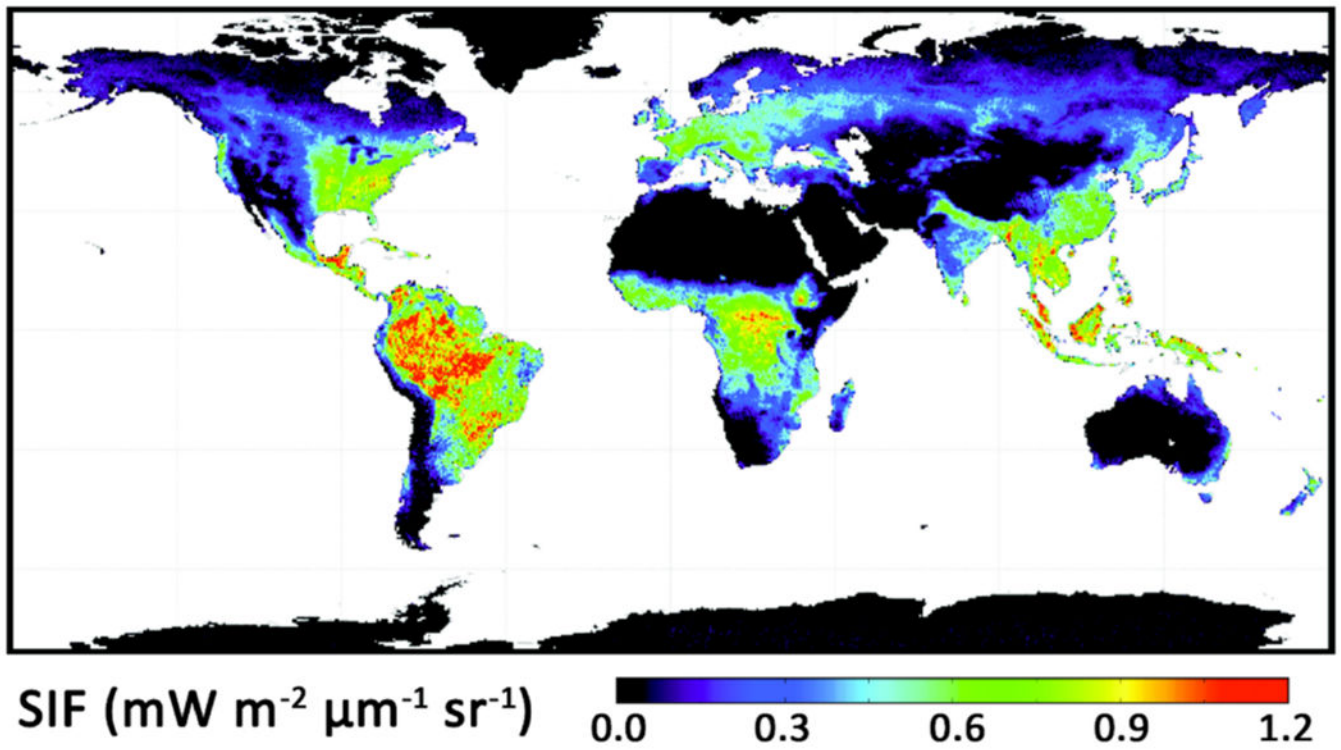
Figure 13.
Global map showing the 2009 annual average of observations for far-red SIF derived from the GOME-2 satellite, utilizing observations acquired throughout 2009. (Source: Joiner et al., 2013.)

Table 1.

Laboratory technologies to measure steady-state fluorescence. Symbols: ✓ standard feature, ⊙ requires specialized configuration, ◇ provides mainly qualitative information.

Technology type	Steady-state CF feature							
	Location within leaf	Amplitude (intensity)	Quenching analysis	Life-time	Red, far-red, full emission	Integrated CF over branch / plant	Effective PSII quantum yield	Heterogeneity of CF over leaf / plant
fluorescence microscopes [1]	✓	◇	–	–	–	–	–	✓
cryo-F-microscopes [2]	✓	✓	⊙		⊙		⊙	
confocal & two-photon microscopes [3]	✓	◇	⊙	–	–	–	–	–
fiber-optic microprobes [4]	✓	✓	–	–	–	–	–	–
imaging systems (PAM etc.) [5]	–	✓	✓	–	–	✓	✓	✓
high-resolution spectrometers (spectro-radiometers) [6]	–	✓	–	–	–	–	–	–
spectro-fluorimeters [7]	–	✓	–	–	✓	–	–	✓
continous excitation fluorometers [8]	–	✓	–	–	–	–	–	–
integrating- sphere fluorometer [9]	–	✓	–	–	–	✓	–	–
laser-induced fluorescence (LIF) systems 10]	✓	✓	✓	–	✓	–	–	✓
τ-LIDARs [11]	–	–	–	✓	–	–	–	–
PAM systems (excluding imaging) [12]	–	✓	✓	–	–	–	✓	–
laser-induced fluorometers measuring fluorescence transients, PSII effective antenna size [13]	–	–	–	–	–	–	✓	–

[1]Buurman et al., 1992; Kalaji et al., 2012; Murchie and Lawson, 2013.

[2]Vácha et al., 2007.

[3]Benediktyová and Nedbal, 2009; Osmond et al., 1999.

[4]Bornman et al., 1991.

[5] Aldea et al., 2006; Calatayud et al., 2006; Genty and Meyer, 1995; Gorbe and Calatayud, 2012; Nedbal et al., 2000; Oxborough, 2004.

[6] Dobrowski et al., 2005; Julitta et al., 2016; Magney et al., 2017; Zarco-Tejada et al., 2003, 2001, 2000a, 2000b.

[7] Boardman et al., 1966; Gitelson et al., 1998; Govindjee, 1995; Mohanty et al., 1972; Papageorgiou, 1975.

[8] Bolhàr-Nordenkampf et al., 1989*; Mohammed et al., 1995*; Öquist and Wass, 1988; Strasser et al., 1995.

[9] Toivonen and Vidaver, 1984.

[10] Buschmann and Lichtenthaler, 1998; Buschmann et al., 2000; Cecchi et al., 1994; Lichtenthaler and Rinderle, 1988*; Omasa et al., 2007; Ounis et al., 2001; Rosema et al., 1991; Stober et al., 1994; Szabò et al., 1992.

[11] Cerovic et al., 1996; Moya et al., 1995.

[12] Magney et al., 2017; Schreiber, 2004; Schreiber et al., 1986.

[13] Keller et al., 2018; Kolber and Falkowski, 1993; Kolber et al., 1998; Nedbal et al., 1999.

*Review papers.

Mohammed et al. Page 91

Table 2.

Current SIF retrieval methods and their characteristics.

Absorption band	Method	Reference	Target SIF (R=red; FR=far-red; F=Full spectrum)	Scale of design (F=field; A=airborne; S=satellite; ms=model simulations)	Spectral channels (M=multispectral; H=hyperspectral)	Retrieval Spectral Range (nm)	Retrieved SIF	Assumed SIF spectral shape	Assumed r spectral shape
			O_2 bands						
	FLD	Plascyk, 1975	R	A	M	486.1; 589.0; 656.3	scalar	constant	constant
	3FLD	Maier et al., 2003	FR	A	M	760	scalar	linear	linear
	SFM	Meroni and Colombo, 2006	R, FR	F (leaf)	H	686.5–690.0; 759.0–764.0	restricted	linear	linear
	cFLD	Gómez-Chova et al., 2006	R, FR	F (leaf)	H	687; 760	scalar	adjusted with correction factor	from apparent R
	iFLD	Alonso et al., 2008	FR	F (canopy), ms	H	750-780	scalar	adjusted with correction factor	adjusted with correction factor
	SFM	Mazzoni et al., 2008	R	F (leaf)	H	686.3-691.6	restricted	polynomial	polynomial
	FLD/SFM	Guanter et al., 2010	R, FR	ms	H	677-697; 750-770	restricted	reference spectrum	linear combination of end-members
Selected Absorption Bands	*SFM*	Meroni et al., 2010	R, FR	F (canopy), ms	H	686.7–691.2; 755.6–765.5	restricted	linear, polynomial, gaussian	linear, polynomial
	nFLD	Daumard et al., 2010	R, FR	F (canopy)	M	683.1-697.1; 757.9-770.5	scalar	reference spectrum	polynomial
	SFM	Mazzoni et al., 2010	R, FR	ms	H	677.0–697.0; 750.0–770.0	restricted	voigt	cubic spline
	SFM	Mazzoni et al., 2012	FR	F (canopy), ms	H	750–770	restricted	voigt, legendre polynomial	polynomials, cubic-spline, legendre polynomial
	3FLD	Damm et al., 2014	FR	A	M	753-771	scalar	linear	linear
	SFM	Cogliati et al., 2015a	R, FR	ms	H	750-770	restricted	gaussian, lorentzian, voigt	polynomial, cubic spline
	iFLD	Wieneke et al., 2016	R, FR	A	M	-	scalar	adjusted with correction factor	adjusted with correction factor
			Fraunhofer lines						
	-	Frankenberg et al., 2011a	FR	S, ms	H	769.5-775; 770.1 (K$_I$)	scalar	constant	polynomial
	-	Joiner et al., 2011/2012	FR	S, ms	H	769.90–770.25 (K$_I$)	scalar	constant	constant

Remote Sens Environ. Author manuscript; available in PMC 2021 January 06.

Absorption band	Method	Reference	Target SIF (R=red; FR=far-red; F=Full spectrum)	Scale of design (F=field; A=airborne; S=satellite; ms=model simulations)	Spectral channels (M=multispectral; H=hyperspectral)	Retrieval Spectral Range (nm)	Retrieved SIF	Assumed SIF spectral shape	Assumed r spectral shape
	SVD	Guanter et al., 2012	FR	F, ms	H	755.8-759.3; 769.2-775.2	scalar	constant	singular vectors
	PCA	Joiner et al., 2014	FR	S, ms	H	712-747; 747-783	scalar	gaussian	polynomial
	-	Köhler et al., 2015	FR	S, ms	H	720-758	scalar	constant/ normalized fluorescence spectrum	linear
	DOAS	Wolanin et al., 2015	R	S	H	681.8-685.5	scalar	reference spectrum	polynomial
	-	Joiner et al., 2016	R, FR	S, ms	H	622–640; 682-692	scalar	gaussian	polynomial
	two step linearized	Grossmann et al., 2018	R, FR	F (canopy)	H	680-686; 745-758	scalar	reference spectrum	polynomial
Full Spectrum	*Spectrum fitting*								
	FSR	Zhao et al., 2014/2018	F	F (canopy), ms	H	640–850	spectrum	linear combination of basis spectra	-
	F-SFM	Liu et al., 2015	F	F (canopy), ms	H	645-805	spectrum	linear combination of basis spectra	linear combination of basis spectra
	SpecFit	Cogliati et al., 2015b	F	ms	H	670-780	spectrum	pseudo-voigt	piecewise cubic spline
	Model inversion								
	-	Verhoef et al., 2018	F	ms	H	400-2255	spectrum	singular vectors from SVD	physically based (RTMo)
	-	Celesti et al., 2018	F	F (canopy), ms	H	400-900	spectrum	physically based (RTMf)	physically based (RTMo)

Table 3.

Current and future satellite missions. Instruments in space or planned for launch that have SIF measurement capability (red SIF wavelengths ~680-690 nm, and far-red ~730-780 nm). A few of these also capture PRI wavelengths (between 520 and 580 nm). This list is not exhaustive; e.g., follow-on missions such as OCO-3 and GOSAT-2 are not included. Pixel quality refers to the combined utility of data products for uses based on influences of sensor specifications (spectral range and parameters retrieved, FWHM, SNR), spatial resolution, temporal collections, and Level 2-4 mission product support.

Mission / Sensor	Status / Launch	Coverage	Footprint (km)	Equatorial Overpass Time	Repeat Cycle	Spectral Range (nm)	FWHM (nm) (SIF)	SIF & PRI meas.	SNR	SIF Pixel Quality	Adequate Support meas.
FLEX / FLORIS	Selected/ ~2022	56°S-75°N	0.3 x 0.3	10:00	27 day	500-780	0.3-2.0	FR, R, full, PRI			
Sentinel-5P/ TROPOMI	In Orbit	Global	7 x 7	13:30	16 day	270-500 675-775 2305-2385	0.5	FR, full, (R)			
MetOp / GOME-2	In Orbit	Global	40 x 40 40 x 80	09:30	29 day	270-790	0.5	FR, full, (R), PRI			
TEMPO	Selected/ ~2019	CONUS	4 x 5	GEO	1 hour	290-490 540-740	0.6	(FR), PRI			
OCO-2	In Orbit	Global**	1.3 x 2.25	13:30	16 day	757-775	0.04	FR			
GOSAT / TANSO-FTS	In Orbit	Global**	10 x 10	13:00	3 day	758-775 1560-1720 1920-2080 5550-14300	0.025	FR			
MTG-S / Sentinel-4	Selected/ 2019	Europe	8 x 8	GEO	1 hour	290-500 750-775	0.12	FR			
GeoCARB	Selected/ 2021	N & S America	~3 x 3	GEO	8 hour	757-772 1591-1621 2045-2085 2300-2345	0.05	FR	N/A	N/A	N/A
TanSat / ACGS	In Orbit	Global**	2 x 2	13:30	16 day	758-778 1594-1624 2042-2082	0.04	FR			

References:
FLEX: Drusch et al. (2017)
TROPOMI: Guanter et al. (2015)
GOME-2: Joiner et al. (2016, 2013)
TEMPO: Zoogman et al. (2016)
OCO-2: Frankenberg et al. (2014)
GOSAT: Joiner et al. (2011); Frankenberg et al. (2011b)
Sentinel-4: Meijer et al. (2014)
GeoCARB: O'Brien et al. (2016)
TanSat: Du et al. (2018)

● Excellent ◐ Very Good ○ Good ◒ Fair ● Poor

** = Global coverage, discontinuous
GEO = Geo-Synchronous Orbit
FR = Far-Red SIF
R = Red SIF
Full = 650-780 nm
(FR), (R) = retrieval possible
PRI = Reflectance @ 530nm, and reference wavelength (usually 570nm)

Table 4.

Studies investigating remotely detected SIF in terrestrial vegetation for photosynthesis and stress detection. Tc: canopy temperature; Ta: air temperature. *Vegetation:* **C:** cropland; **F:** forest; **G:** grassland; **O:** orchard; **V:** various biomes. *Scale:* **G:** ground-based; **A:** airborne-based; **S:** satellite-based. *SIF:* **R:** red; **FR:** far-red; **PR:** fluorescence peak ratio; **F-SIF:** full SIF emission.

Objective	Vegetation	Scale	SIF	Publication examples
Photosynthesis and its estimation				
absorbed PAR	C, F, O	G	FR	Cui et al., 2017a; Miao et al., 2018; Wagle et al., 2016; Yang et al, 2015; Zhang et al., 2016a
diurnal dynamics	C, F	G, A	R, FR	Cogliati et al., 2015a; Damm et al, 2010; Middleton et al., 2017; Schickling et al., 2016; Sobrino et al., 2011
GPP (empirical)	C, F, G, V	G, A, S	R, FR	Alden et al., 2016; Berkelhammer et al., 2017; Chang et al., 2016; Gentine and Alemohammad, 2018; Goulas et al., 2017; Guan et al., 2015; Hu et al., 2018a; Guanter et al., 2014; Köhler et al., 2018b; Li et al., 2018a; Sun et al., 2018, 2017; Wieneke et al., 2016
GPP (modelled)	V	S	FR	Luus et al., 2017; MacBean et al., 2018; Parazoo et al., 2014; Qiu et al., 2018; Thum et al., 2017; Verma et al., 2017; Wagle et al., 2016; Yoshida et al., 2015
light use efficiency	c, F, G, V	G, S	R, FR	Cheng et al., 2013; Miao et al., 2018; Song et al., 2018; Walther et al., 2018; Verma et al., 2017; Yang et al., 2015
NPP	C	S	FR	Patel et al., 2018
phenological stage	C	G	R, FR	Daumard et al., 2012; Miao et al., 2018
seasonal dynamics	C, F, G, O, V	G, A, S	R, FR	Koffi et al., 2015; Joiner et al., 2014; Meroni et al., 2011; Parazoo et al., 2013; Rascher et al., 2015; Rossini et al., 2010; Smith et al., 2018; Wang et al., 2018; Wieneke et al., 2018; Wyber et al., 2017; Zarco-Tejada et al., 2013b
vegetation type	C, F, G, V	G, A, S	R, FR	Damm et al., 2015a; Guan et al., 2016; Guanter et al., 2012; Li et al., 2018b; Liu et al., 2017; Madani et al., 2017; Rascher et al., 2009; Rossini et al., 2016; Sun et al., 2018
Stress detection				
bacterial infection	O	A	FR	Zarco-Tejada et al., 2018
fungal infection	C, F	A	FR	Calderón et al. 2015; Hernández-Clemente et al., 2017
heat	C	S	FR	Guan et al., 2016; Song et al., 2018
herbicide	C, G	G, A	R, FR	Pinto et al., 2016; Rossini et al., 2015
nitrogen deficit	F	G	PR	Freedman et al., 2002
transpiration	F	G	F-SIF	Lu et al., 2018b
water deficit, drought	C, F, O, V	G, A, S	R, FR, PR	Daumard et al., 2010; Koren et al., 2018; Lee et al., 2013; Ma et al., 2016; Sanders et al., 2016; Sun et 1., 2015; Wang et al., 2016; Wieneke et al., 2018, 2016; Xu et al., 2018; Zarco-Tejada et al., 2012; Zuromski et al., 2018
Ancillary indices				
chlorophyll content	C, O	G, A, S	R, FR	Panigada et al., 2014; Zhou et al., 2016; Zarco-Tejada et al., 2018, 2013b; Zhang et al., 2014
EVI	V	S	FR	Ma et al., 2016
MTCI	C	S	FR	Zhang et al., 2014
NDVI	C, F, G	G, A	R, FR	Garzonio et al., 2017; Rascher et al., 2009
PRI	C, G	G, A, S	FR, PR	Middleton et al., 2018; Paul-Limoges et al., 2018; Schickling et al., 2016; Verma et al., 2017
Tc-Ta; *or* Tc	C, F, O	A	FR	Calderón et al. 2015; Middleton et al., 2017; Zarco-Tejada et al., 2018, 2012

Table 5.

Drivers of steady-state fluorescence, processes that may be affected, and ecological and temporal scales of influence. *Process:* **A:** absorption of incident light; **R:** re-absorption of fluorescence; **S:** fluorescence scattering; **PQ:** photochemical quenching; **NPQ:** nonphotochemical quenching; **OP:** other photoprotection. *Ecological scale:* **L:** leaf; **C:** canopy; **E:** ecosystem; **B:** biome. *Temporal scale:* **ST** (short-term)**:** seconds, minutes, hours, diurnal; **MT** (medium-term)**:** days, weeks; **LT** (long-term)**:** months, years; **SV:** seasonal variation. **Definitions of ecological scales**: Leaf: a single leaf or leaf cluster on a single plant; Canopy: a single plant or monospecific closed canopy stand; Ecosystem: a mixed-species stand with closed or open heterogeneous structure; Biome: a major habitat (e.g., tundra, grassland, tropical rainforest) with multiple

ecosystems and heterogeneous structure. (Note: For photosynthetic pathway, switching between pathways occurs in some species.)

Fluorescence driver	Process potentially affected						Ecological scale				Temporal scale			
Vegetation traits and processes	A	R	S	PQ	NPQ	OP	L	C	E	B	ST	MT	LT	SV
age														
carboxylation capacity														
chlorophyll content														
chloroplast movements														
electron transport rate														
epicuticular wax														
evapotranspiration														
fraction functional PSII reaction centres														
fraction open PSII reaction centres														
leaf area index, LAI distribution														
leaf inclination, heliotropism														
leaf internal anatomy														
leaf thickness														
light use efficiency														
mesophyll conductance														
non-chlorophyll pigments														
non-foliar photosynthesis														
phenological stage														
photodamage														
photoinhibition (reversible)														
photorespiration														
photosynthetic pathway (C_3, C_4, CAM)														
photosystem state transitions														
photosystem stoichiometry (PSII : PSI)														
PSII efficiency (quantum yield)														
species, plant functional type														
stomatal conductance														
surface albedo														
thermal dissipation – constitutive														
thermal dissipation – regulated														
water content														
vegetative competition														
Environmental, atmospheric, and stress factors														
air temperature; cold or heat stress														
atmospheric aerosols, pollutants, ozone														
carbon dioxide concentration														
cloud cover														
daylength														
herbicide stress														
incident light intensity														
incident light spectral quality														
nutrient deficiency, toxicity														
oxygen concentration														
pest stress (insect, viral, fungal, bacterial)														
relative humidity, vapour pressure deficit														
solar zenith angle														
surface (atmospheric) pressure														
water stress														
wind stress														